

TOP-FUEL DRAGSTER WING DESIGN USING CFD
AND ITS INFLUENCE ON VEHICLE
DYNAMIC PERFORMANCE

By

TONY MICHAEL BURATTI

Bachelor of Science

Oklahoma State University

Stillwater, Oklahoma

1998

Submitted to the Faculty of the
Graduate College of
Oklahoma State University
in partial fulfillment of
the requirements for
the Degree of
MASTERS OF SCIENCE
December, 2000

TOP-FUEL DRAGSTER WING DESIGN USING CFD
AND ITS INFLUENCE ON VEHICLE
DYNAMIC PERFORMANCE

Thesis Approved:

Thesis Advisor

Dean of the Graduate College

ACKNOWLEDGEMENTS

I am deeply grateful to my parents, Richard M. and Joyce K. Buratti, for their love, support and encouragement. They have instilled in me the value of hard work and dedication which has helped me to become who I am today. Special thanks goes to my grandmother, Frances Henson, for her love and support that she has provided.

I also extend my appreciation to the faculty and staff of the Mechanical and Aerospace Engineering department at Oklahoma State University who have adopted me and encouraged me to be successful. I would also like to thank the other members of my committee, Dr. David G. Lilley and Dr. Gary E. Young, for their suggestions and comments throughout this research.

Mr. Brian Vermillion of Advanced Racing Composites has provided support through his knowledge, information, and insight into the racing community. I appreciate all his time and resources that he has provided in support of my research and education. I would also like to thank Dr. Kajal K. Gupta of NASA Dryden Flight Resource Center for his support and sponsorship.

Lastly, I wish to express my sincere appreciation to my graduate advisor, Dr. Andrew S. Arena Jr., for his continual support and guidance throughout the last couple of years. He has been inspirational through his teachings and will continue to serve as a great mentor throughout my professional career.

TABLE OF CONTENTS

Chapter	Page
I. INTRODUCTION	1
1.1 Background	1
1.2 Research Objective.....	3
II. LITERATURE REVIEW.....	4
2.1 Dynamics of Vehicles	4
2.1.1 Tire Tread Momentum Theory	5
2.1.2 Critical Speed Model.....	6
2.2 Characteristics and Dynamics of Rotating Wheels	10
2.2.1 Dynamics of Tires	10
2.2.2 Tire Aerodynamic Studies.....	11
2.2.3 Top-Fuel Dragster Tires	17
2.3 Wing Design.....	20
2.3.1 Multi-element Wings	20
2.3.2 Limitations on Rear Wing Design for Top-Fuel Dragsters.....	22
2.3.3 Typical Top-Fuel Dragster Wings	22
2.3.4 Endplate Design	25
III. METHODOLOGY	26
3.1 Modeling the Dragster	26
3.1.1 Wheel Properties Used.....	27
3.1.2 Rear Wing Properties Used.....	28
3.1.3 Equations of Motion.....	28
3.2 Validation of the Dragster Model.....	31
3.3 STARS CFD Module	35
3.4 Implementing the Dragster Wing into STARS	36
3.4.1 Geometry Specifications in STARS.....	37
3.4.2 Grid Specifications in STARS	40
3.4.2.1 SURFACE Module	41
3.4.2.2 VOLUME Module	42
3.4.3 Boundary Condition Specification in STARS	42
3.4.3.1 SETBND Module.....	44
3.4.4 Solver Control Specifications	45
3.4.4.1 EULER Module	45
3.5 The Effects that Endplates have on Rear Wing Performance	46

Chapter	Page
3.6 Box Wing Design	47
IV. RESULTS	53
4.1 Effects of Endplate on Three-Element Dragster Wings	53
4.1.1 Pressure Contours	54
4.1.2 Cross-Flow Velocity	59
4.1.3 Velocity at the Tip of the Wing.....	69
4.1.4 Down Force to Drag Ratio	71
4.1.5 Mach Number and Coefficient of Pressure Distribution	73
4.2 Gap Spacing Comparisons for a Three-Element Dragster Wing	76
4.3 Angle of Attach Comparisons of Three-Element Dragster Wings.....	78
4.4 World Record Performances	80
4.5 Using the Dragster Model to Analyze the Problem	80
4.6 Steady Results of Boxwing Design	89
4.6.1 Decalage Angle Comparisons	89
4.6.1.1 Pressure Plots	90
4.6.1.2 Mach Plots	93
4.6.2 Boxwing and Three-Element Wing Comparisons	96
4.7 Dragster Performance Comparisons using the Dynamic Model	100
4.7.1 Performance Data for Various Rear Wings	101
4.7.2 Performance Data for Various Input Power Curves	103
V. CONCLUSIONS AND RECOMMENDATIONS	107
5.1 Conclusions	107
5.1.1 Dynamic Dragster Model.....	107
5.1.2 Endplate Effects on a Top-Fuel Dragster Rear Wing	108
5.1.3 Boxwing Design.....	108
5.2 Recommendations	109
5.2.1 Dynamic Dragster Model.....	109
5.2.2 Endplate Design Improvements	110
5.2.3 Boxwing Design.....	111
5.2.4 Stability of the Dragster	111
BIBLIOGRAPHY	112
APPENDIX A-1.....	115
STARS-CFD Geometry Data File (<i>fin.sur</i>).....	115
APPENDIX A-2.....	127
STARS-CFD Background Mesh Data File (<i>fin.bac</i>).....	127
APPENDIX A-3.....	129
STARS-CFD Boundary Conditions Data File (<i>fin.bco</i>).....	129
APPENDIX A-4.....	130

Chapter	Page
STARS-CFD Parameter Control File (<i>fin.cons</i>).....	130
APPENDIX B-1.....	131
STARS-CFD Geometry Data File (<i>boxwing.sur</i>)	131
APPENDIX B-2.....	139
STARS-CFD Background Mesh Data File (<i>boxwing.bac</i>)	139
APPENDIX B-3.....	141
STARS-CFD Boundary Conditions Data File (<i>boxwing.bco</i>)	141
APPENDIX B-4.....	142
STARS-CFD Parameter Control File (<i>boxwing.cons</i>)	142
APPENDIX C-1.....	143
Selig 1223 Airfoil Coordinate Data.....	143
VITA.....	145

LIST OF TABLES

Table	Page
3-1: Lift and Drag Coefficients for the Tires from Cogotti's Research	27
3-2: Surface Region Flags.....	43
3-3: Curve Segment Flags.....	43
4-1: Down Force and Drag for the Three Test Cases Analyzed	72
4-2: Increase of Lift to Drag Ratio for the Three Test Cases Analyzed	73
4-3: Lift and Drag Coefficients for the Dragster Model.....	82

LIST OF FIGURES

Figure	Page
1-1: Schematic of a top-fuel dragster.....	1
2-1: Drag Tire Schematic.....	5
2-2: Schematic of an AA/FD Dragster with Forces.....	8
2-3: Schematic of the Contact Patch.....	11
2-4: Schematic of Magnus Effects.....	13
2-5: Experimental Study of Flow Past a Stationary and Rotating Wheel.....	14
2-6: Pressure Distribution Around the Wheels of a Vehicle.....	14
2-7: Reynolds Number Effects on the Coefficient of Drag.....	15
2-8: Flow Pattern Around a Smooth Cylinder at Various Re Number.....	16
2-9: Static View of a Top-Fuel Dragster Tire.....	17
2-10: Tire Expansion on Top-Fuel Dragster Burnout.....	18
2-11: Top-Fuel Dragster Tire at the Start of a Run.....	19
2-12: Effects of Multiple Elements on the Coefficient of Lift.....	21
2-13: Endplate Size Dimensions.....	24
3-1: Dragster Run Schematic Showing Two Areas.....	29
3-2: Validation of Position vs Time for a Top-Fuel Dragster (1/4 Mile).....	32
3-3: Validation of Speed vs Time for a Top-Fuel Dragster (1/4 Mile).....	33
3-4: Validation of Acceleration vs Time for a Top-Fuel Dragster (1/4 Mile).....	34

Figure	Page
3-5: Validation of Speed vs Position for a Top-Fuel Dragster (1/4 Mile).....	35
3-6: Wing Geometry Specification	38
3-7: Rendered View of a Half-Span model with a Style 3 Endplate	39
3-8: Half Model of Dragster Rear Wing Mesh Density.....	40
3-9: Three Different Endplate Geometry Analyzed.....	46
3-10: Selig 1223 Airfoil	48
3-11: Effect of the Number of Elements on an F-1 Type Wing	49
3-12: Decalage Angle	50
3-13: Rendered View of half model Boxwing with a 12° Decalage Angle.....	52
4-1: Pressure Contours of the Wing without an Endplate.....	54
4-2: Pressure Contour of Wing with Style 3 Endplate.....	56
4-3: Pressure Contour of Wing with New Style Endplate	57
4-4: Pressure Gradient for Style 3 Endplate	58
4-5: Cross Flow Velocity Cuts Represented by Vertical Lines	60
4-6: Cross-Flow Velocity 7 in. back from L.E. w/o an Endplate	61
4-7: Cross-Flow Velocity 14 in. back from L.E. w/o an Endplate	62
4-8: Cross-Flow Velocity 20 in. back from L.E. w/o an Endplate	63
4-9: Cross-Flow Velocity 7 in. back from L.E. with Style 3 Endplate.....	64
4-10: Cross-Flow Velocity 14 in. back from L.E. with Style 3 Endplate.....	65
4-11: Cross-Flow Velocity 20 in. back from L.E. with Style 3 Endplate.....	66
4-12: Cross-Flow Velocity 7 in. back from L.E. with New Endplate	67
4-13: Cross-Flow Velocity 14 in. back from L.E. with New Endplate	68

Figure	Page
4-14: Cross-Flow Velocity 20 in. back from L.E. with New Endplate	68
4-15: Velocity at the Wingtip without an Endplate	69
4-16: Velocity just inside Style 3 Endplate.....	70
4-17: Velocity just inside New Endplate	71
4-18: Pressure Distribution at the Tip of the Wing for Three Configurations.....	74
4-19: Mach Distribution at the Tip of the Wing for the Three Configurations	75
4-20: Velocity Profile of Wing with Original Gap Spacing	76
4-21: Velocity Profile of Wing with Modified Gap Spacing.....	77
4-22: Pressure Plots for Angle of Attack Comparisons.....	79
4-23: Input Power Curve and Acceleration Power Curve versus Time.....	81
4-24: Power Curves along with Drag Power versus Time.....	83
4-25: Elapsed Time and Speed Data for Varying Drag Coefficient	84
4-26: Elapsed Time and Critical Speed Data for Varying Drag Coefficient	85
4-27: Elapsed Time and Speed Data for Varying Lift Coefficient	86
4-28: Elapsed Time and Critical Speed Data for Varying Lift Coefficient	88
4-29: Pressure Plot for Boxwing at 0 Degree Decalage Angle.....	91
4-30: Pressure Plot for Boxwing at 8 Degree Decalage Angle.....	92
4-31: Pressure Plot for Boxwing at 12 Degree Decalage Angle.....	93
4-32: Mach Number Plot for Boxwing with 0 Degree Decalage Angle.....	94
4-33: Mach Number Plot for Boxwing at 8 Degree Decalage Angle.....	95
4-34: Mach Number Plot for Boxwing at 12 Degree Decalage Angle	96
4-35: Coefficient of Lift vs Angle of Attack	97

Figure	Page
4-36: Coefficient of Drag vs Angle of Attack	98
4-37: Coefficient of Drag vs Coefficient of Lift.....	99
4-38: Coefficient of Lift to Drag vs Coefficient of Lift.....	100
4-39: Elapsed Time and Speed Data with Different Wing Configurations	102
4-40: Elapsed Time and Speed Data with Different Wing Configurations	103
4-41: Model Power Input Curves to look at Horsepower Effects.....	104
4-42: Power Curve Input Effects on Elapsed Time and Top Speed	105

NOMENCLATURE

CFD	Computational Fluid Dynamics
NHRA	National Hot Rod Association
A	Aerodynamic reference area-projected frontal area of the vehicle
AR	Aspect Ratio
C_D	Coefficient of drag
C_L	Coefficient of lift
D_{free}	Free diameter of the tire, unrestrained, inches
F_v	Vertical tread force, lbf, impact momentum
L.E.	Leading Edge
M_{grd}	Mass of tread, lb_m/g , W/g
\dot{M}_{grd}	Mass rate of tread, $lb_m/g \cdot \text{sec}$
N_i	Rear axle input speed, RPM
N_r	Real axle speed, RPM, $N_i/3.2$
P	Specific effective power
Re	Reynolds number
RPM	Revolutions per minute
S	Wing area
SR	Slip Ratio

a	Distance to vehicles cg from the front wheels
b	Wing span
c	Chord length of an airfoil
d	Distance from the vehicle cg to vehicles center of pressure
g	Acceleration due to gravity
h	Height of endplate
m	Mass of the vehicle
s	Horizontal distance traveled
\dot{s}	Longitudinal velocity
\ddot{s}	Longitudinal acceleration
s_L	Aerodynamic radius, $s_L = \frac{m}{\frac{1}{2}\rho AC_L}$
Λ, Δ	Fraction of lift on driving wheels including weight transfer effect
γ	Traction coefficient
η	Vehicle driving efficiency
λ	Fraction of weight on driving wheels including weight transfer effect
μ	Coefficient of rolling resistance
ρ	Air density

CHAPTER 1

1. INTRODUCTION

1.1 Background

The dynamics of a Top-Fuel Dragster Car, depicted in Figure 1-1, are quite complicated to model and pose problems for many research areas of interest. The Top-Fuel Dragster is the fastest of drag racing vehicles. It accelerates at almost 4 longitudinal g's completing a quarter mile run in less than five seconds. It reaches over 100 mph in less than a second and finishes the run with speeds in excess of 320 mph. They are powered by a supercharged engine that puts out over 6000 horsepower and the massive tires spin at almost 8000 rpm. For a single run these dragsters consume more than 5 gallons of nitro methane fuel. The vehicles weight is around 2150 pounds, including the driver, giving it a phenomenal power to weight ratio that puts it in a class like no other.

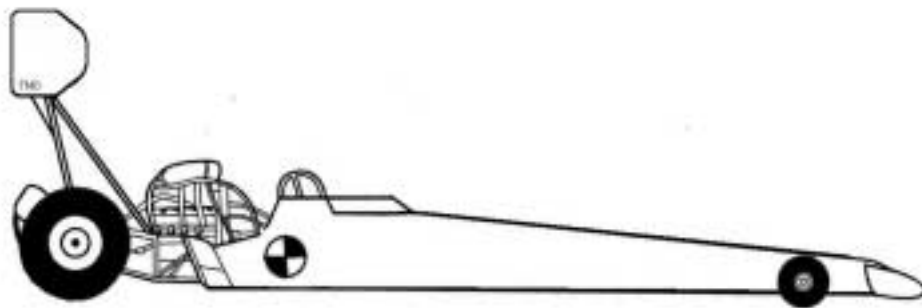


Figure 1-1: Schematic of a top-fuel dragster

Lift and drag are very important factors for this type of racing event. Many components are responsible for creating this lift and drag but only a couple greatly affect the dragsters performance. These components include the body, rear wheel dynamics, and the rear wing.

The performance of the enormous rear tires, 36.0" x 17.0"-16's, add to the complexity of the problem. During the run the tires stretch and deform due to a large engine torque of around 4500 ft-lbs as well as the rotational inertial of the tire tread. Normal operating pressure is 4 psig to 5 psig creating a tire footprint of over 250 square inches at the start of the run. The tire constantly changes in size and can expand adding an additional 4.5 inches to the diameter during a run. The rotational inertia of the tire delivers a down force to the car. On the other hand, the flow over the wheels has a great affect on the performance of the car because it results in a positive lift at the rear axle.

The rear wing is used to increase the amount of down force to the rear tires. Increasing this down force increases the normal force between the tire and track surface, which theoretically should increase the potential to use the engine power to accelerate the dragster. If there is little normal force then there is potential for the car to experience wheel slip and thus not have traction to accelerate.

The reason every top fuel dragster team doesn't make a rear wing that has an enormous amount of down force is the fact that when lift is generated so is drag. This drag is referred to as induced drag and is a function of the square of the velocity. This increase in drag therefore takes more horsepower away from the acceleration horsepower and results in a reduced maximum speed that can be achieved during the run. The

question is therefore how much down force is needed and at what time during the run is the maximum amount of down force critical?

1.2 Research Objective

The emphasis of the present work is two fold. First is to develop an accurate dynamic model for a quarter mile run of a top-fuel dragster. The model will be as complete as possible accounting for the significant forces encountered on the vehicle. The performance of the vehicle will be determined by the elapsed time and final speed.

The second portion of this work will be to study the effects that the aerodynamic characteristics of a dragster and rear wing have on the performance of the dragster using the model. From this data an alternative wing will be designed and analyzed. This data will be entered into the model and compared to the current style of wings being used.

Most emphasis has gone into improving the rear wing characteristics but this will not necessarily improve the performance of the dragster. The dynamic solver will be used to determine if the new wing will improve the performance of the overall vehicle. Therefore the focus will be in improving the performance of the car and not just focus on improving the rear wing characteristics. A computational fluid dynamic (CFD) solver will be used to analyze the wing characteristics and this information will be used in the dynamic dragster model.

CHAPTER 2

2. LITERATURE REVIEW

This literature review covers several aspects of a dragster. First two dynamic models will be discussed in detail and one will be modified and used for the current research. Second the dynamics of the tires will be discussed to find out more about modeling the tire dynamically and all the modeling problems that it might pose. The other part of the tire research review will be on the aerodynamics of the tires since they are large and rotate at high rpm. To end the chapter other aerodynamic studies will be done for different wing designs talking about the general style of dragster wing used now and the rules limiting the wings.

2.1 Dynamics of Vehicles

It is good to first look at the interaction between the vehicles aerodynamic characteristics and wheel dynamics and see how they affect the overall vehicle performance. Better and improved vehicle performance is what is truly desired and not just the improvement of the components. Granted the improvements in components can lead to better vehicle performance but how much and at what time during the run is the question. The dynamics of the vehicles and how it is affected by the dynamics and

aerodynamics of the tires, the aerodynamic surfaces, and the aerodynamics of the vehicle's body is what is looked at next.

2.1.1 Tire Tread Momentum Theory

Because Top-Fuel Dragsters accelerate at over 4 longitudinal g's for several seconds this means that there is an effective tire friction factor of over 4 [Hallum, 1994]. This is not possible and therefore Hallum offers a theory on his tread momentum principle.

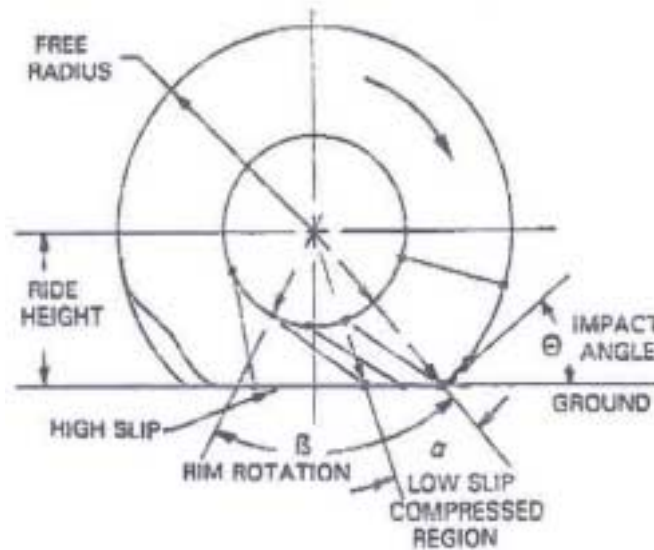


Figure 2-1: Drag Tire Schematic

A schematic of a dragster tire is depicted in Figure 2-1 above. In this schematic the tire contact angles, tread radius, tread sidewall twisting-straightening, and rotational angles are all shown. Hallum states that the normal force applied to the ground under the compressed area is about equal to the rate of change of vertical tread momentum at the contact. This force, for one tire is given by equation (2-1).

$$F_v = \dot{M}_{grd} \cdot V_{grd} \cdot \sin \theta \quad (2-1)$$

where

$$\dot{M}_{grd} = \dot{M}_{grd} \left(\frac{N_r \cdot RPM}{60} \right)$$

$$V_{grd} = \pi \cdot \left(\frac{D_{free}}{12} \right) \left(\frac{N_r}{60} \right)$$

For this method there are three initial inputs into the system, which are start line ride height (16.5 inches), rear axle RPM at initiation (0 RPM), ground velocity (0 ft/sec), and acceleration due to rear static weight times the tire friction. The rear axle RPM and ground velocity are from real data but it would seem that the ground velocity would be something that should be calculated. The ride height was assumed and a constant friction factor was used. The output is the tread horizontal momentum change and the acceleration of the dragster.

This model did not give a whole lot of information as to how it works and proved difficult to use when trying to implement. Therefore a different model was sought and discovered that would prove more beneficial to the current research effort.

2.1.2 Critical Speed Model

A different model was proposed by [Hawks and Sayre, 1973] in which they study the optimum straight-line performance of an automobile. They introduce the equations of motion for a straight-line acceleration including both the aerodynamic lift and pitching moment. Their results concluded that aerodynamic down force can improve performance

if the acceleration is limited by traction and that aerodynamic lift is beneficial when power is the limiting factor.

Most of the trends in those days, when considering high-performance automobile design, was to place emphasis on producing down force for the purpose of improving cornering speeds. It was thought that these aerodynamic devices that were being used degraded straight-line performance due to the drag but then it would be made up in the cornering.

Hawks and Sayre found that, in certain circumstances, the straight-line performance improved along with the cornering speed due to the introduction of these aerodynamic down force generating devices. Their studies looked at the performance of three vehicles - an AA/FD Competition Fuel Dragster, a Ford Galaxie sedan, and the Lola T-140 Formula A car with several different aerodynamic devices.

It was found that below a certain speed, referred to as the critical speed, the vehicle can spin its wheels. This force corresponds to the friction coefficient multiplied by the normal force on the tires. When there are aerodynamic forces acting on the vehicle then the force becomes a function of the vehicle's speed squared. This increase in down force comes with the penalty of increased drag due to the induced drag of the aerodynamic surfaces as discussed previously. If the increase in driving force is greater than the increase in drag then an improvement in performance will result.

Some of the assumptions that were made for this model include a rigid body in rectilinear motion; the automobile is driven through one pair of wheels; acting on the automobile are the driving force, the rolling resistance, the aerodynamic forces of lift and drag, and the aerodynamic pitching moment; and there is an ideal transmission. It was

also assumed that below the critical speed, wheel spin is impending and the driving force is dependent on the product of the friction coefficient and the normal force on the driving wheel. Above this critical speed the driving force is proportional to the maximum power and inversely proportional to the speed. The rolling resistance is assumed to be constant for simplicity.

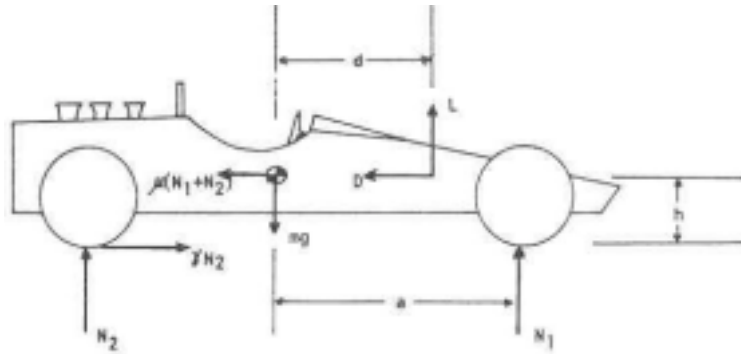


Figure 2-2: Schematic of an AA/FD Dragster with Forces [Hawks and Sayre, 1973]

When looking at the model in a more detailed manner the schematic of an AA/FD Dragster and the forces acting upon it should be used and is depicted in Figure 2-2. Using the vertical force equation and the moment equation to find the normal loads on the tires, the equation of motion in the longitudinal direction can be derived. The longitudinal acceleration for a speed that is less than the critical speed is shown in equation (2-2).

$$\ddot{s} = [\gamma\lambda - \mu]g - \frac{1}{2} \frac{\rho A}{m} [C_D + (\gamma\lambda - \mu)C_L] \dot{s}^2 \quad (2-2)$$

Equation (2-3) is the acceleration where the speed is greater than the critical speed.

$$\ddot{s} = \frac{\eta P}{m\dot{s}} - \mu g - \frac{1}{2} \frac{\rho A}{m} [C_D + \mu C_L] \dot{s}^2 \quad (2-3)$$

where

$$\lambda = \frac{a}{1 - h\gamma}$$

$$\Lambda = \frac{a - d}{1 - h\gamma}$$

Since the critical speed is the speed at which the traction-limited driving force equals the power-limited driving force it can be found by equating (2-2) and (2-3). The resulting equation is a cubic equation in critical speed where the critical speed is the smaller positive root of equation (2-4).

$$\dot{s}^3 - \frac{\lambda g}{\Lambda} s_L \dot{s} + \frac{P s_L}{m \Lambda \gamma} = 0 \quad (2-4)$$

where s_L is the aerodynamic radius and is given by

$$s_L = \frac{m}{\frac{1}{2} \rho A C_L}$$

For the current research effort the critical speed model will be modified and used in order to look at particular components of the dragster and how they affect the performance. Actual parameters will be used when known but other parameters will be estimated to develop a good model. This model will be validated using top-fuel dragster data. Further research will be done to show patterns of the affects that changing the aerodynamic characteristics have on the performance. The model will also be used to

look at a current wing used and see what types of changes can be made to it, if any, that will help lower the elapsed time and increase top speed.

2.2 Characteristics and Dynamics of Rotating Wheels

The tire is one of the most important considerations of the racecar because it is the linkage between the vehicle and the racing surface. There are many studies on the dynamics of tires and the various things that affect the performance of the tire. The bulk of the studies in this area have been for passenger cars but some of this can be used for the current research. There will also be some discussion of the dynamics and aerodynamics of various parts of the vehicle. After talking about passenger car tires and the dynamics and aerodynamics, a section dealing with just top-fuel dragster tires will be discussed.

2.2.1 Dynamics of Tires

The main bulk of the material for the dynamics of tires deals with lateral forces or cornering forces. The research done in this field is for passenger tires and deals mainly with trying to model a tire for passenger cars. For example several researchers look at tire interaction with different surface terrain, how things differ when there is an uneven vehicle, how the effects of braking and cornering affect traction, the effects of wheel orientation, temperature and pressure variations, and various combinations of each.

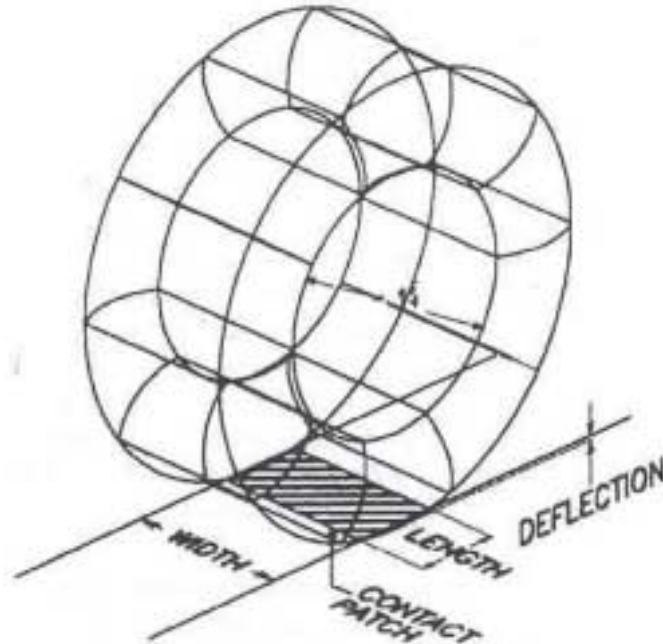


Figure 2-3: Schematic of the Contact Patch

The concern for the current research is that for straight-line acceleration where it deals with the longitudinal forces. When accelerating there are longitudinal forces between the tire and the ground that arise in an area referred to as the tire footprint as can be seen in Figure 2-3. The longitudinal forces have similarities to the lateral or cornering forces inasmuch as there is an elastic distortion region, referred to as longitudinal stretching, and a sliding or frictional region [Milliken and Milliken, 1995]. In addition to these longitudinal forces there are other important forces that arise that come from the aerodynamics of the tires.

2.2.2 Tire Aerodynamic Studies

Tire aerodynamics are not the main focus of this work but for modeling purposes it is necessary to understand some of the characteristics of the tires when developing an

accurate dynamic model. Wheel aerodynamics is a topic that is not fully understood. The information that is generated is based upon research done for the automotive industry. A lot of time has been put into experimental wind tunnel setups where the concern becomes ground interference. Once placed in the wind tunnel, a tire setup can consist of several things:

1. The tire can be stationary (not allowed to rotate) varying the gap distance between the floor and the bottom of the tire.
2. It can be powered by a motor and vary the gap between the floor and the bottom of the tire.
3. The wind tunnel has a movable floor and the wheel is powered by a motor and placed on the moving floor.

All these tests in the wind tunnel are used to try to match existing tire aerodynamic data. It might not be possible to have the ideal setup in the wind tunnel because they might not have a moving floor, they might not be able to power the wheel, etc. The ideal setup would be to have a wind tunnel vehicle that is able to rotate the wheels at their appropriate speeds with zero ground clearance.

Studies have been done looking at the first setup where the tire is stationary and the gap is varied. It was shown by using wool tufts around the wheels that for the stationary wheels the difference between a sealed and unsealed ground clearance was almost imperceptible [Stapleford and Carr, 1970]. It was stated that the boundary layer effect restricted the flow of air under the wheels when the gap was opened. But when the wheels were rotating, as in the second setup mentioned above, an additional airflow was induced through these gaps and the flow pattern had changed considerably. The principal

effect of the rotation was an asymmetric pressure distribution causing a large negative lift to be generated in accordance with the Magnus effect, which is discussed next.

For inviscid flow past a cylinder has a symmetric flow pattern and by symmetry the lift and drag are zero. But for a rotating cylinder it will drag some of the fluid around producing circulation. This in effect causes the flow to be asymmetric and the average pressure is greater on the upper half of the cylinder than on the lower half of the cylinder causing lift to be generated. This is known as the Magnus effect and is pictured in Figure 2-4. This figure was provided by [Munson, Young, and Okiishi, 1994].

In the figure, the first picture (a) is of a uniform upstream flow past a cylinder without circulation. The second picture (b) is a free vortex at the center of the cylinder while the last picture (c) is the combination of the free vortex and uniform flow past a cylinder. This combination gives nonsymmetrical flow and thus produces lift.

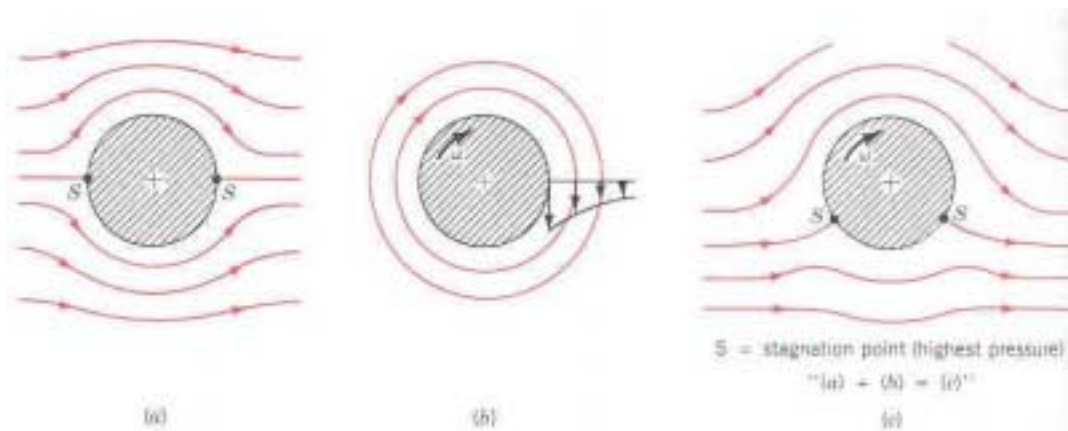


Figure 2-4: Schematic of Magnus Effects

Further explanation is given by [Katz, 1995] where he talks about and shows the difference in separation points for a rotating and non-rotating wheel in a wind tunnel. As seen in Figure 2-5 the separation point on the rotating wheel (left) occurs much sooner

than the separation point on the stationary wheel (right). This figure was provided by [Katz, 1995].

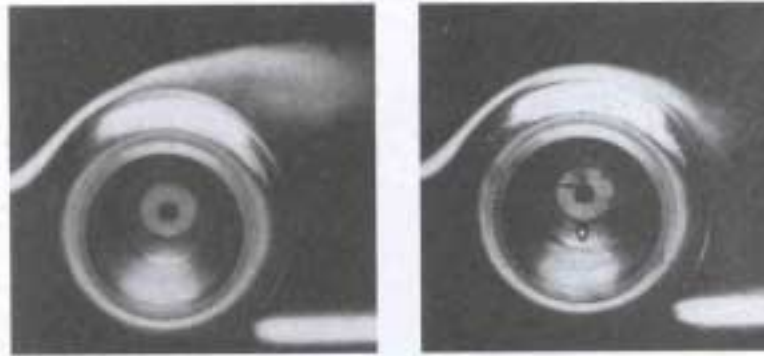


Figure 2-5: Experimental Study of Flow Past a Stationary and Rotating Wheel [Katz, 1995]

This early separation for the rotating wheel can be explained by studying Figure 2-6 which was provided by [Milliken and Milliken, 1995]. For the stationary wheels the suction pressure is greater on the top of the wheels and thus causes a greater positive lift upwards. When the rotation is introduced the separation point is further upstream reducing the suction pressure and thus reducing this positive lift. The figure below is from wind tunnel tests and the rotating wheel had an effective "zero" ground clearance while the stationary wheel had a 0.25 inch ground clearance [Stapleford and Carr, 1969].

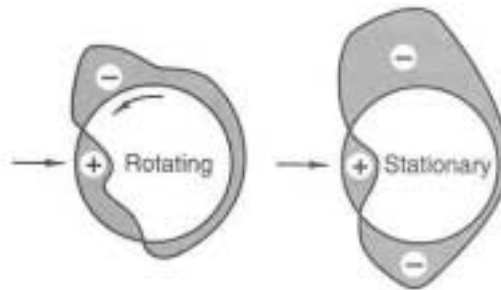


Figure 2-6: Pressure Distribution Around the Wheels of a Vehicle

Another thing that greatly affects the characteristics of tire performance is Reynolds number. A little bit of information was provided by [Cogotti, 1983] about the effects of Reynolds number. He also provides his tire data along with the corresponding critical Reynolds number, which is based upon the turbulence and surface roughness. This critical Reynolds number greatly affects the drag coefficient.

When looking at the Re number effects on a smooth cylinder, as seen in Figure 2-7, the coefficient of drag is greatly affected. The figure below is not used for any data in this work but it is merely to show how great Re number effects can be on an object similar to the dragster tire. The figure was provided by [Munson, Young, Okiishi, 1994]. The calculated Re number for the top-fuel dragster tire at a top speed of 330 mph, based upon its diameter, is 9.25×10^6 .

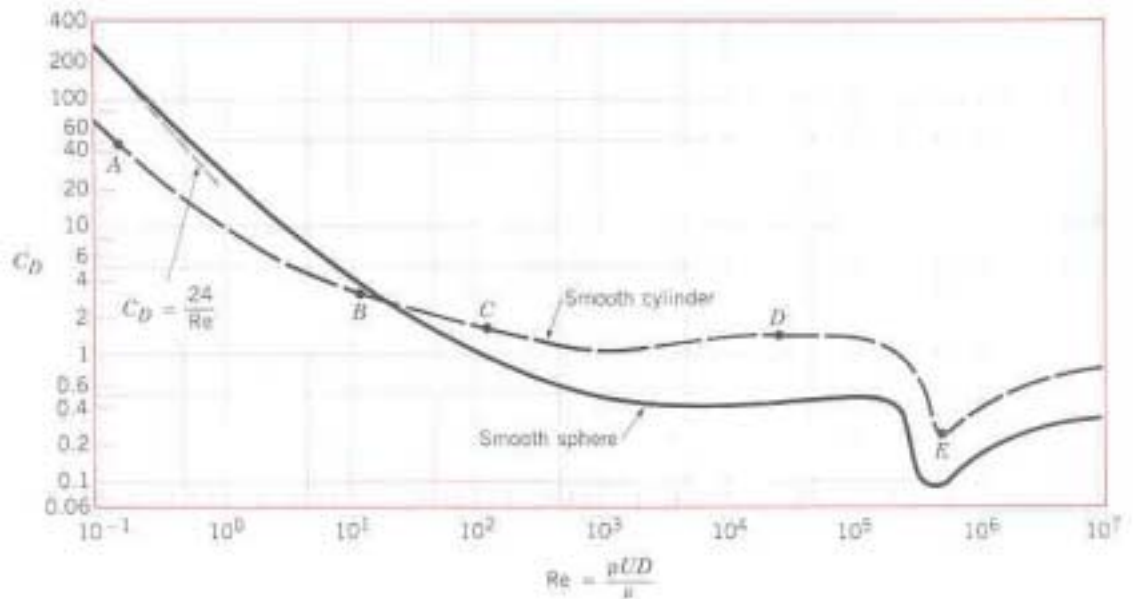


Figure 2-7: Reynolds Number Effects on the Coefficient of Drag [Munson, Young, Okiishi, 1994]

The letters in the previous figure correspond to flow patterns in Figure 2-8, below. The wheel would see a similar flow pattern as it speeds up but in this case there is no ground effects present and the cylinder is not spinning so the flow pattern is for visual purposes only. This helps show the different flows that are encountered during the dragsters run which make the analysis that much more difficult.

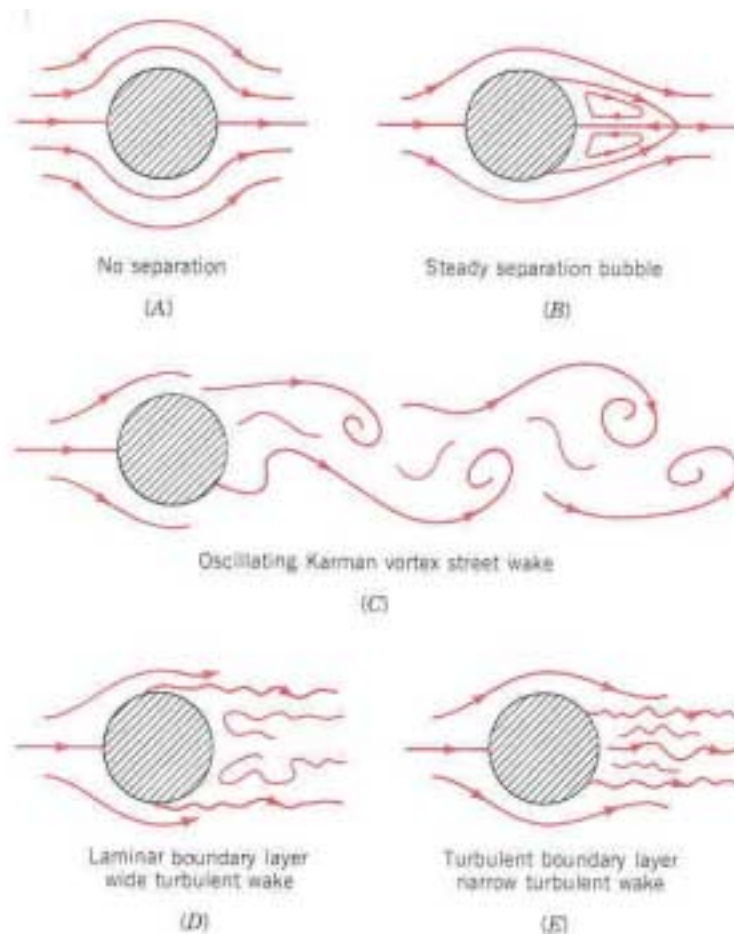


Figure 2-8: Flow Pattern Around a Smooth Cylinder at Various Re Number

One thing in common with all of these papers is that they all seem to come to the conclusion that wheel aerodynamics are very difficult to measure experimentally and their full interaction with the rest of the vehicle is still in a state of confusion. This was

mainly for passenger type tires without the added complications of the top-fuel dragster tire where the high torque, low pressure, high speeds, and large tire deformations add to the complexity of the problem.

2.2.3 Top-Fuel Dragster Tires

As mentioned before the top-fuel dragster has enormous rear tires, 36.0" x 17.0"-16's as seen in Figure 2-9. The side walls of the 36-inch diameter tire are very flexible and weighs around 47 pounds. The main tread of the tire comes in at a weight of around 30 pounds for its 17-inch width.



Figure 2-9: Static View of a Top-Fuel Dragster Tire

With a large engine torque of around 4500 ft-lbs coupled with the normal operating tire pressure of 4 psig to 5 psig gives way to the large 4.5 inches of diameter expansion that the tire sees. In Figure 2-10, there is a static picture before a burnout as well as a picture of the same vehicle during the burnout. The tire has changed shape dramatically both in the width and the diameter of the tire.



Figure 2-10: Tire Expansion on Top-Fuel Dragster Burnout

The tire footprint is over 250 square inches at the start of the run. With the wheels spinning at almost 8000 rpm the rotational inertia of the tire can deliver an enormous amount of down force to the car. When viewed in slow motion at the start of the run the tremendous torque is applied and the tire is balled up at the front of the contact patch as seen in Figure 2-11. The dragster squats and the weight transfers to the rear tires. The wheel rim spins at a faster rate than the rest of the tire causing the sidewalls to wrinkle up at the bottom. Once the tread reaches the rear part of the contact patch it speeds up to catch up with the rest of the wheel rim. This momentum causes great forces that are responsible for the incredible acceleration according to [Hallum, 1994].



Figure 2-11: Top-Fuel Dragster Tire at the Start of a Run

The deformation and wrinkling of the tire due to the large amount of torque applied can be seen above. At the bottom of the tire is the word "Goodyear" and due to the wrinkles in the sidewall it is not entirely visible.

The other perspective of the top-fuel dragster tire is the aerodynamics involved. The flow over the wheel has a great affect on the performance of the car because it results in a positive lift at the rear axle as mentioned before. The flow over a stationary semicircle can be used as an example for this lift effect. Starting out with the basic lift equation, the lift on a stationary semicircle shape was derived in [Munson, Young, Okiishi, 1994] to be the following:

$$L = \left(0.88 + \frac{1.96}{\sqrt{\text{Re}}} \right) \left(\frac{1}{2} \rho U^2 A \right) \quad (2-5)$$

It can be seen that lift is created when there is flow over a semicircle. This is not what is used for determining the lift over that wheels because it is not accurate for a 3D cylinder that is rotating. This is just used to show that there is lift produced due to the flow over the rear wheels and that as the speed increases the lift force becomes greater.

2.3 Wing Design

To keep these rear wheels in contact with the race surface aerodynamic surfaces are used. There are two wings, the front and rear, on a top-fuel dragster car, which help the performance in different ways. The primary purpose of the front wing is to keep the vehicle from pitching up in the front and flipping over. Since the rear wing is mounted as far aft as possible, there is a tendency for the front wheels to be lifted off of the track. The counteracting balance comes from the negative lift produced by the front wing. The required down force of the front wing is enough to keep the overall vehicle from flipping over and provide enough pressure to the front wheels so that the driver has control over the steering. The rear wing is more of the focus of this research.

2.3.1 Multi-element Wings

Sometimes when designing a wing it is desired to produce more down force. Different methods used to obtain more down force are increasing the wing area, increase the camber of the airfoil, and delay flow separation by slotted flap design or multi-elements [Katz, 1995]. Since the wing area is fixed by the NHRA regulations, which will be presented in detail in the next section, then the alternative is to use wings with multi-elements.

Experimental studies on multi-element wings proved that larger lift coefficients could be obtained. These experiments were first performed by Handley Page and the results can be seen in Figure 2-12. This figure was provided by [Smith, 1975]. The

airfoil was a RAF 19 and they are separated by a number of slots. The numbers represent the number of slots with a two-element airfoil having one slot, a three-element airfoil having two slots, and so on. It can be seen that higher angles of attacks can be reached and the coefficient of lift can reach as much as 4.

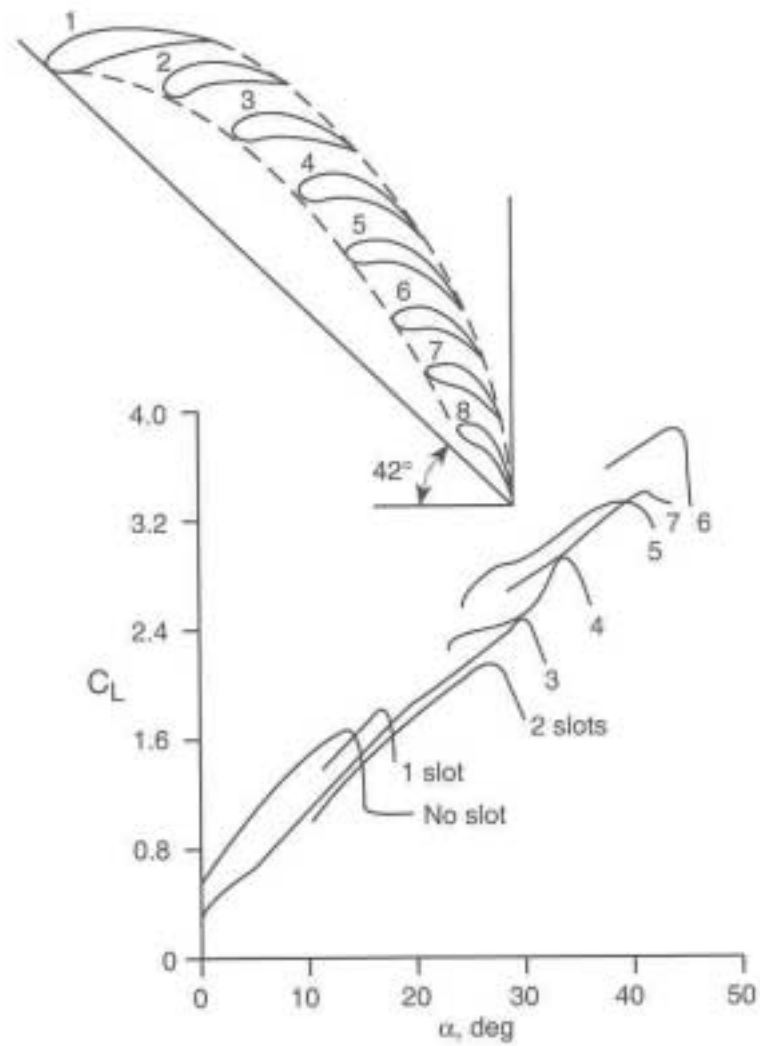


Figure 2-12: Effects of Multiple Elements on the Coefficient of Lift [Smith, 1975]

These slots allow high pressure air from the bottom side of the wing to exit through the gap and flow over the top of the next element. This will tend to reduce the separation while increasing lift and reducing drag.

2.3.2 Limitations on Rear Wing Design for Top-Fuel Dragsters

Since Top-Fuel Dragsters compete in sanctioned races, the governing body or the National Hot Rod Association (NHRA), has instilled rules and regulations that must be met. According to the NHRA 2000 Rulebook the rear wing is limited in type, size, and position. The wing must be locked into place as to prevent adjustment of any part of the wing during the run. The combined total area of all wings, canards, and airfoils mounted behind the front spindle can be no more than 1500 square inches. The position of the rear wing is limited by its height and aft placement. The trailing edge may not extend more than 50 inches behind the centerline of the rear axle and the height of any part of the wing may not exceed 90 inches measured vertically from the ground.

2.3.3 Typical Top-Fuel Dragster Wings

A typical rear wing design for a top-fuel dragster is a three-element wing with endplates. The material has been aluminum but with the advances in composites most are made of carbon fiber and Kevlar for the outer skins as well as the endplates.

Typical rear wings have an aspect ratio of around 2.4. The aspect ratio of a wing is defined by equation (2-6) as being the ratio of the span of the wing squared to the area of the wing.

$$AR = \frac{b^2}{S} \quad (2-6)$$

The higher the aspect ratio the better the performance of the wing. When a wing is generating lift, it has a reduced pressure on the upper surface and an increased pressure on the lower surface. The air wants to get to the lower pressure and thus flows over the tip of the wing. This escaping air reduces the pressure difference near the tip of the wing and thus reduces the lift near the tip. For a wing with the same area this effect is greater for lower aspect ratio wings because the span of the wing is less than that of a high aspect ratio wing. For the high aspect ratio wing the pressure difference at the tip is less significant because it affects a smaller portion of the overall wing. This is why the higher the aspect ratio the better the performance characteristics.

To increase this aspect ratio means increasing the span of the wing or decrease the area of the wing. Increasing the span of the wing can only be done to a certain limit constrained by the width of the dragster. It can be extended past the width of the vehicle but during the race if any part of the dragster crosses the middle dividing line on the drag strip then that dragster is disqualified. This is the main reason that the span of the wing is kept at or below the width of the vehicle.

The effects of increasing this wing span were presented by [Winn, Kohlman, Kenner, 1999] which showed improvement as expected but increasing the span is not desirable as discussed earlier. They show increasing the span of the wing by 3 feet. This is great from an aerodynamic perspective but when it is looked at from the perspective of the race team or the driver it would add one more complication to the race. The driver would have to worry about staying that much further away from the center line.

In an attempt to increase the performance by decreasing this loss an addition to the wing called an endplate can be used. The endplate, seen in Figure 2-13 and provided by [Katz, 1995], maintains a pressure difference between the upper and lower portion of the wing that not only improves the performance of the wing at the tip and thus improves the overall wing performance. Therefore there is an effective aspect ratio calculation that can be made that is presented by [Raymer, 1992] and is shown in equation (2-7).

$$AR_{effective} = AR \cdot \left(1 + 1.9 \cdot \frac{h}{b} \right) \quad (2-7)$$

Thus by increasing the height to span ratio of the endplate a greater effective aspect ratio can be obtained. The effects of changing the endplate design will be discussed later in another section.

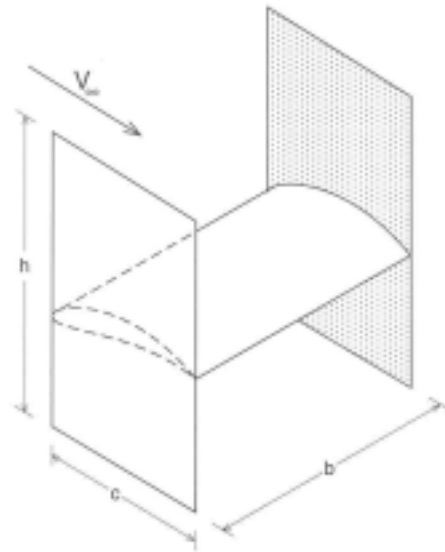


Figure 2-13: Endplate Size Dimensions

2.3.4 Endplate Design

As previously mention the effects of the endplates have proven to provide a more effective wing in the case of the low aspect ratio wing such as the rear wing of a dragster. The endplates on a typical dragster has been shaped based upon a "coolness" factor instead of on an aerodynamic performance factor. CFD analysis was performed on a three-element top-fuel dragster wing to study the aerodynamics involved. After careful analysis it was determined that due to the huge pressure difference between the top and bottom of the wing the flow was spilling over the top of the endplate and would disrupt the flow on the bottom surface of the wing. This reduced the amount of potential down force that the wing could generate. After determining this, adjustments were made to reduce this spillover effect and new endplates were designed and rerun in STARS. Vast improvements were made in the down force to drag ratio.

Although this improvement to the wing design was beneficial to the wings down force to drag ratio it has not been proven that the enormous amount of down force generated is necessary to the overall vehicle performance. This is where the study of the dynamics of the vehicle, which includes the aerodynamics, will be beneficial to the understanding of the overall effect of the dragster rear wing. It is also the intent of the author to show how much these improvements in wing design affects the performance of the vehicle such as the elapsed time and top speed for a quarter mile run.

CHAPTER 3

3. METHODOLOGY

This chapter is broken down into several sections that include the methodology behind the dragster model. The description of the STARS CFD code used and the implementation of a dragster wing into STARS. Also the setup to determine how the endplates effect the rear wing performance will be discussed followed by the development of a new type of dragster wing.

3.1 Modeling the Dragster

Several approaches were explored when trying to come up with a good dragster model. First the equations of motion for the dragster needed to be derived by studying all the forces acting on the vehicle. These included all of the lift and drag properties of the vehicle, the weight and weight transfer, the dimensions of certain parts of the dragster, and the performance of the engine and overall drive train. The lift and drag properties will be explored first building up to the full equations of motion.

3.1.1 Wheel Properties Used

The wheels were one of the more difficult components to get true data for because of the dynamics of these types of tires as discussed earlier. Lift and drag are generated by a number of different ways not just due to the flow around the tire but due to the rotation of the tires as well. In the previous chapter the aerodynamics of a rotating object was discussed. For the lift and drag characteristics of a rotating tire, research done by [Cogotti, 1983] will be used. Wind tunnel tests were done with the tires in direct contact with the balance and the wheel was powered.

C_d	0.579
C_l	0.18

Table 3-1: Lift and Drag Coefficients for the Tires from Cogotti's Research

Since the model was looking at general trends in aerodynamic effects on dragster performance a complicated tire model was not sought after. The data found on modeling tires was so detailed and was concerned with so many different aspects of the tires that it was decided that a simple tire model will be sufficient. Sure the tire can be analyzed and modeled in greater detail but the current research is concerned with finding general trends for the purpose of analyzing the rear wing and not concerned with advanced tire models.

3.1.2 Rear Wing Properties Used

The rear wing had two different sources of drag - induced drag and area drag. The first portion of drag, induced drag, is provided by the STARS code. This entails entering the dimensions of the object into a computer and using CFD to determine the aerodynamic properties of the object. STARS and implementing the wings into STARS is discussed later in this chapter.

The second type of drag used is area drag. The area drag is estimated by breaking the dragster wing into different components and estimating these different component drags.

The lift component for the wing is determined using STARS. The wetted area of the wing is provided by STARS and the plan form area of the wing is set by the NHRA rules.

3.1.3 Equations of Motion

After all the parameters are determined the next step is to determine the equations of motion for the dragster. The equations of motion are derived by summing the forces on the dragster. There are two regions that determine which equation is going to be used which can be seen in Figure 3-1. The first region is the traction limited acceleration portion of the track. This is where the acceleration power is so great that the wheels would slip if the throttle was held wide open. There is not enough down force to grip the wheels to the ground therefore the driver must ease on the throttle until they reach a point

at which this is no longer a scenario where the wheels can spin. This point is called the critical velocity of the vehicle.

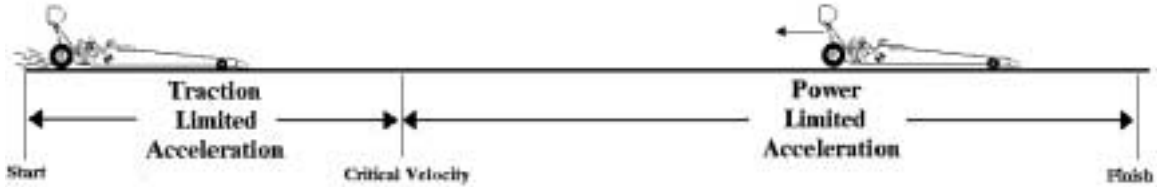


Figure 3-1: Dragster Run Schematic Showing Two Areas

This critical velocity point is the transition between the traction limited acceleration and the power limited acceleration. In the power limited acceleration region there is so much down force that the power used to accelerate the vehicle is not large enough to spin the wheels. In other words, the normal force from the wheels to the ground multiplied by the friction factor of the tires is greater than the force generated by the torque from the engine.

The two different equations of motion are shown below. The first equation of motion, Equation (3-1), is the traction limited acceleration which is valid below the critical velocity. After this critical velocity is reached the second equation of motion can be utilized which is the power limited acceleration shown in Equation (3-2).

For $\dot{x} < v_{cr}$

$$\ddot{x} + \left[\frac{1}{s_D} + \frac{\gamma\Lambda - \mu_{rr}}{s_L} \right] \dot{x}^2 - [\gamma\lambda - \mu_{rr}]g = 0 \quad (3-1)$$

For
 $\dot{x} > v_{cr}$

$$\ddot{x} - \frac{P}{m\dot{x}} + \left[\frac{1}{s_D} - \frac{\mu_{rr}}{s_L} \right] \dot{x}^2 + \mu_{rr}g = 0 \quad (3-2)$$

where

$$\lambda = \frac{a}{1 - h\gamma}$$

$$\Lambda = \frac{a - d}{1 - h\gamma}$$

The idea of this model is to use the lift and drag coefficient data along with the other vehicle properties such as the effective input engine power and vehicle dimensions to find the critical velocity of the vehicle. Since the critical speed is the speed at which the traction-limited driving force equals the power-limited driving force it can be found by equating (3-1) and. (3-2). The resulting equation is a cubic equation in critical speed where the critical speed is the smaller positive root of equation (3-3).

$$\dot{s}^3 - \frac{\lambda g}{\Lambda} s_L \dot{s} + \frac{P s_L}{m \Lambda \gamma} = 0 \quad (3-3)$$

where s_L is the aerodynamic radius and is given by

$$s_L = \frac{m}{\frac{1}{2} \rho A C_L}$$

After the critical velocity is found the corresponding position and time are calculated using the acceleration from equation (3-1) and simple dynamics. From this point the differential equation for velocity less than the critical velocity can be solved.

Using the critical velocity and position as inputs and the corresponding time as the starting time the second differential equation (3-2) for velocity greater than critical velocity can be solved.

Plotting can be done of position, velocity, and acceleration for the given vehicle data. In the results section this model will be implemented using dragster characteristics and this will be compared to position, velocity, and acceleration from an actual dragster run.

Once the model is established and validated it can be used in a number of ways. First of all trends can be found to see how aerodynamic characteristics will affect the performance of a dragster. Once this is known the second approach will be to use it to come up with a new wing design that will allow the performance of the dragster to improve either by elapsed time, by top speed, or maybe both.

3.2 Validation of the Dragster Model

In order to validate the model it was necessary to match the position, velocity, and acceleration data from an actual dragster run. Speed versus distance and position versus time data was found [Winn and Kohlman, 1999] and used for the validation. In order to get the speed versus time curves the position versus time data had to be differentiated. Double differentiation of the position versus time data was used to compare the acceleration data of the model.

The first validation plot is position versus time which is shown below in Figure 3-2. In this plot the two different regions of analysis, both below and above the critical

velocity, can be seen. The circles are the actual data and the lines are from the model. The model matches the actual data very well.

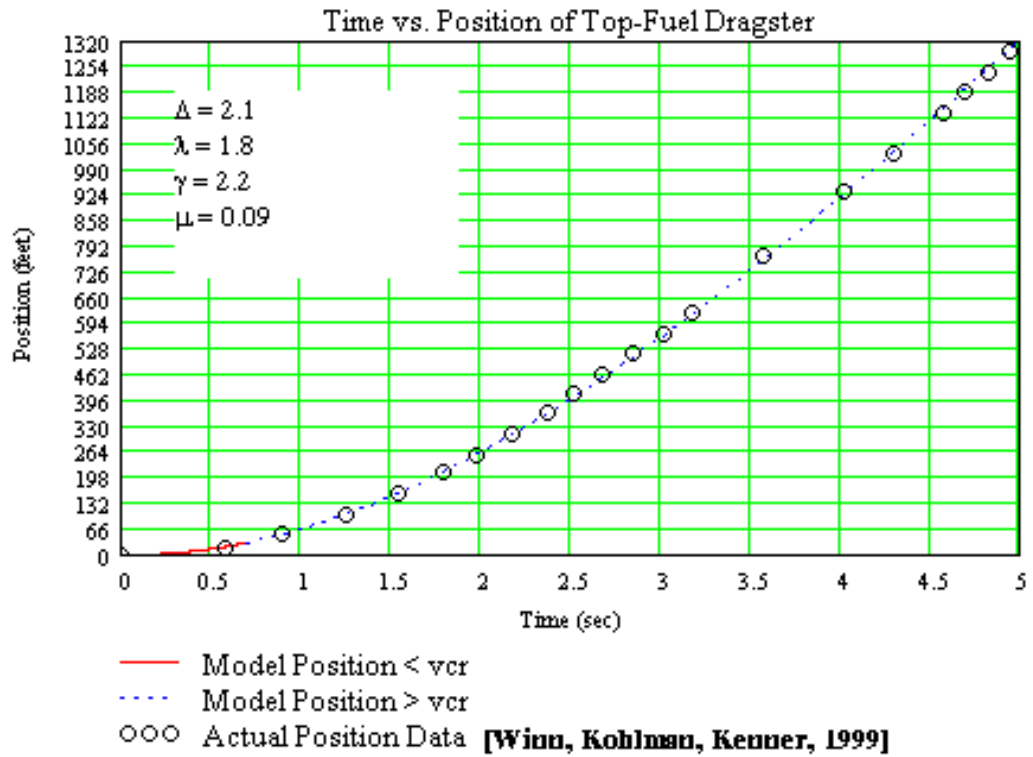


Figure 3-2: Validation of Position vs Time for a Top-Fuel Dragster (1/4 Mile)

In order to get speed versus time data the data from Figure 3-2 had to be differentiated. This data is represented by the circles in Figure 3-3, below, along with the model data depicted by the lines. Once again the model shows the regions where the two different equations of motion were used by plotting a solid line and a dashed line. The speed where these two lines meet is the critical velocity. This data matches up fairly well but a small error can be seen which is due to the differentiation of the data. Once differentiated the error that was there in the position versus time plot is enlarged.

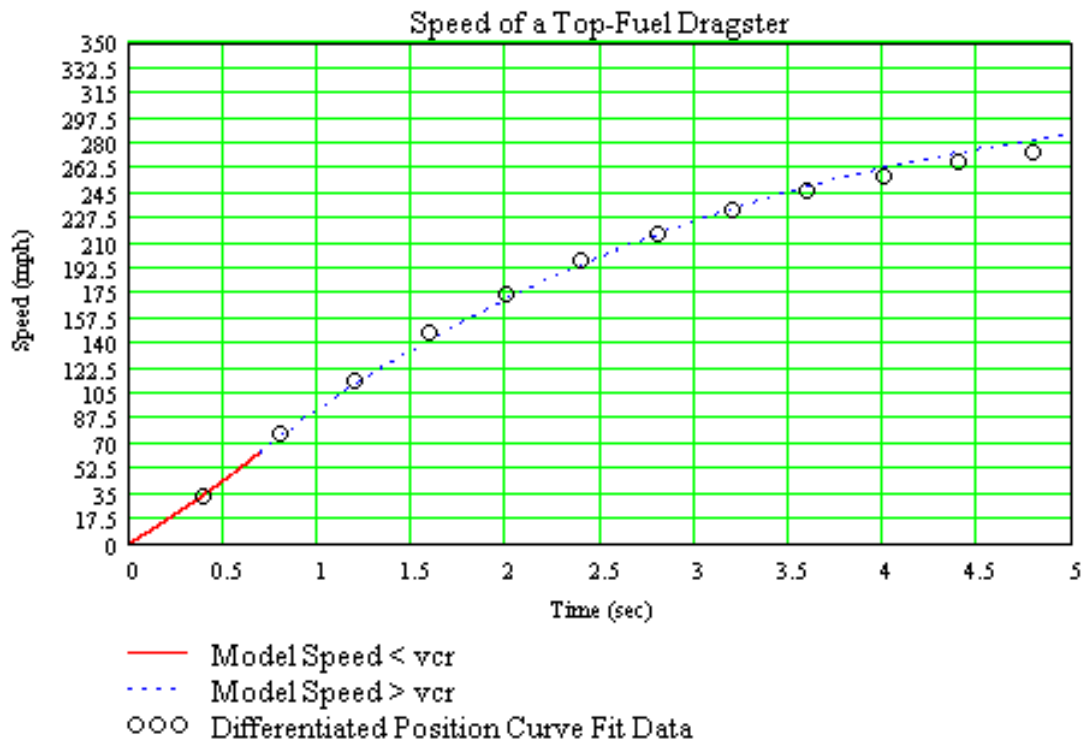


Figure 3-3: Validation of Speed vs Time for a Top-Fuel Dragster (1/4 Mile)

Acceleration data versus time was not readily available and therefore the position versus time data was double differentiated to get the actual data in Figure 3-4 below. The model still matches the trend of the actual data.

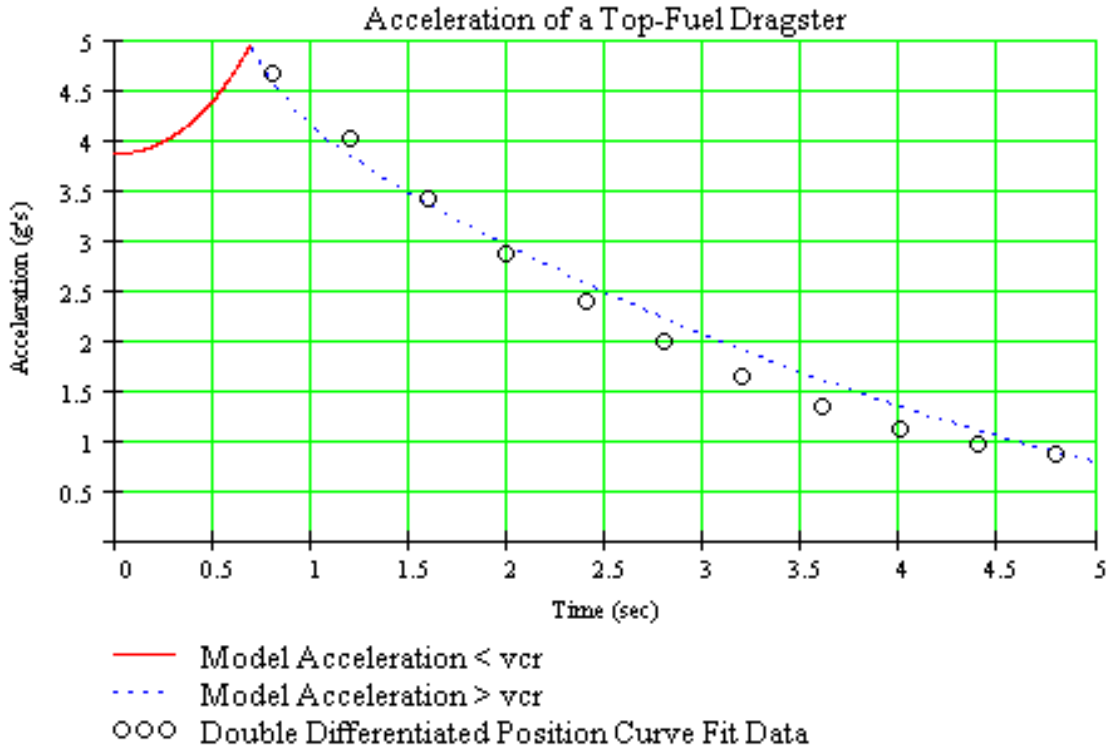


Figure 3-4: Validation of Acceleration vs Time for a Top-Fuel Dragster (1/4 Mile)

There was also actual speed versus position data that was used to validate the model. This data is shown in Figure 3-5 with the actual data depicted by circles. Once again the model matches the data very well.

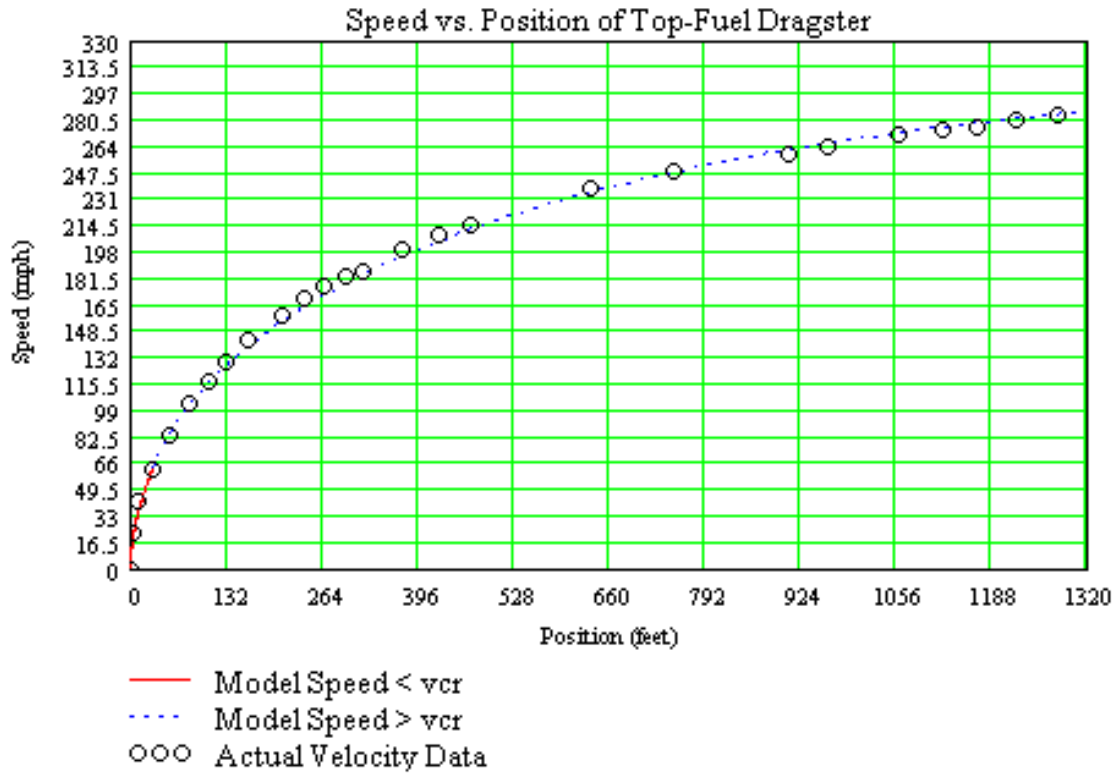


Figure 3-5: Validation of Speed vs Position for a Top-Fuel Dragster (1/4 Mile)

3.3 STARS CFD Module

One of the research tools used for this project is portion of a set of codes developed at NASA Dryden Flight Research Center known as STARS. STARS stands for Structural Analysis RoutineS, which is a highly integrated computer program for multidisciplinary analysis of flight vehicles including static and dynamic structural analysis, CFD, heat transfer, and aeroservoelasticity [Gupta, 1997]. For the current effort, only the CFD module of the code will be utilized for analyzing the aerodynamic characteristics of the wings.

The CFD module is an Euler based code that applies finite element CFD on an unstructured grid. The mesh generation uses the advancing front technique to generate the unstructured mesh, which had been proven to be effective in complex structures. When implementing the CFD module it is pertinent to follow a set of steps. This module consists of the following four major parts and should be run in the order that they are listed:

- SURFACE - generates a surface triangulation
- VOLUME - generates a three-dimensional computational domain
- SETBND - defines the boundary conditions in the domain
- EULER - steady or unsteady Euler flow solver

The easiest way to explain these different modules is to implement an actual problem into STARS step-by-step. The steps used and the data file structures and contents will be discussed in more detail in the next section. The problem that is being used is the rear dragster wing that has a style 3 endplate. The differences in the wings and endplates will be discussed later.

3.4 Implementing the Dragster Wing into STARS

As mentioned before there are four main modules or steps to follow, in order, before the user gets the solution. The first step in order to analyze the dragster wing in STARS is to setup the geometry data into the format so that STARS can read it. After the geometry is entered a mesh generation is enacted and a refinement in the density of the grid is performed until a suitable mesh is found. The last step before running the flow

solver is to specify the boundary conditions for the geometry and flow domain. The aforementioned modules are discussed in more detail in the following subsections.

3.4.1 Geometry Specifications in STARS

The geometry is made up of curves and surfaces that define the geometry of the dragster wing and the geometry of the flow domain. The geometry data file is a formatted data file that will be referred to as *case.sur*, where *case* can be any name that the user specifies. The dragster rear wing geometry file can be found in Appendix A-1.

The lines are oriented in a specific direction, defined in the direction of the arrows in Figure 3-6, according to the way STARS reads in the geometry. The lines are defined by means of an ordered set of points. The curve component is a continuous cubic spline, which is interpolated through these points. The model is a half span model with a symmetry plane. Using this symmetry plane cuts down on the computational time of the job without sacrificing the accuracy of the solution.

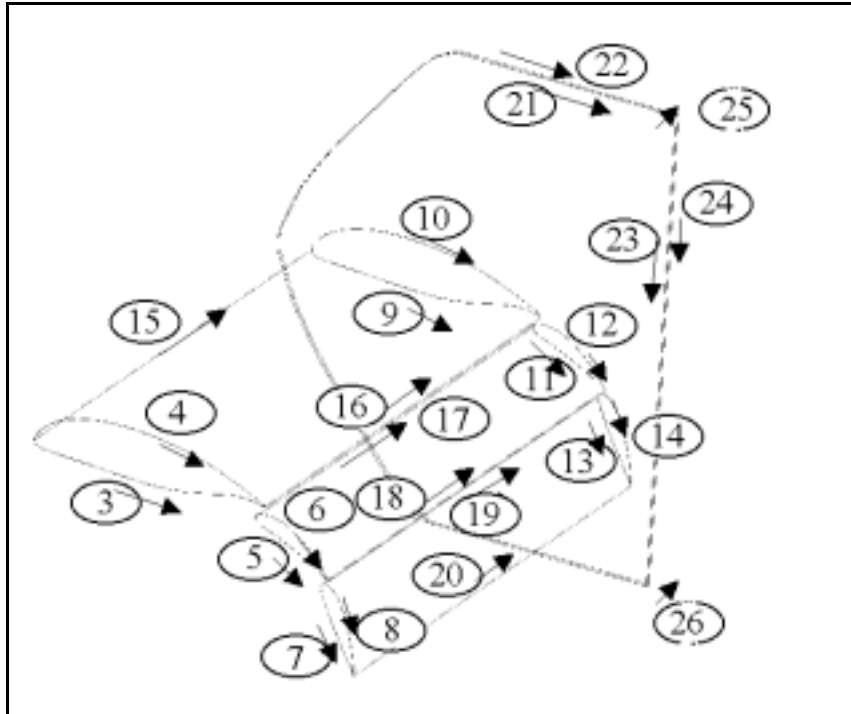


Figure 3-6: Wing Geometry Specification

It might be noticed that the numbering in Figure 3-6 starts out at three. The first two numbered lines define the flow domain that surrounds the geometry. The flow domain is a large hemisphere. There are ten chord lengths between the wing geometry and the outer surface of the hemisphere. The flat side of the hemisphere is the symmetry plane and is where the half span model of the rear dragster wing is attached.

After the curves are defined the next step in STARS is to specify the surfaces of the geometry. This is done by specifying each line that makes up the surface in a specific order. There are two possibilities that STARS will see depending on the order that the lines are specified - either a surface or a whole in a surface. When defining the surface the right hand rule must be used. The direction of the lines are important to this step and when using the right hand rule the fingers curl in the direction of the specified lines and

the thumb has to point into the flow. If the thumb points into the geometry then the surface was not specified correctly.

When this is completed the wing looks like Figure 3-7. For the dragster wing that was analyzed, the largest and main element is based upon a set of data points. The chord length of this element is 14.1 inches long. This main element is set at zero angle of attack. The second element is an NACA 9400 type airfoil with a chord length of 5.25 inches. It is set at a 28-degree angle of attack with respect to the chord line of the main element. The third and final element is an NACA 4300 type airfoil with a chord length of 5.25 inches. It is set at a 65-degree angle of attack with respect to the main element chord line.

The configuration of the wing analyzed was 0° - 28° - 65° . The configuration, 0° - 28° - 65° , refers to the angle of attack of each of the three individual elements. The wing was adjustable to different configurations but this configuration was the one most commonly used and therefore was the configuration that was used in the analysis.

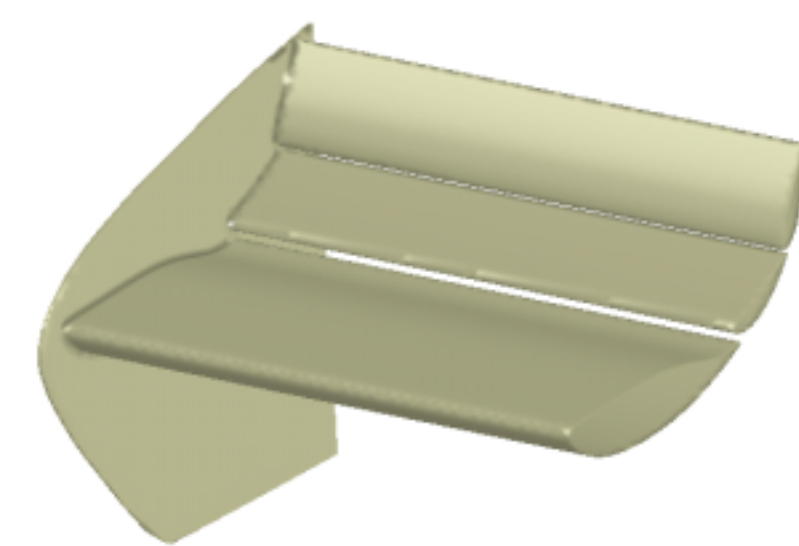


Figure 3-7: Rendered View of a Half-Span model with a Style 3 Endplate

3.4.2 Grid Specifications in STARS

Once the geometry is defined a mesh density must be specified in the (.bac) file, which is listed in Appendix A-2. The mesh density must be small enough on the geometry in order for the solution to be accurate. The half model of the wing can be seen in Figure 3-8. The symmetry plane, where the half span model is attached, has a larger triangular mesh than the wing surface. This allows the solution to converge faster because the amount of calculations that the code has to go through is greatly reduced.

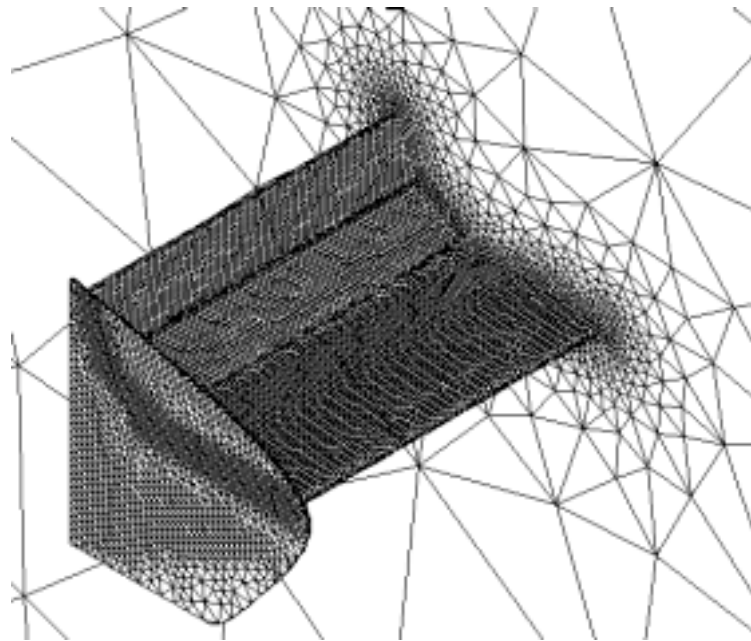


Figure 3-8: Half Model of Dragster Rear Wing Mesh Density

The density of the mesh can be specified in a number of ways. In the (.bac) file the user can specify any number of sources in order to get the specified mesh density. The user can choose from three types of sources being a point source, a line source, or a triangle source.

A point source allows for a sphere like mesh density that can change the size of mesh to start out with, how large of a sphere, and how far out until the mesh size is double of the original starting size. Point sources can be used on the front of an airplane body, such as the nose of the X-29 experimental aircraft, in order to make the geometry mesh tighter.

The line source differs from a point source in that it is cylinder like and there is a specified length instead of a sphere. The line sources are typically used in the leading and trailing edges of a wing because of the sharp transition in geometry.

The triangle source is a mesh density in the shape of a three dimensional triangle. They can be used in a number of ways for a number of different situations. In the dragster wing case two triangle sources are used per wing in a way as to make a rectangle running thru the chord of the wing to refine the mesh on the surface of the wings. They are also used on the endplates since the endplate is so thin it allowed for a refined mesh so that the solution around the endplate is accurate.

3.4.2.1 SURFACE Module

After generating the geometry data file and the background mesh data file the first step is to run the SURFACE module. The SURFACE module generates a couple of data files. The first is a (.RST) file, where the .RST is just the suffix that is added to the problem name, e.g. *fin.RST* or *wing.RST*. This file is an auxiliary file in which all of the information about the generation processed is dumped. This allows the user to re-start the SURFACE module if the program is stopped before completion.

The second file generated is a (.*fro*) file that stores the information about the triangulation of the surface in the three-dimensional and the parametric space. This file is used for input to the VOLUME and SETBND modules, which will be discussed later. The (.*fro*) file is not listed in the appendix because it takes up 1060 pages of numbers in 10 point font and the information is not pertinent to developing a model in STARS.

3.4.2.2 VOLUME Module

The VOLUME module only requires two files to run - the background mesh file (.*bac*) and the surface triangulation file (.*fro*), that was generated from the SURFACE module. The Volume module outputs a restart file (.*RVT*) and a tetrahedral mesh file (.*gri*). The restart file (.*RVT*) can be read by the VOLUME module in case the program was interrupted or unable to finish. It is similar to the restart file of the SURFACE module. The (.*gri*) file holds the description of the tetrahedral mesh. This is one of the input files to the SETBND module. The (.*gri*) file is extremely large, over 7200 pages of numbers in 10 point font, and therefore is not listed in the appendix.

3.4.3 Boundary Condition Specification in STARS

After running the SURFACE and VOLUME modules, it is now time to look at the boundary conditions. The boundary condition specifications, (.*bco*) in STARS, is pretty straightforward and can be found in Appendix A-3. The user is required to flag the curve segments and surface regions in a formatted data form. The surface region flags define the type of boundary conditions to be applied to a certain surface and are defined in Table

3-2. If the surface was a symmetry plane then that surface would be flagged with a 2 as indicated in the table.

Flag	Surface Type
1	Wall
2	Symmetry
3-4	Far Field
5-6	Engine Inlet
7-8	Engine Outlet

Table 3-2: Surface Region Flags

The user must also specify the curve segment flags. These identify points in the triangulation, which lie on the surface regions, where the normal to the surface is not defined. These are singular points in the geometry and at these points there is no wall boundary corrections applied. Such points include the trailing edges of wings or any similar geometry. The flags for the curve segments can be found in Table 3-3.

Flag	Singularity
0	No Singularity
1	All are Singular
2	Singular Point at First and Last
3	Singular Point at First Only
4	Singular Point at Last Only

Table 3-3: Curve Segment Flags

3.4.3.1 SETBND Module

After the boundary conditions are specified, the third module can be run. This is the SETBND module, which is the flow solver preprocessor. It transforms the element-based description of the tetrahedral mesh into the side-based data structure employed by the EULER module. The SETBND module requires the surface triangulation file (*.fro*), the tetrahedral mesh file (*.gri*), and the boundary conditions file (*.bco*).

The output to the SETBND module is a file that contains the combination of both the surface triangulation file (*.fro*) and the tetrahedral mesh file (*.gri*) into a single file referred to as the (*.plt*) file. This file can then be used for another module that is sometimes used, which is the REMESH module. The (*.plt*) file is a binary file and is not listed in the appendix.

The REMESH file is not discussed as one of the main modules because it is not necessary to run this module in order to obtain a solution. The REMESH module looks at the concentration of flow activity and can refine the mesh density in this area in order to acquire a more accurate solution.

The other output file from the SETBND module is the solver data file (*.geo*). This file contains the side-based data structure representing the computational mesh and all the information required by the flow solver. The (*.geo*) file is another large data file that is binary and is not listed in the appendix.

3.4.4 Solver Control Specifications

This solver control file (*.cons*) contains a set of flow conditions and algorithmic constants for the Euler flow solver and a sample can be found in Appendix A-4. The flow solver contains built-in defaults that can be overwritten by the user if another value is specified in the solver control file. This is where the the free-stream Mach number, the angle of attack, side slip angle, as well as fluid properties must be specified. Other algorithmic properties include the number of timesteps, dissipation coefficients, CFL number, and residual smoothing parameters to name a few.

3.4.4.1 EULER Module

Now that the control specification file is generated and all three previous modules had be run then the last module can be started. The solver module or the EULER module is the unstructured Euler flow solver which performs numerical computation of the steady-state solutions of the transient form of the Euler equations of compressible inviscid flow.

The SOLVE module needs both the solver data file (*.geo*) and the solver control file (*.cons*) in order to run. The module outputs nodal values of flow variables (density, velocity, and pressure) in a (*.unk*) file. The EULER module also outputs another file that contains the history of the convergence of the L-2 norm of the residuals of the conserved variables in a (*.rsd*) file. This can be used as a convergence criterion that will be discussed in a later chapter. Once the EULER module has run and the solution has converged, the CFD portion of the STARS code has been completed.

The final step would be to view the solution with a postprocessor where a variation of figures and graphs both two- and three-dimensional can be generated. Several of these figures are shown in the results section of this paper.

3.5 The Effects that Endplates have on Rear Wing Performance

CFD was used to analyze the flow over an existing top-fuel dragster wing both with and without an endplate. This wing geometry, that was discussed in the previous section was used for each of the three test cases analyzed. Therefore, the three wings vary only in the endplate design as can be seen in Figure 3-9 below. The first case was to study of the dragster wing without an endplate. The second case used one endplate design that was currently being used on a dragster wing built by Advanced Racing Composites (ARC). This will be referred to as a style 3 endplate. The third and final wing used an endplate that tried to improve the performance characteristics of the wing by changing just the geometry of the endplate. This endplate is referred to as the new endplate.



Figure 3-9: Three Different Endplate Geometry Analyzed

The CFD analysis was run to depict a race at the top design speed at the highest racing altitude. This meant using a Mach number of 0.434, which corresponded to a design velocity of 325 mph at an altitude of 5500 feet (Denver, CO).

The CFD solver starts out at the given free-stream Mach number and after converging gives a resulting flow-field on the wing. Therefore, it is necessary to determine when the solution converges. STARS can output flow parameter residuals (*.rsd*) file and maximum Mach numbers for every time step. The steady-state solution convergence criteria for maximum Mach number was used instead of the residuals of flow parameters. It was determined that the maximum Mach number is a much better convergence indicator than the flow parameter residuals [Stephens, 1998].

Since the input files for the STARS modules can be long and detailed, when changing geometry, a spreadsheet was used to create the geometry and background mesh data files. The spreadsheet was set up to allow many different parameters to be changed. Changes could be made to the span of the wing, the angle of attack of each of the airfoils, the gap spacing in between each of the wing elements, the position of the wing inside the flow domain, as well as the type of endplate to be use. This spread sheet saved a lot of time in the generation of the input data files.

3.6 Box Wing Design

After analyzing the dragster model and looking at the trends to improve performance some thought went into a different rear wing design. A simpler design that was made of less components would be a plus but most important improved dragster performance was sought.

Previous work had been done with a high-lift low Reynolds number airfoil that showed some potential for this type of project. The airfoil is a Selig 1223 that was found at the University of Illinois at Urbana-Champaign airfoil data website. It was decided that the approach would be to use this airfoil with a boxwing type design instead of the typical three-element design that is seen today on top-fuel dragsters. The boxwing type design will be talked about later on in this section.

The Selig 1223 airfoil, as seen in Figure 3-10, has a large coefficient of lift. This airfoil was designed to be a heavy lifting airfoil. The airfoil data points can be found in Appendix C-1.

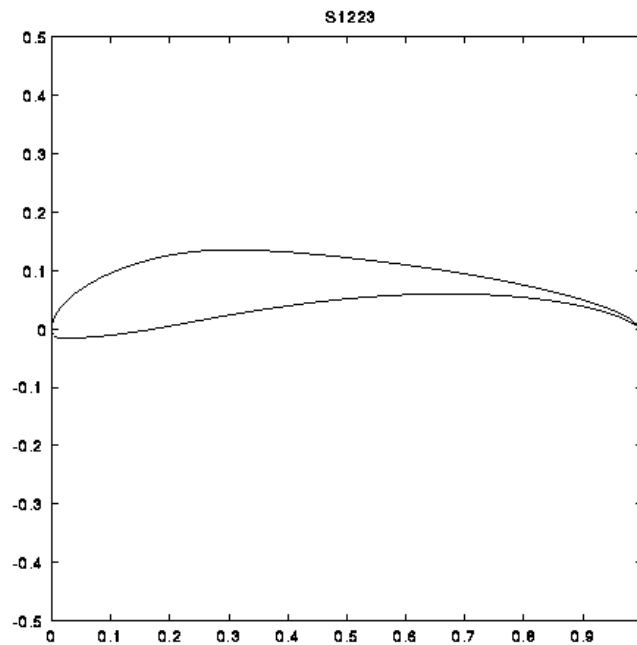


Figure 3-10: Selig 1223 Airfoil

This airfoil has a very thin trailing edge as can be seen in the figure above. This requires some knowledge of manufacturing as well as the materials that will be used to built the wing. With materials like carbon fiber, which is one of the currently used

materials for dragster wings, this airfoil is not a problem. Because the wing's thin trailing edge you need a material that is strong so that it would not break off. Carbon fiber could be used to make this trailing edge strong enough.

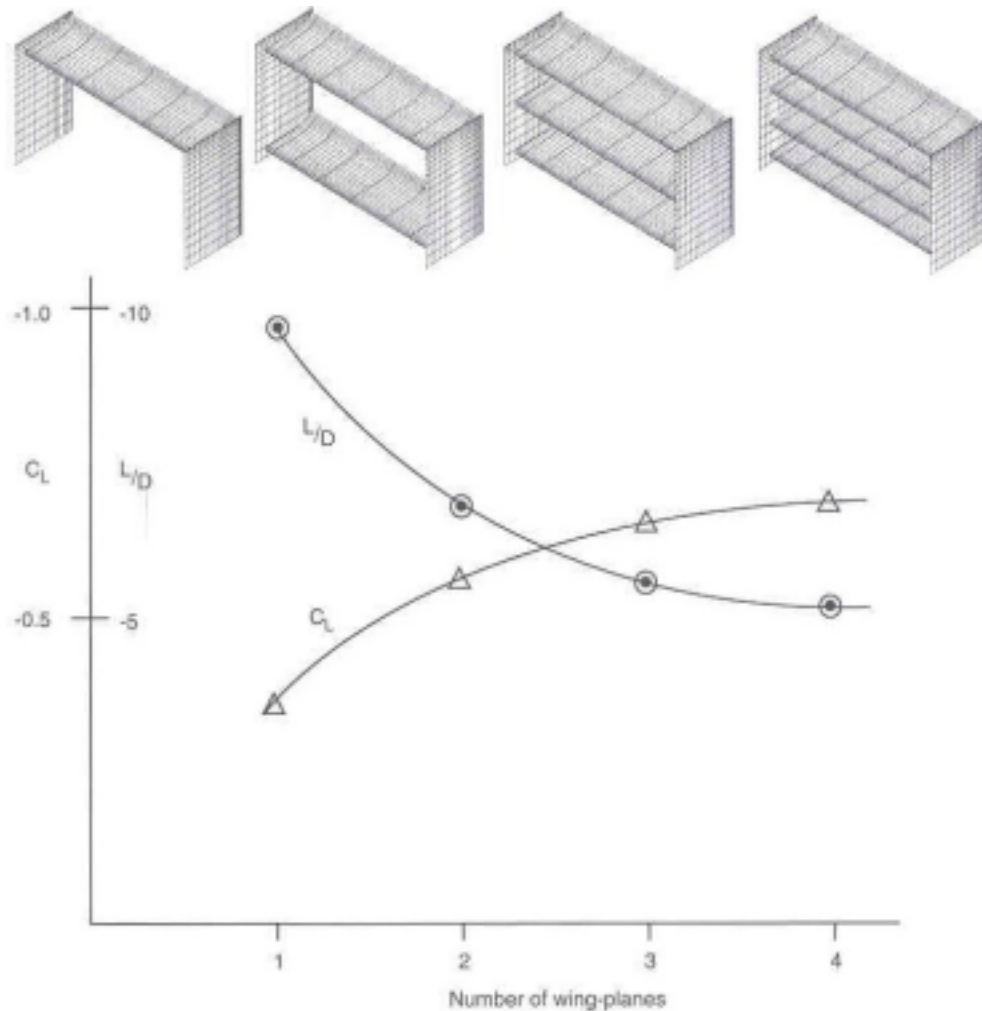


Figure 3-11: Effect of the Number of Elements on an F-1 Type Wing [Katz, 1995]

Next the effect of the wing was considered using simple back of the envelope calculations. It was thought that a single wing with the Selig 1223 airfoil did not produce adequate lift. Therefore a boxwing design seemed more appropriate. Looking at Figure 3-11, provided by [Katz, 1995], it can be shown that the number of elements should not

exceed 2. The figure shows that as the number of elements increase so does the coefficient of lift or down force. The other plot in the figure is the ratio of down force to drag and as the number of elements increases this down force to drag ratio decreases. This means that with more elements the wing is producing more drag. These two curves meet in between two and three elements showing that, for this application where drag matters, two elements is ideal.

The final wing design consisted of one chord length separation between the wings both horizontally and vertically. When looking at Figure 3-12 the vertical separation refers to distance h where the wing would be moved one chord length. The horizontal separation refers to the distance x and is one chord length as well.

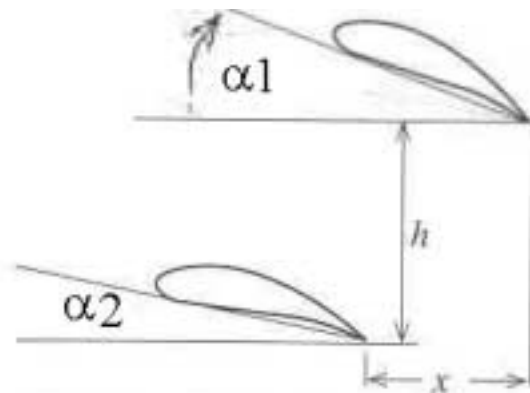


Figure 3-12: Decalage Angle

The two wings are identical in chord and span which would cut down building time because only one type of wing would be needed. This would eliminate the production of three different types of wings as is the case for the currently used multi-element wings. The wings are set at a different angle of attack which changes the performance

characteristics of the wings. The difference in the angle of attack between the top wing and the bottom wing is known as decalage angle. When looking at Figure 3-12 above, the decalage angle will be the difference between α_1 and α_2 . If the bottom airfoil was set at 5° angle of attack and the top airfoil was set at 15° then the decalage angle would be the difference in the two or 10° .

A study was done to look at the effect that decalage angle has on the performance characteristics of the wing. Therefore three decalage angles were tested computationally, using STARS, and the angles were set at 0° , 8° , and 12° . Further computation was done by varying the overall angle of attack of the whole boxwing starting at 0° and ranging up to, in some instances, 25° . A half model of the boxwing design is pictured below in Figure 3-13.

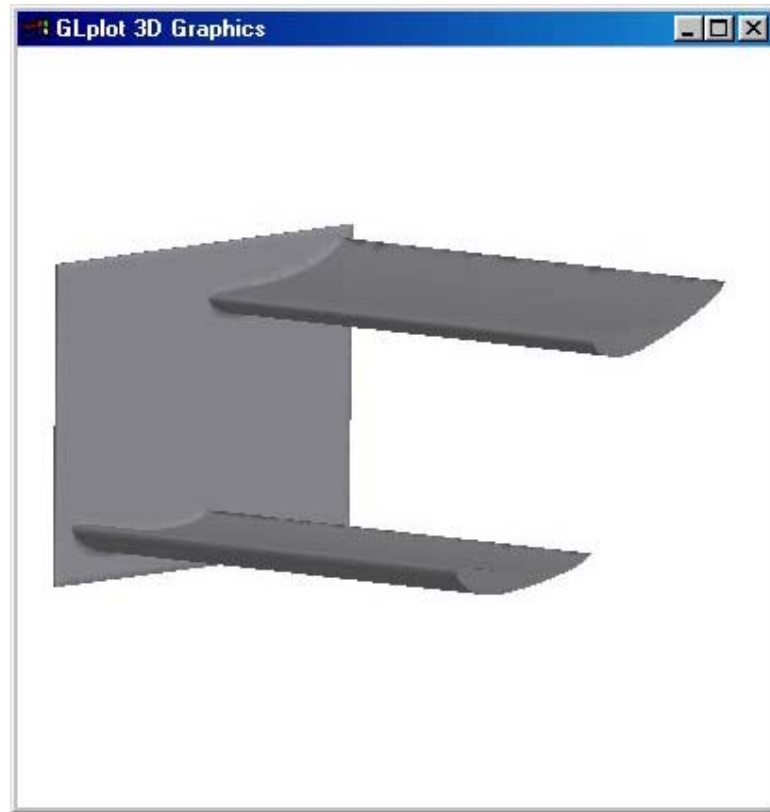


Figure 3-13: Rendered View of half model Boxwing with a 12° Decalage Angle

No studies were done on the shape of the boxwing endplates. Therefore a simple square endplate was used for the computational analysis. This will be talked about further in the results section.

Since a lot of variations to the wing were going to be performed it was beneficial to make a spreadsheet that would produce the STARS input data file after the wing parameters were changed. The spreadsheet allowed for each angle of attack of the two wings, the endplate dimensions both vertically and horizontally, the chord of the airfoil, the length of the wing, as well as the position of the wing in the flow domain all to be changed. This saved a lot of time between data runs.

CHAPTER 4

4. RESULTS

This chapter is broken down into several sections including the results of the endplate effects on the performance characteristics of the wing, the gap spacing comparisons for a multi-element wing, and angle of attack comparisons between wings. The results of the boxwing design will also be addressed. Finally the dynamic model comparisons of a dragster run will be shown and discussed. This section will look at various wings used and show how each affected the performance of the dragster.

4.1 Effects of Endplate on Three-Element Dragster Wings

The effects of endplates section explores several ways that endplates can effect wing performance by studying a three-element wing without an endplate as well as two different endplate designs. This section is broken down into several subsections including pressure contours, cross flow velocities, velocities at the tip of the wings, down force to drag ratio, and Mach number and coefficient of pressure distribution over the wing.

4.1.1 Pressure Contours

When looking at the three-dimensional pressure contours generated by STARS the effects of the endplates can be easily seen. The wing without the endplate, Figure 4-1, shows how three-dimensional the airflow can be without the endplate. In these pressure plots the tip of the wing is the closest to the reader and the symmetry plane is the farthest. On the main element the suction pressure along the tip of the wing is dramatically decreased due to the spillover caused by the large pressure gradient present towards the tip of the wing. This can be seen by looking at the various color differences that are represented in the pressure bar on the right hand side of the figure.

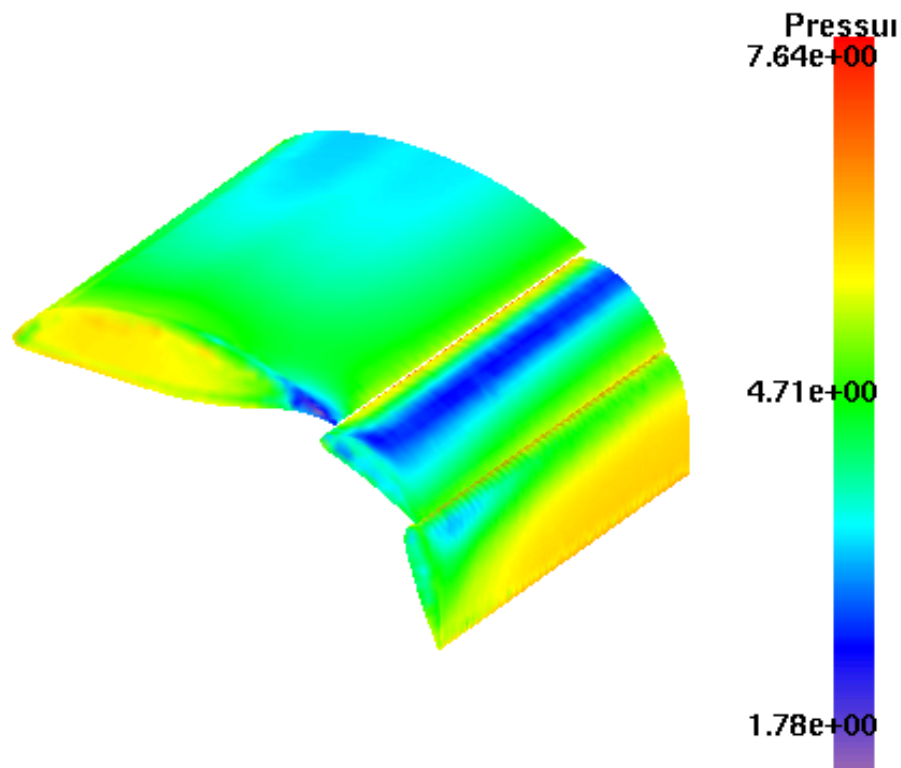


Figure 4-1: Pressure Contours of the Wing without an Endplate

This effect is not only visible on the main element but can also be seen on the second and third elements as well. In Figure 4-1, only towards the tip of the wing the pressure contours tend to dissipate as compared to the pressure contour at the mid-span of the model. The wings with the endplates have a more uniformly distributed suction pressure strip along the entire length of the second element.

As for the last element on the three-element wing, the advantage of the endplate can once again be easily seen. The non-uniform pressure gradient appears to be in the shape of a quarter of an ellipse. Towards the tip of the third element in Figure 4-1, the wing without the endplate, a very distinct non-uniform pressure gradient can be seen. Although the pressure on wings with the endplates is not entirely uniform it is relatively more so than the wing without the endplate. This does not appear on the two wings with endplates as seen in Figure 4-2 with the style 3 endplate and Figure 4-3 with the new endplate design. For the two figures with endplates, the edge that appears closest to the reader is where the endplate is located. However, the endplate has been removed during the post-process plotting so that the pressure on the elements at the tip of the wing can be viewed.

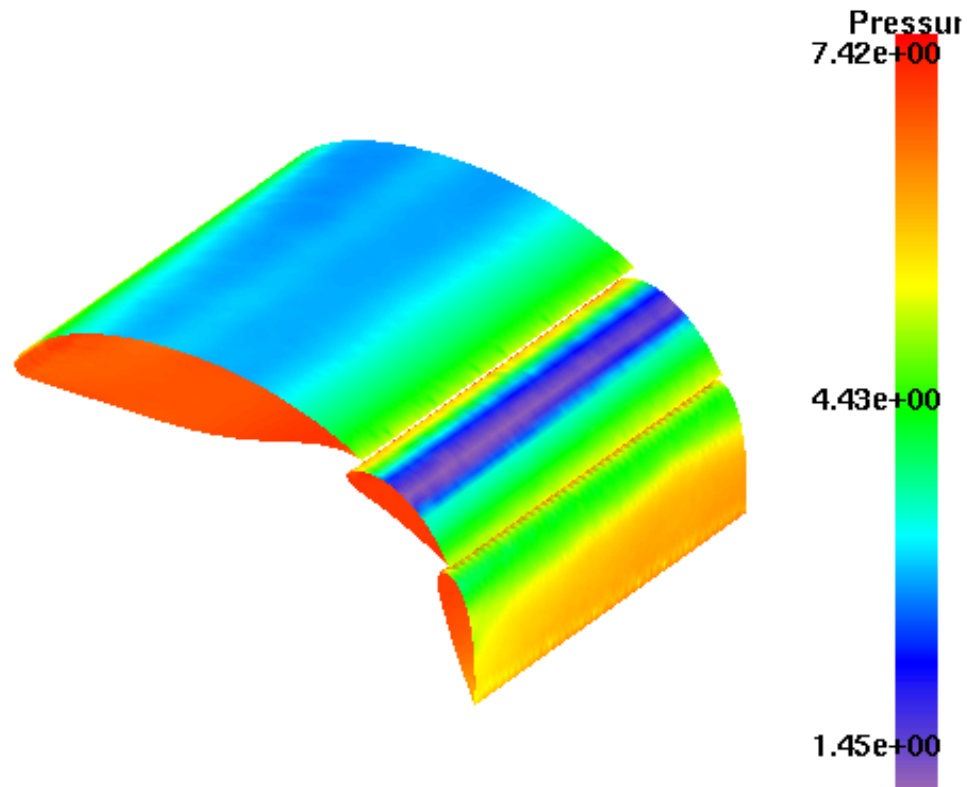


Figure 4-2: Pressure Contour of Wing with Style 3 Endplate

On the wing with the style 3 endplate, Figure 4-2, the main element has evenly distributed pressure sections as we move from the leading edge of the main element and move back. The second element has a very uniform pressure distribution which is recognized when comparing the tip sections of Figure 4-1 and Figure 4-2. It is not until the third element that we see the tip pressure start to dissipate. The flow here is extremely high, over Mach 1, and the angle of this third element is at 65° to the free stream. When the conditions are remembered it is hard to believe that the pressure distribution at this section of the wing is as uniform as it appears.

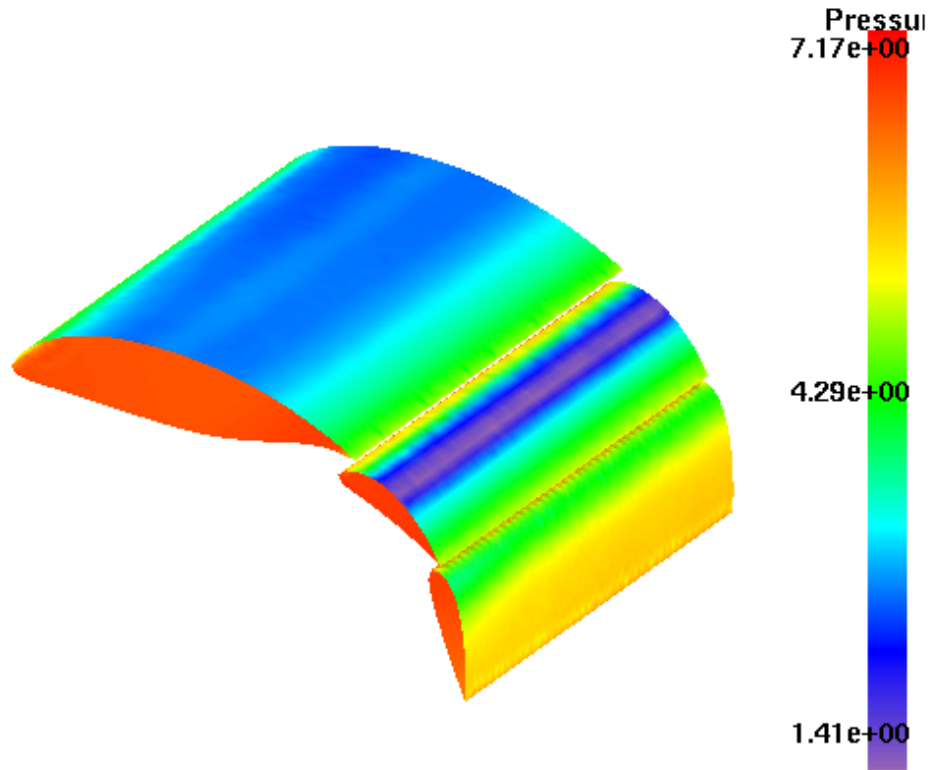


Figure 4-3: Pressure Contour of Wing with New Style Endplate

The first and second elements of the wing with the new style of endplate in Figure 4-3 appear as uniform as they were in Figure 4-2 with the style 3 endplate. The third element for the new endplate design however appears to be more uniform than that of the third element of the style 3 endplate. This larger new endplate controls the flow better by reducing this spillover effect.

From another perspective, Figure 4-4 shows a side view of the endplate with the symmetry plane in the background. This then can be somewhat viewed as the gradient pressure that the endplate sees and thus shows once again why the airflow favors to spillover the top edge of the endplate. The bottom does not seem to be as great of a pressure gradient and thus only moderate spillover affects occur. This figure helped in

deciding how the new endplate geometry should be manipulated in order to reduce this pressure gradient.

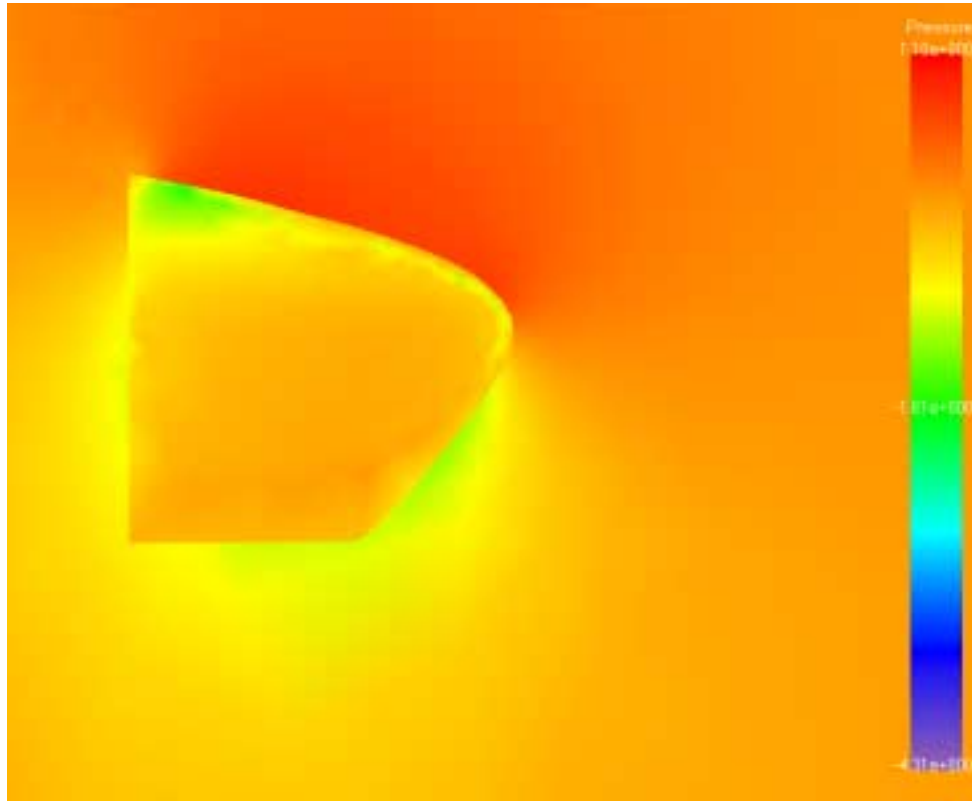


Figure 4-4: Pressure Gradient for Style 3 Endplate

The figure above was produced during the initial studies of the flow around the three-element wing with the style 3 endplate and led into an investigation of the effects that endplates have on wing performance as well as my development of the new endplate design.

It can be seen the high-pressure on top, represented by the darker area in the figure, extends way above the wing as well as above the top of the endplate. Ideally, from the pressure gradient standpoint, it would be best to extend the endplate up until the pressure

in the far field is the same as the pressure on the endplate. There are two reasons why this is not done. First there is a point by which the overall drag will outweigh the benefit of extending the endplate. The second factor could be to make the structural strong enough without bearing a lot of weight on the vehicle. I admit that these are only a few of the many considerations that must be addressed for a real design but I was just concerned with minor changes to endplate geometry for improvement.

A simple change in the endplate geometry was decided so the top of the endplate is just the mirror image of the bottom. This change implemented the two changes that I felt were necessary to improve the performance characteristics of the dragster wing. First of all the overall height of the endplate above the wing was increased. Second there was an increase in height at an earlier stage in the flow.

4.1.2 Cross-Flow Velocity

A different view point can be looked at that shows how the flow over this three-element wing is effected by endplate geometry. This different perspective is cross flow velocity cuts that show the flow on a cut plane at user specified locations on the wing. Cross-flow velocity cuts were taken at three different positions parallel to the flow velocity axis.

The first position was at a distance 7 inches back from the leading edge of the main airfoil as depicted in the far left picture of Figure 4-5. This was chosen to look at early spill over effects generated by the main element. The second cross-flow cut was at 14 inches back from the leading edge of the main element and can be seen in Figure 4-5 as well. This position cuts through the trailing edge of the main element and the leading

edge of the second element. The other picture in Figure 4-5 is the last cross-flow cut was located 20 inches back from the main element's leading edge. This is at the trailing edge of the last element where the most severe circulation can be seen. Each of these cut planes will be looked at separately although they each show similar results.

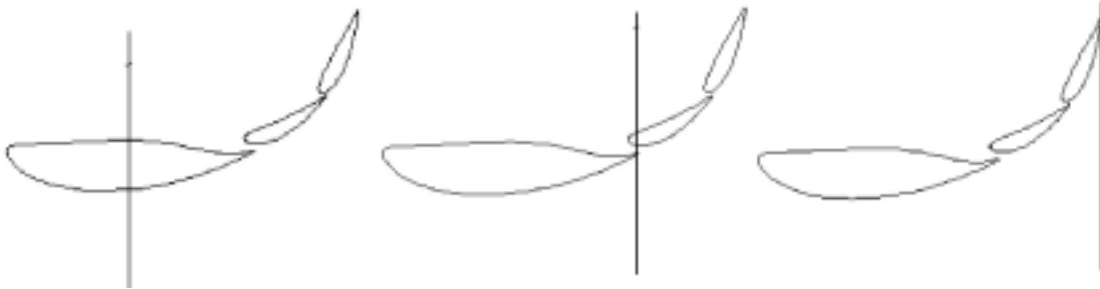


Figure 4-5: Cross Flow Velocity Cuts Represented by Vertical Lines

For the first cut plane at 7 inches back from the leading edge of the main element the spillover effect is minimal but the effects are very distinct. In Figure 4-6, without the endplate present, a circulation can be seen coming from the top of the wing around the tips of the wing to the suction side as discussed earlier. The figure shows a number of different size and oriented lines. The length of the line is proportional to the speed of the air around the dragster wing. The longer the line the faster the air is traveling. The orientation of the line is the direction of the air at that instance for the steady-state solution. The mid span of the half model is at the readers left hand side of these figures and the tip of the wing is on the right hand side. There is no endplate present to deflect this flow from circulating to the lower pressure side of the wing. From Figure 4-1 the three dimensional effects of can be seen from a different perspective from that discussed and shown earlier.

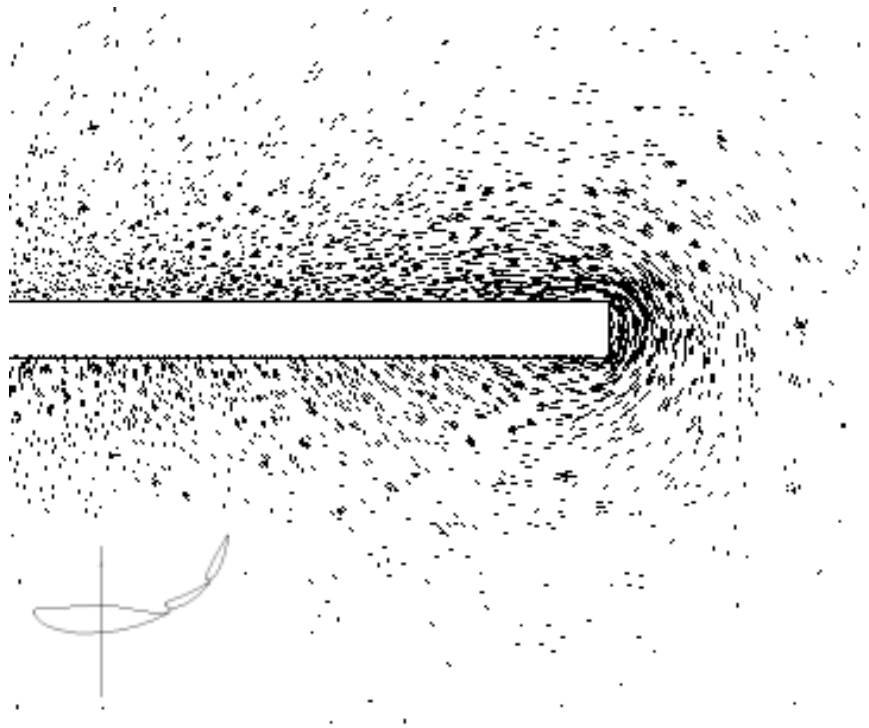


Figure 4-6: Cross-Flow Velocity 7 in. back from L.E. w/o an Endplate

If we now look at the second cross-flow plane cut, 14 inches back from the leading edge of the main element, the circulation strength is increased. Figure 4-7 shows the increased velocity of the flow coming around the tip of the wing.

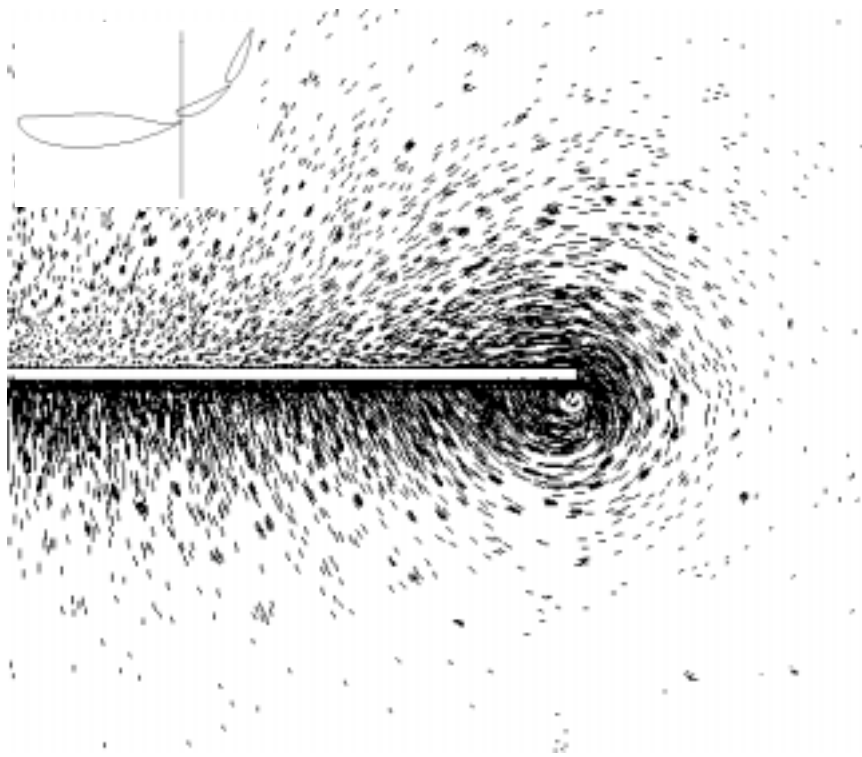


Figure 4-7: Cross-Flow Velocity 14 in. back from L.E. w/o an Endplate

The same effects can once again be seen in the cross-flow velocity plane cut towards the trailing edge of the third element.

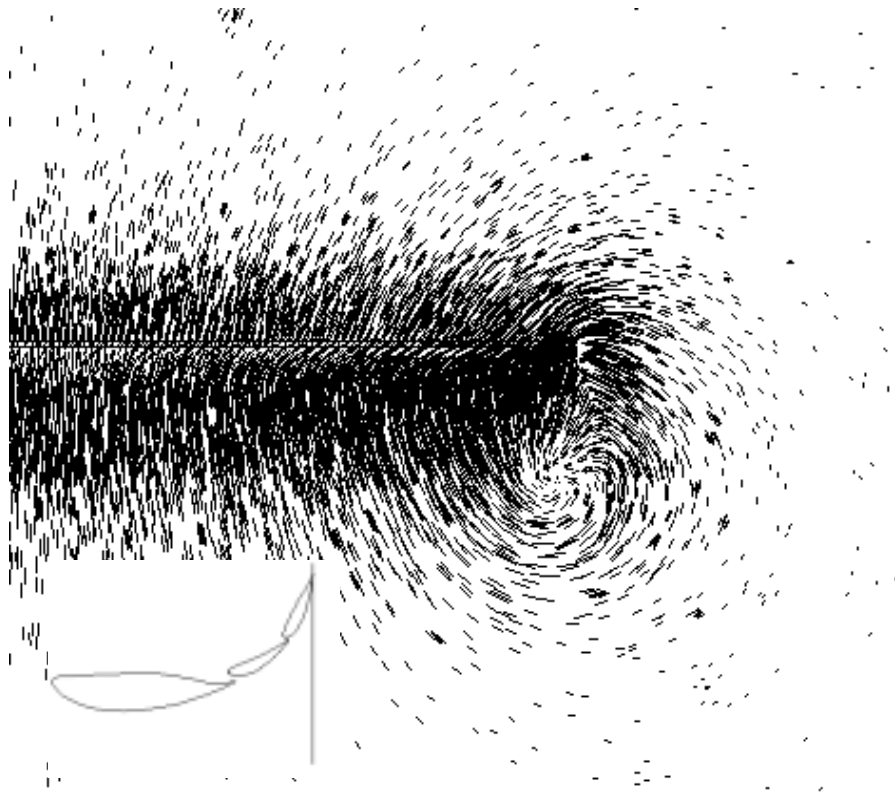


Figure 4-8: Cross-Flow Velocity 20 in. back from L.E. w/o an Endplate

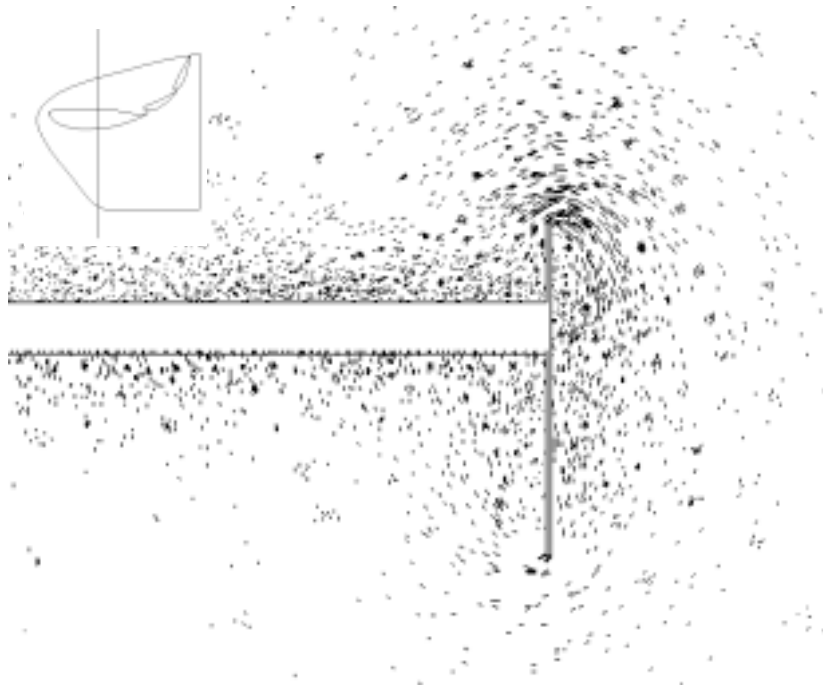


Figure 4-9: Cross-Flow Velocity 7 in. back from L.E. with Style 3 Endplate

Comparing that to the wing with the style 3 endplate, Figure 4-9, it can be seen that the airflow hits the inside of the endplate and is forced to flow up and over the endplate. At the top of the endplate the circulation is still present but it is less noticeable and certainly less severe. This circulation is disruptive to the suction side of the wing causing a decrease in suction as was shown in Figure 4-1 where the pressure is very noticeably changed. This is why endplates are so important to a low aspect ratio wing such as this rear dragster wing. Now since this circulation arose this early on in the flow it was decided that the height of the new endplate design needed to be increased at this location. This was also seen previously from the pressure gradient in Figure 4-4.

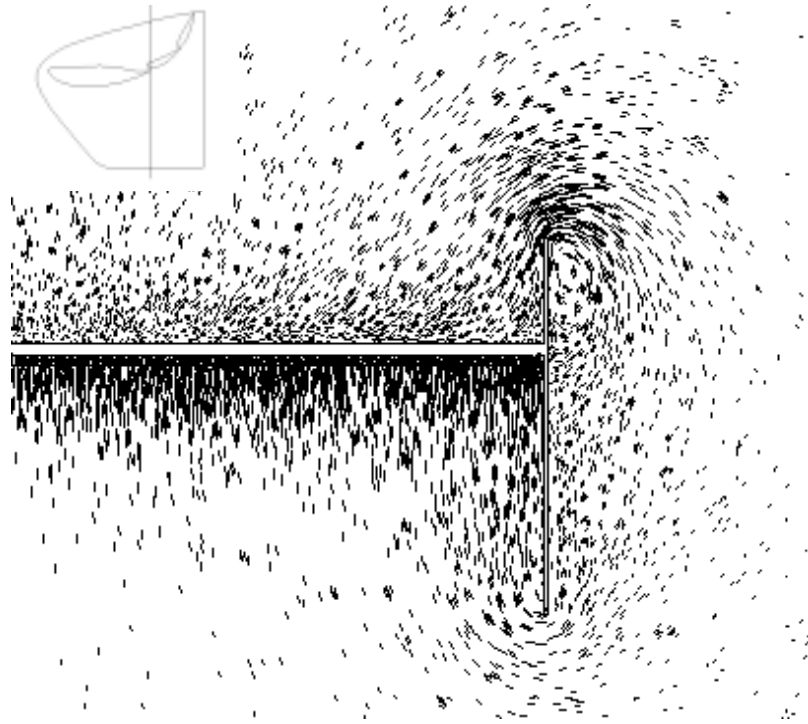


Figure 4-10: Cross-Flow Velocity 14 in. back from L.E. with Style 3 Endplate

The spillover effects are increased as seen in Figure 4-10. Again the high pressure gradients that are present matched with the shortness of the endplate above the airfoil section allow this flow to spill over and disrupt the flow.

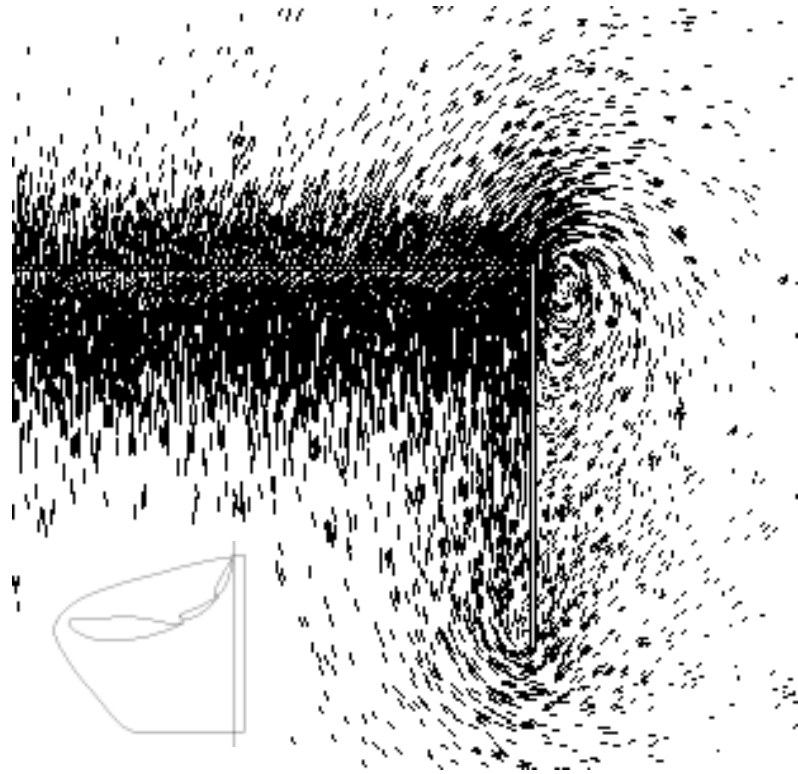


Figure 4-11: Cross-Flow Velocity 20 in. back from L.E. with Style 3 Endplate

The style 3 endplate has hardly any height above the trailing edge of the third element so the effects of the endplate are very minimal. The lower portion of the style 3 endplate is beneficial to reducing the circulation around the suction side of the wing.

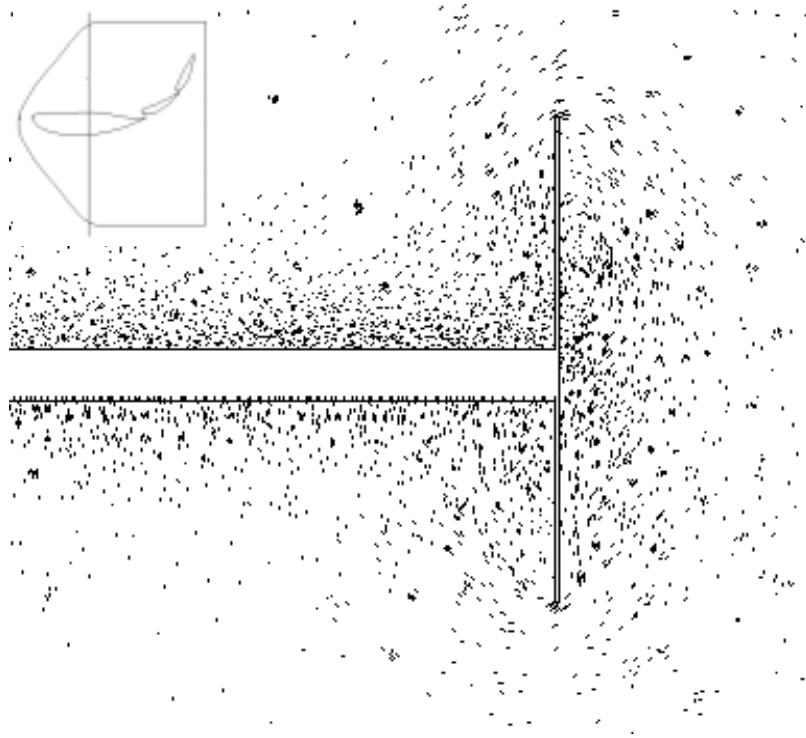


Figure 4-12: Cross-Flow Velocity 7 in. back from L.E. with New Endplate

Now looking at the new endplate design in Figure 4-13 the effects of the increased height still shows an improvement in the reduction of the spillover effect. The airflow has to travel a longer distance up over the endplate while decreasing its pressure gradient to the airflow on the outside of the endplate. Thus there is a decrease in the spillover.

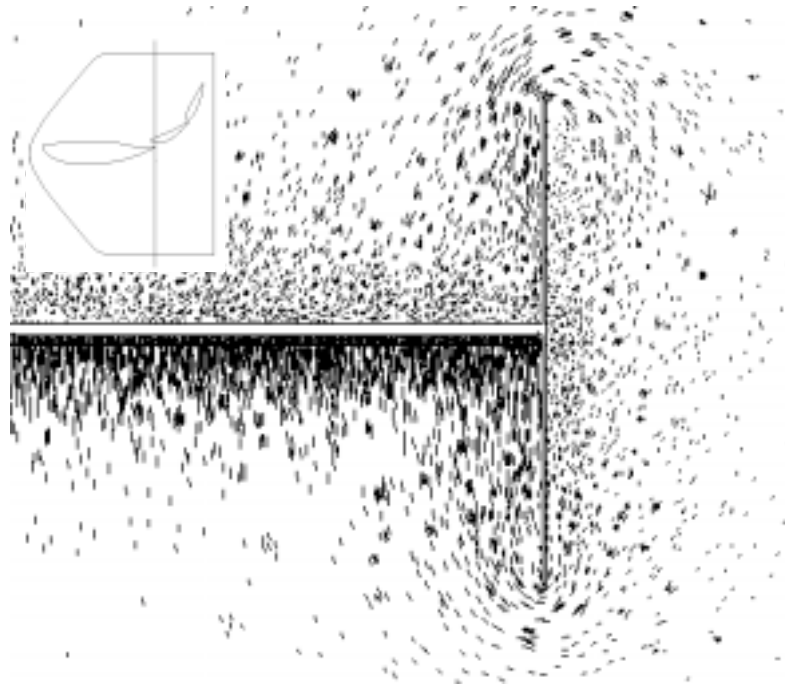


Figure 4-13: Cross-Flow Velocity 14 in. back from L.E. with New Endplate

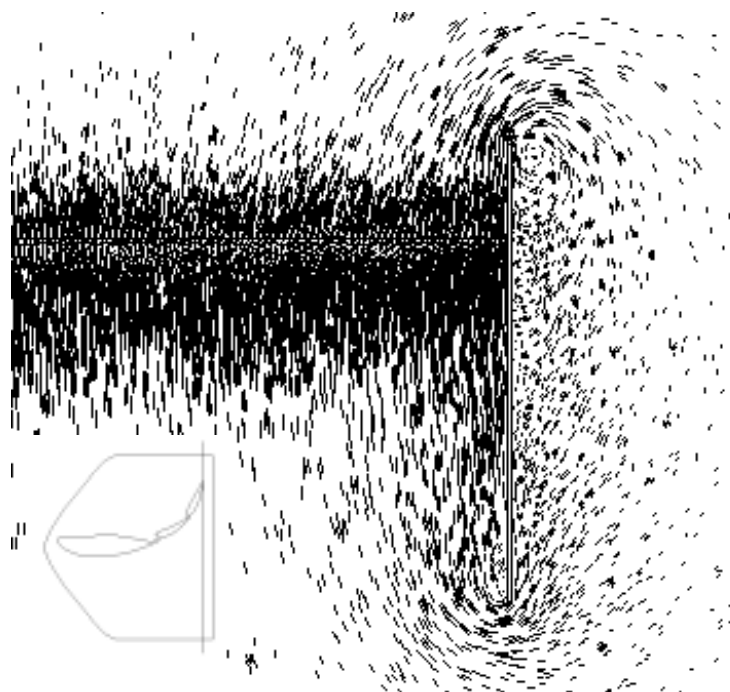


Figure 4-14: Cross-Flow Velocity 20 in. back from L.E. with New Endplate

Once again it was necessary on the new endplate design to increase the height above the third element in an attempt to reduce this circulation over the top of the endplate. It was once again very beneficial to incorporate this height change as can be seen in the reduced circulation in Figure 4-14.

This cross-flow velocity is only one view of what is going on as far as the flow velocity on and around the endplate. Therefore, it is necessary to look at a cut plane velocity profile parallel to the endplate.

4.1.3 Velocity at the Tip of the Wing

The velocity around the tip of the wing can give even more insight to the benefits of the endplates. In Figure 4-15, a cut plane at the tip of the wing, shows the circulation generated by the wing and how disruptive and almost how chaotic the airflow is behind the three-element wings due to the lack of an endplate.

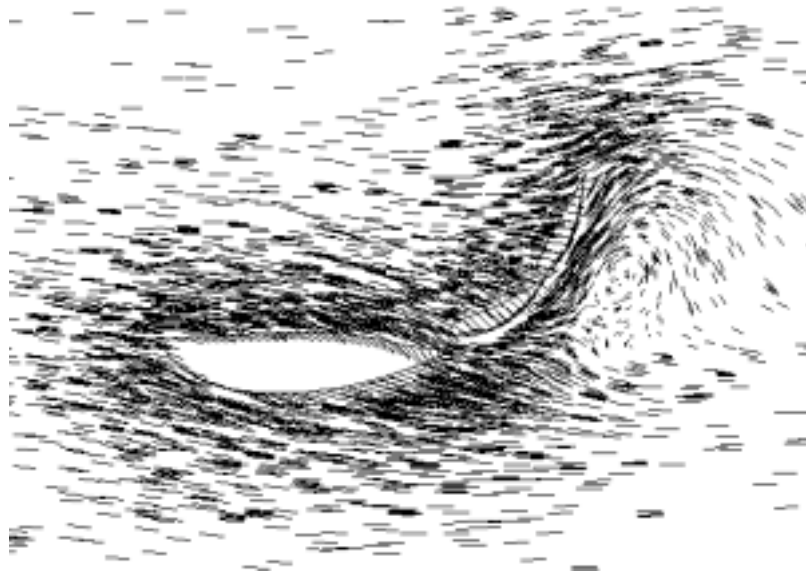


Figure 4-15: Velocity at the Wingtip without an Endplate

If there were an endplate attached the spillover flow would be reduced making for a less disruptive flow on the bottom of the wing. This is shown by looking at the flow on top and on bottom of the wing with an endplate present as in Figure 4-16. There are no distinct disruptive flows coming around the wingtips because the flow as you can see has to travel over the endplate. Figure 4-16 is a good example to show that the flow moves up the inside of the endplate which would then spillover and mix with the existing flow on the outside of the endplate. Once again it should be noted that the idea is to reduce the amount of flow spilling over.

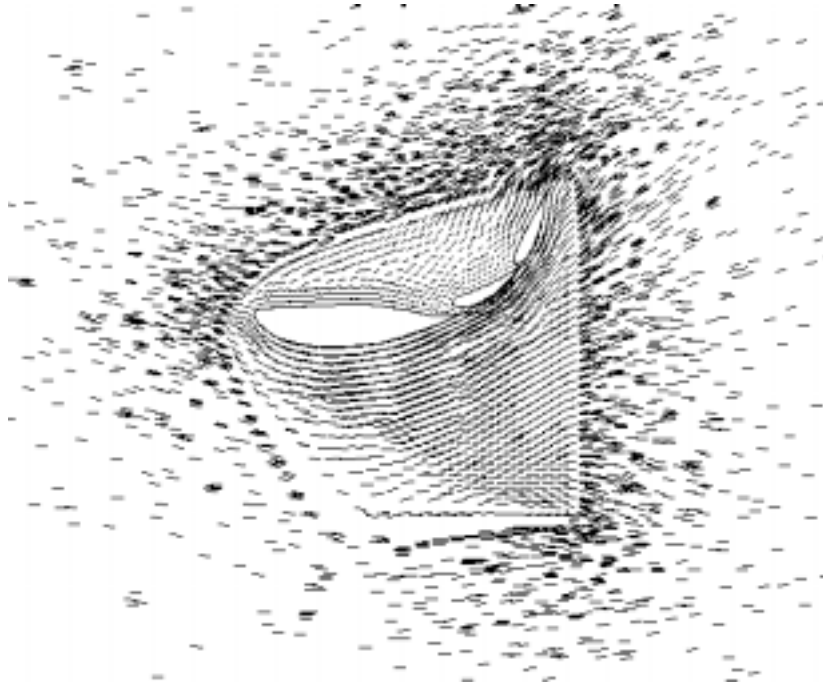


Figure 4-16: Velocity just inside Style 3 Endplate

Compare the velocity just inside the endplate of Figure 4-16 with the style 3 endplate to Figure 4-17 with the new endplate design. It can be seen that the flow at the

top of the new endplate design, Figure 4-17, is not as vertical as the flow at the top of the style 3 endplate. This indicates that there is less severity to the disruptive nature of the flow as airflow spills over. The angle of the velocity at the top of the new endplate design becomes very similar to that of the style 3 endplate towards the tail end of the endplate. This is due to the last wing element being at such a high angle, 65° , causing the flow to accelerate in the direction of its projected chord line.

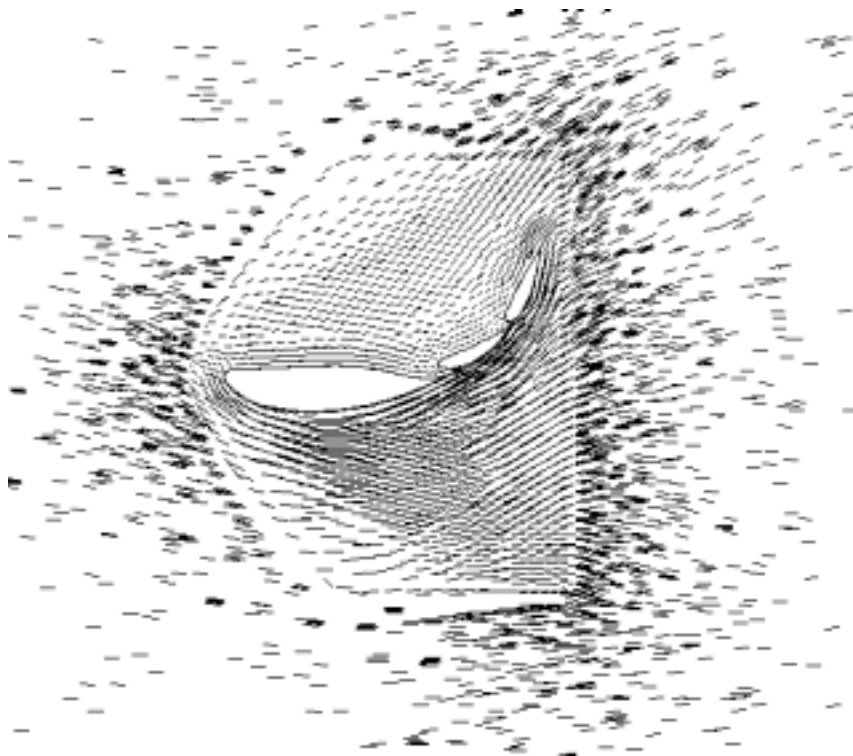


Figure 4-17: Velocity just inside New Endplate

4.1.4 Down Force to Drag Ratio

Another important parameter to look at the effects that endplate geometry have on the ratio of down force to drag. This parameter allows easy comparison between the

different geometry. The idea is to maximize the ratio of down force to drag. It should be noted that it is not being said that we want to maximize the amount of down force but we want to maximize the ratio, ie get the most down force with the least amount of drag.

The forces that are calculated using STARS are not the actual down force and drag forces directly. They are in fact non-dimensional lift and drag coefficients. However they are not non-dimensional in the true sense but the coefficient of pressure is divided by a factor of two. We can utilize these coefficients without further manipulation since the ratio of the down force to drag is being calculated.

If we look at Table 4-1 at the wing without the endplate and compare it to the either of the wings with an endplate. There is a large difference in the amount of down force created by the wing with endplates. The drag however for the wing without the endplate is smaller but this is not important because we are concerned with the ratio of the two parameters.

	Down Force	Drag	L/D Ratio
No Endplate	741.9	232.4	3.19
Style 3 Endplate	960.7	258.5	3.72
New Endplate	967.6	242.6	4.0

Table 4-1: Down Force and Drag for the Three Test Cases Analyzed

If we look at the actual increase in the down force to drag ratio we can get a better feel for how much of an improvement changing the endplate can have. As shown in Table 4-2 there is a 16.6% increase in the ratio when we attach the style 3 endplate to the basic wing. This ratio is further increased by 25.4% when we look at adding the new endplate design. This data shows that the new endplate design is effective because it

increases the down force to drag ratio by 7.2% over the style 3 endplate while only adding a minimal amount of area to the overall wing.

Geometry being Compared	Percent Increase of Lift to Drag Ratio
No Endplate to Style 3	16.6
No Endplate to New Design	25.4
Style 3 to New Design	7.2

Table 4-2: Increase of Lift to Drag Ratio for the Three Test Cases Analyzed

4.1.5 Mach Number and Coefficient of Pressure Distribution

The Mach number and coefficient of pressure distribution at the tip of the wing can be useful in showing where the maximum amount of flow velocity and suction is occurring, respectively. This gives the analysis a more physical comparison than just looking at the three-dimensional color pressure plots as was shown in the beginning of the section.

The pressure distribution in Figure 4-18 shows the coefficient of pressure for each of the three test cases analyzed. The first case where there was not an endplate, the coefficient of pressure on the suction side is about -2.5 on the first element as compared to -3 for the wings with the endplates. For the second wing element the difference in pressure on the suction side between the wing with an endplate and the wing without an endplate is about 1.5. The suction side of the third element and the positive pressure sides of all three-elements do not show a dramatic difference but there is still a moderate change.

Pressure Distribution for 0°-28°-65° Configuration
Mach=0.434, $\alpha=0^\circ$

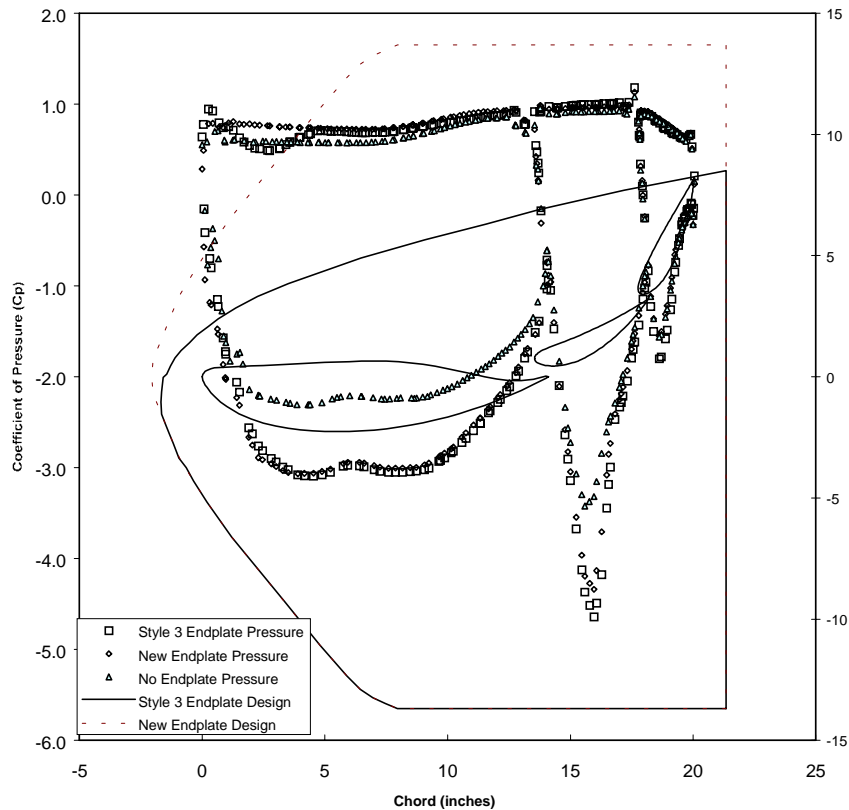


Figure 4-18: Pressure Distribution at the Tip of the Wing for Three Configurations

For the difference between the coefficient of pressure on the two endplates it is very difficult to tell from this data which is better. Although if you look closely at the positive pressure side of the wing, or top of the wing, you will notice that the new endplate design gives a little bit higher pressure.

As for the Mach number distribution in Figure 4-19 it can be seen that the Mach number for the wings with the endplates allowed for a larger amount of data points to become supersonic. The maximum Mach number for the wing without the endplate only reaches about eight-tenths the speed of sound on the first element. Comparing this to the

first element for the wings with endplates, the Mach numbers almost reaches the speed of sound. For the second wing element the effect of the endplate is about the same. On the third wing element there is not a noticeable difference.

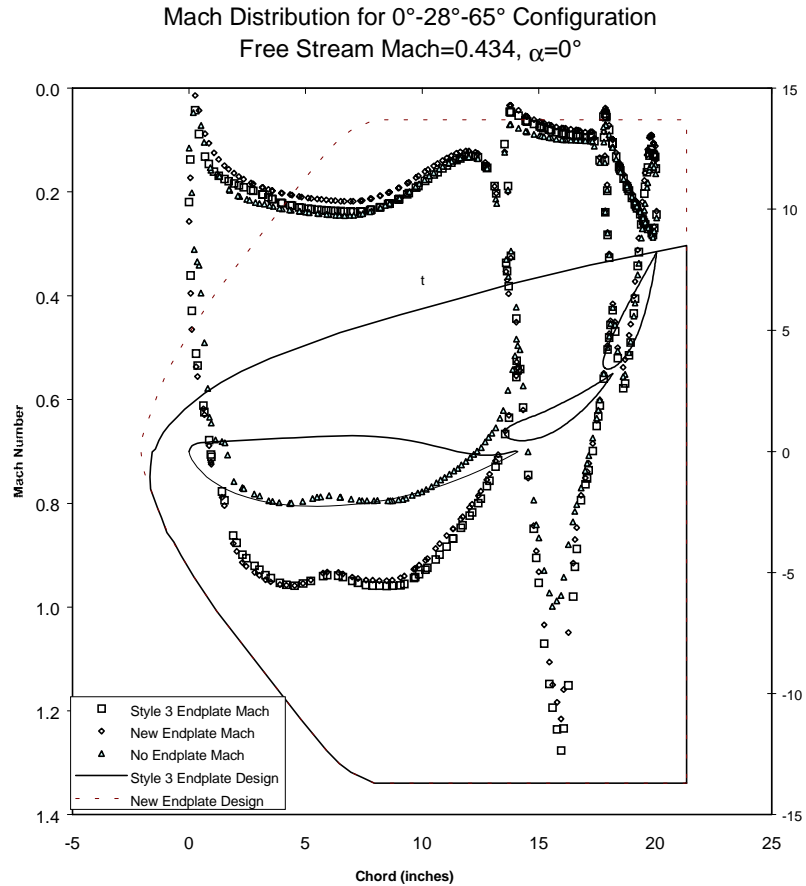


Figure 4-19: Mach Distribution at the Tip of the Wing for the Three Configurations

The topside of the wing shows a pretty uniform Mach number distribution between the three test cases analyzed. There is a slight increase in Mach number for the new endplate design over the style 3 endplate. It is believed that this can be linked to the reduced spillover affect seen on the top of the endplate.

4.2 Gap Spacing Comparisons for a Three-Element Dragster Wing

Gap spacing can affect the performance characteristics of these wings as well. Therefore the effects of gap spacing between the elements of a multi-element wing will be studied. This gap spacing is critical because it allows a certain amount of flow to pass between the elements and this amount of flow is very sensitive when looking at the performance of a multi-element wing.

The best way to look at this is a velocity cut plane at the mid span of the half model as seen in Figure 4-20. The multi-element wing has a 0° - 28° - 65° configuration at a Mach number of 0.434 for an overall angle of attack of 0° . As a reminder the configuration, 0° - 28° - 65° , refers to the angle of attack of each of the three individual elements.

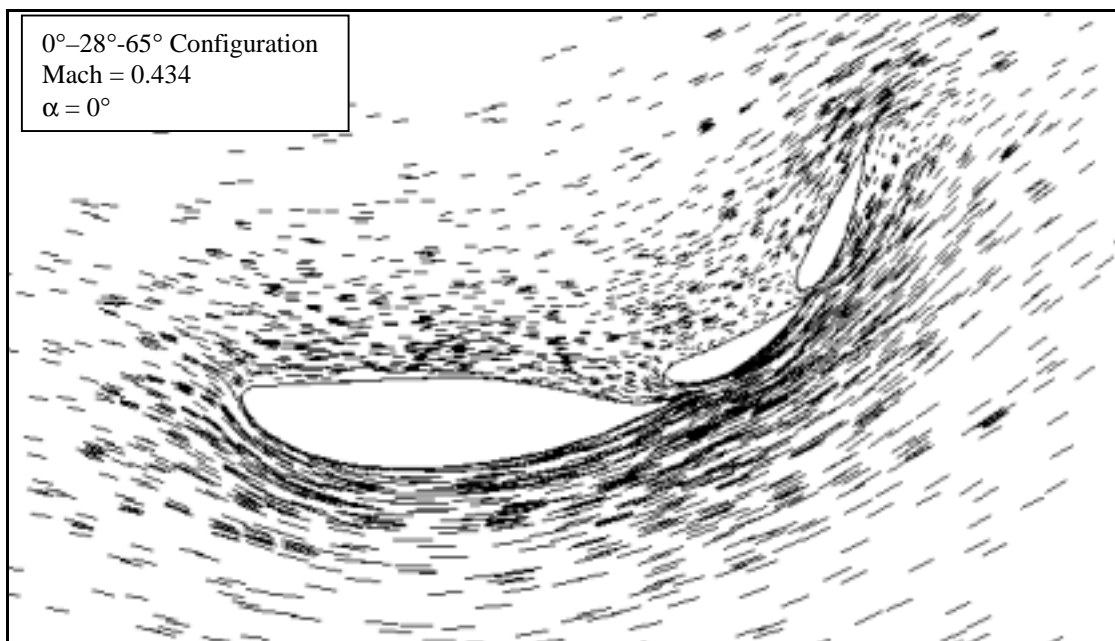


Figure 4-20: Velocity Profile of Wing with Original Gap Spacing

Pay attention to the gap size in between the elements as well as the flow field around and in between the gaps when looking at Figure 4-20 and Figure 4-21. It can be seen in Figure 4-20 that the flow around the second element, particularly the flow right in front of the second element, is more smooth looking than the flow around the second element in Figure 4-21. In the latter mentioned figure the gap size is too large and allows too much air to flow to pass. This causes a Venturi affect before the second element letting a massive amount of air through the gap which disrupts the flow. The same effects can be seen in the flow around the third element.

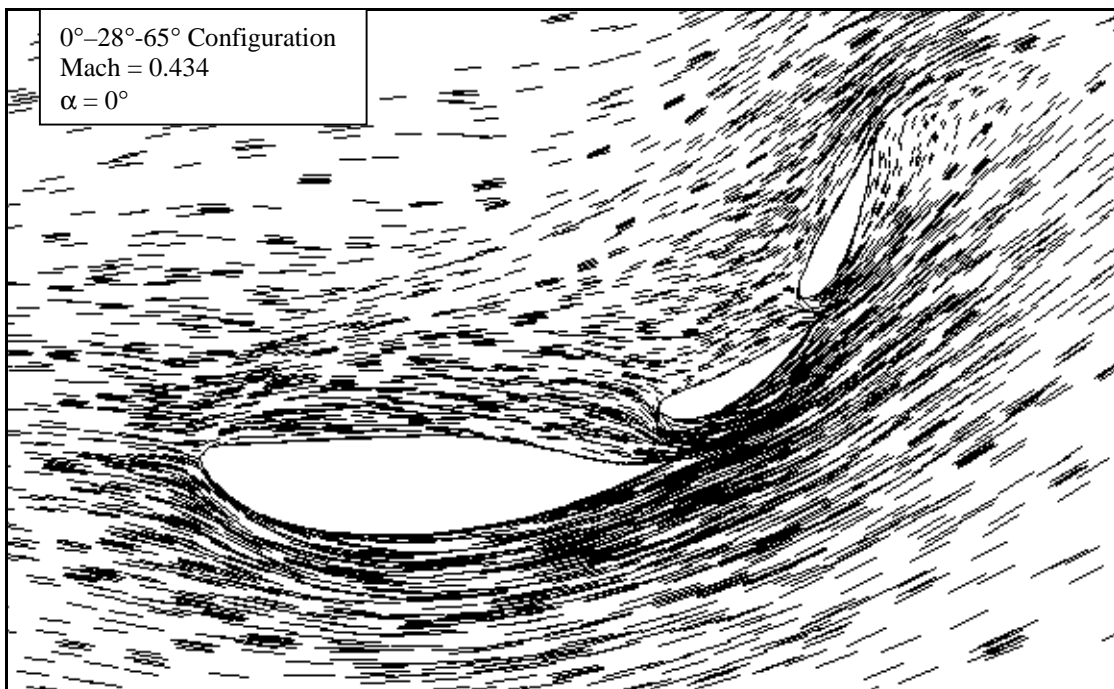


Figure 4-21: Velocity Profile of Wing with Modified Gap Spacing

When looking at the flow at the trailing edge of the third element another effect can be seen. With the increase in gap spacing the appears to be a flow separation. An Euler flow solver is unable to predict flow separation but the chaotic flow just aft of the trailing

edge of the third element shows signs of flow separation. It almost appears to have a circulation around this area and is very disruptive to the flow.

When the gap size was increased there was a decrease in the amount of down force generated. The decrease in down force was 6.8% under the amount of down force generated by the original gap spacing. The increased gap spacing also resulted in an increased the down force to drag ratio by 15.7%.

4.3 Angle of Attach Comparisons of Three-Element Dragster Wings

The effects of angle of attack on dragster wing with the style 3 endplate was studied to see how it affected the performance of the wing. The configuration was a 0° - 28° - 65° wing that was varied at two different angles of attack being 0° and 5° . The reason for this analysis is due to the top-fuel dragster teams wanting to vary the angle of attack on the rear wing to change the performance characteristics. These comparisons were looked at both through pressure cut plane data as well as down force and drag data, which was generated using STARS.

The pressure distribution data, as seen in Figure 4-22, is a pressure cut plane at mid span of the half model. As seen in the figure below there is little differences for the last two elements in the coefficient of pressure between each of the two angles of attack. However, the main difference appear on the first element and are mainly present toward the leading edge of that element. When the whole wing is rotated 5° , tilted forward, the suction pressure has a greater distribution than the wing at 0° angle of attack. When looking from three quarters of the way back from the leading edge of the first element all the way back to the trailing edge of the third element there is little difference.

Pressure Distribution for 0°-28°-65° Configuration
Mach=0.434, $\alpha=0^\circ$ and $\alpha=5^\circ$

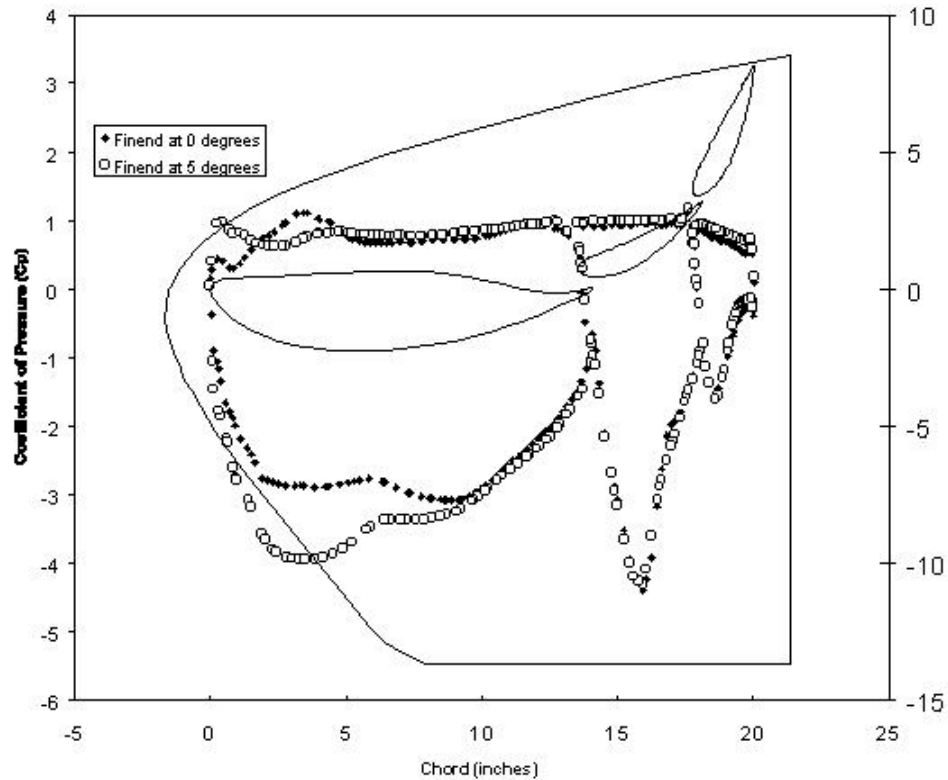


Figure 4-22: Pressure Plots for Angle of Attack Comparisons

For a feel on how much it affects the performance of the wing it is necessary to look at the down force and drag of the wing. An increase in angle of attack to $\alpha = 5^\circ$ increases the down force by 8.9%. This might be considered good if all we were interested in was down force the drag must be considered in our case. The drag also increased but increased by 20.4%. This is greater than the increase in down force and therefore it decreases the down force to drag ratio by 9.7%. Based upon wing performance alone this increase in angle of attack would be a mistake.

4.4 World Record Performances

It should be noted that the improvement to the endplate design over the previously used style 3 endplate helped two top-fuel dragster teams break two different world records. Two weeks after the introduction of this new endplate Larry Dixon piloted a dragster owned by Don Prudhomme to the quickest elapse time record in the quarter mile history. At Houston Park Raceway in April of 1999 he posted a 4.486 second run beating the previous record by 0.03 seconds. Weeks later, with the same new endplate design, Tony Schumacher at the Checker-Schuck's Kragen Nationals downed the top-fuel dragster speed record reaching 330.23 mph in the quarter mile.

Granted the wing was not the only factor involved in the record-breaking runs but given the vast improvements they can be considered to be somewhat responsible. These wings can require close to 2000 hp to drag them through the air. The new endplate design reduced the drag and thus reduced the needed horsepower to drag the wing through the air. This additional horsepower can then go to acceleration and thus potentially allowing the vehicle to reduce the elapsed time or increase the top speed.

4.5 Using the Dragster Model to Analyze the Problem

Since the model matched the actual data well it is now the objective to see what affects the aerodynamics has on the performance of the dragster.

The first figure below, Figure 4-23, shows the actual input power to a dragster. This is used for the input power to the dragster for the validation analysis in the previous section. Along with this input power is the power left over to accelerate the dragster and

is labeled acceleration power. This is the power after the drag and various friction components are taken away from the trust component. This acceleration power is an output from the model. There is a point on the plot that is labeled critical horsepower and this is the point where the vehicle hits critical velocity. At any time below this the model is assuming that it is on the verge of slipping which was discussed in earlier sections.

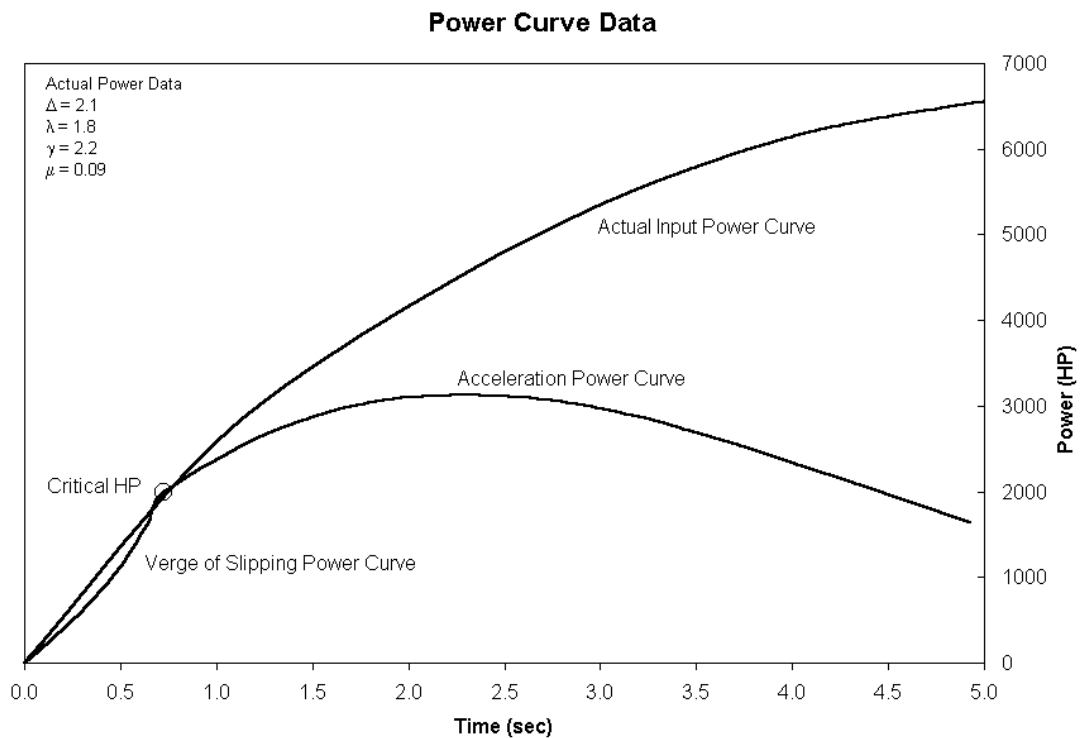


Figure 4-23: Input Power Curve and Acceleration Power Curve versus Time

Looking at difference in power between the two curves is an indication into how much power is being lost. The acceleration power is critical because this is the power being used to accelerate the vehicle. Therefore it is necessary to determine where these loses are coming from.

In the next figure, Figure 4-24, there are two additional lines. One is the amount of power that the car absorbs due to drag and friction. Looking at the drag coefficient of the wing in comparison, Table 4-3, with the rest of the components under consideration showed that it was a major factor in this power loss.

Coefficient of Drag Scaled to Wing Area

Wheels	Cl	-0.14142	Cogotti for Rotating Wheels
	Cd	0.45489	Cogotti for Rotating Wheels
Wing Induced	Cl	-2.47700	STARS
	Cd	0.60100	STARS
Wing Area Top	Cd	0.00963	Estimated
Wing Area Endplate	Cd	0.00380	Estimated
Body	Cd	0.01733	Estimated by 3D Wedge

Table 4-3: Lift and Drag Coefficients for the Dragster Model

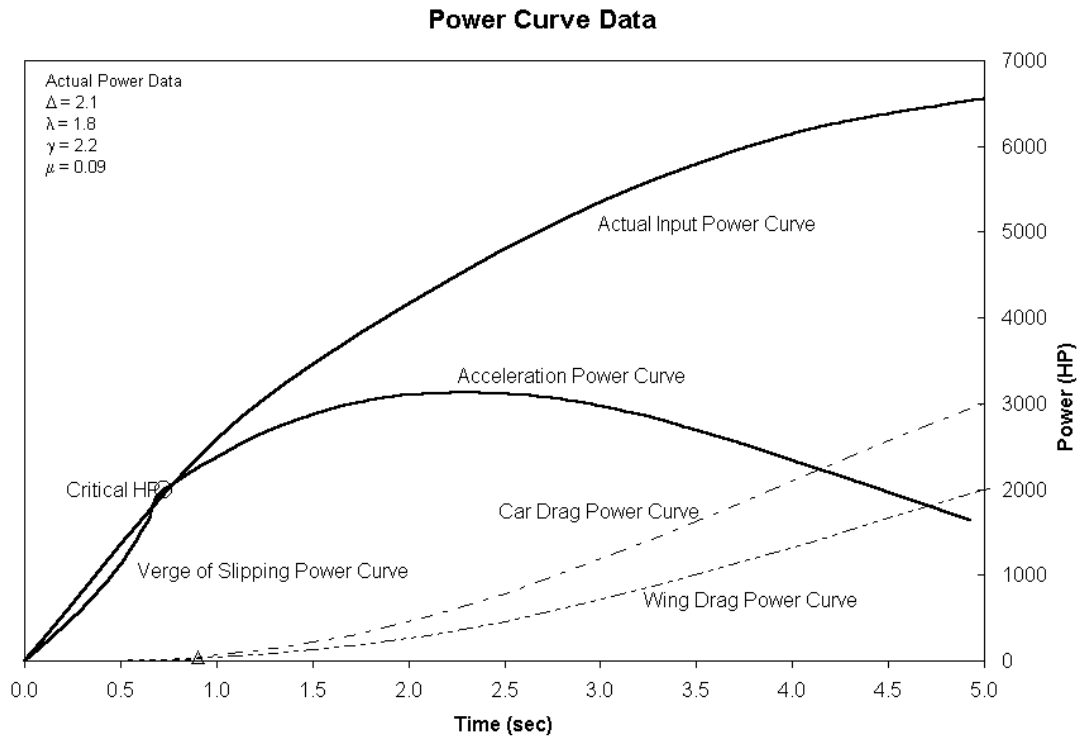


Figure 4-24: Power Curves along with Drag Power versus Time

At the end of the race the wing is making up almost two thirds of the total loss of power of the dragster. It is necessary to find out how changing this drag would affect the performance of the dragster. In order to do this the model was run with different drag coefficients while keeping constant the lift to drag ratio. This was done for four drag coefficients and six different lift to drag ratios and the results can be seen in Figure 4-25.

Performance Data for a Top-Fuel Dragster (1/4 mile)

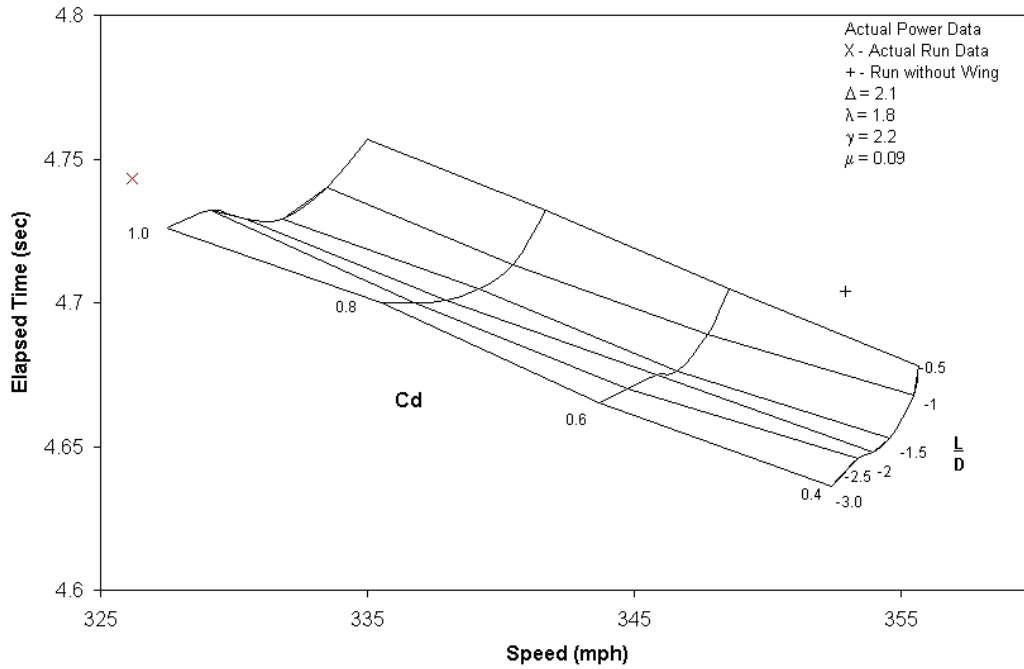


Figure 4-25: Elapsed Time and Speed Data for Varying Drag Coefficient

This figure shows how much reducing the drag coefficient can improve the elapsed time of the dragster as well as how much it can increase the top speed. The X on the figure shows a dragster whose lift and drag characteristics were estimated and the wing data was generated from STARS for the finnew wing design. The finnew design is a wing that is currently being used by several dragster teams. The elapsed times and top speed are not current with the times and top speeds of today's dragsters but it must be understood that the input power used was from actual data that might not meet the input power data of a dragster now. The idea of this is to not look at the times and speeds that were achieved but to look at the trends of changing the parameters.

Another point on the graph to look at is the + mark. This run is the same dragster but the wing is taken off so that it produces not down force or drag force. It has a lower elapsed time because the reduction in drag but the catch is that the driving style would have to change. This can better be seen below in Figure 4-26.

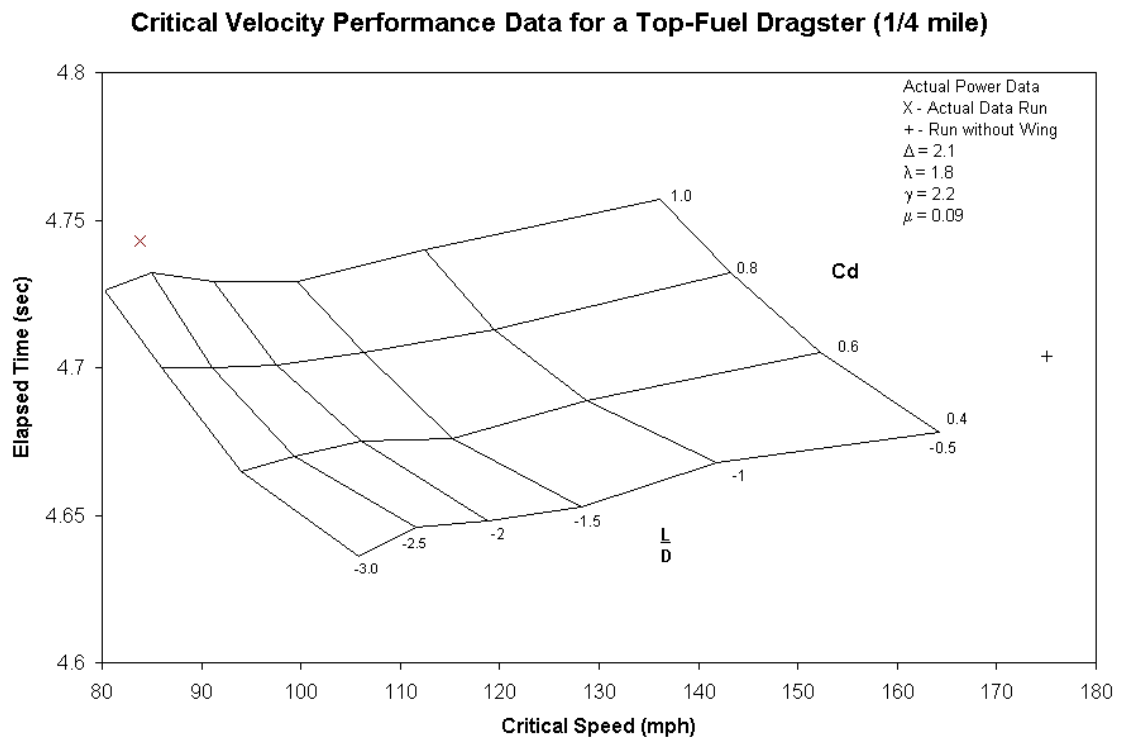


Figure 4-26: Elapsed Time and Critical Speed Data for Varying Drag Coefficient

The critical speed is over twice that of the dragster with the wing. This means that there is not enough down force early on and with the given input power curve it is not able to give full power until it reaches this speed. If it had more power earlier than this point than the tires would slip and loose traction. This means that the driver must be less

aggressive during the race in the dragster without the wing. This shows how important reducing this drag can be as far as performance is concerned.

The question then is whether running a dragster without a wing is the best or is there some other way that is better. It is still not know how the lift coefficient affects the performance of the dragster. The question must be answered then how much lift does the dragster need and at what point on the track is the lift needed? The best way to figure this out is to vary the lift coefficient for a fixed lift to drag ratio. This data is plotted below in Figure 4-27.

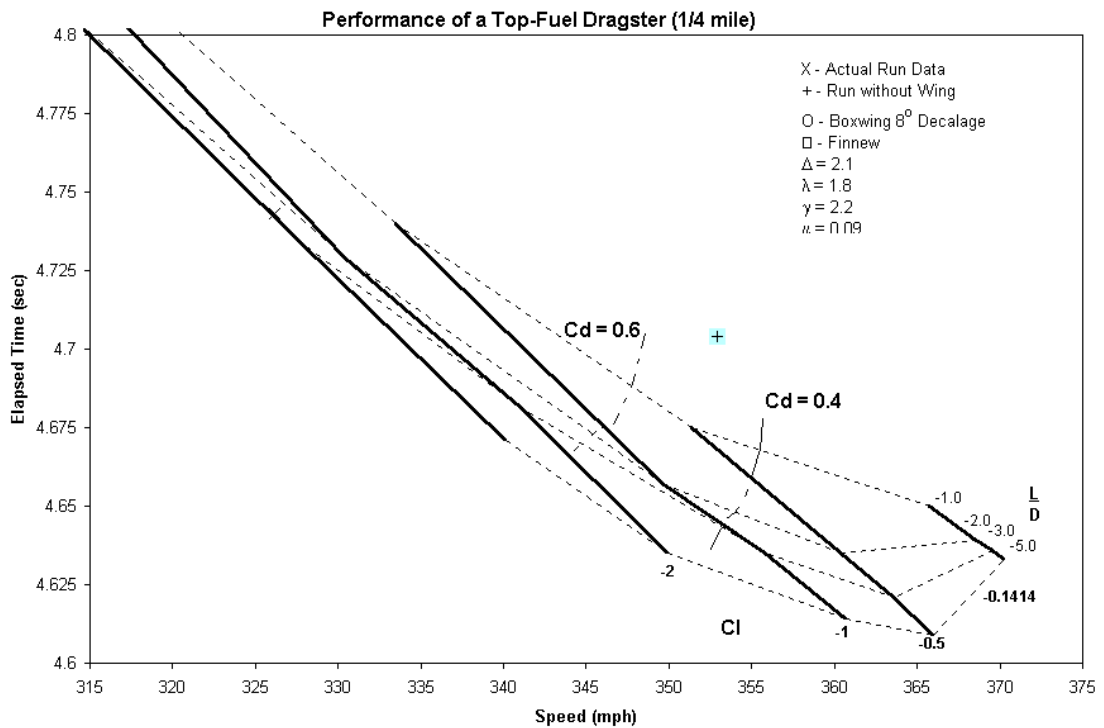


Figure 4-27: Elapsed Time and Speed Data for Varying Lift Coefficient

Looking at the constant drag coefficient lines ($C_d=0.6$ and $C_d=0.4$) backs up the theory from before that to get a better elapsed time it is necessary to reduce the drag coefficient. The lift coefficient can be looked at as well showing that for a constant lift to drag ratio reducing the lift coefficient from -3 to -0.5 will reduce the elapsed time and increase the top speed of the dragster. Once the dragster gets below a lift coefficient of around -0.5 the elapsed time increases. This starts to show that reducing the lift coefficient down to zero does not help the performance of the dragster.

In this region where there is a low lift coefficient and a high lift to drag ratio the performance of the dragster suffers because of the critical speed is too great for the car to have its best run. This can better be seen in Figure 4-28. The elapsed time is around 175 mph. This is somewhat misleading because the drag coefficient for the dragster cannot be this low unless significant modifications to the aerodynamics of the overall car is made. Looking at the run of the dragster without the wing it has a drag coefficient between 0.4 and 0.6. The drag from the large open wheels and the body of the dragster are to blame for this drag.

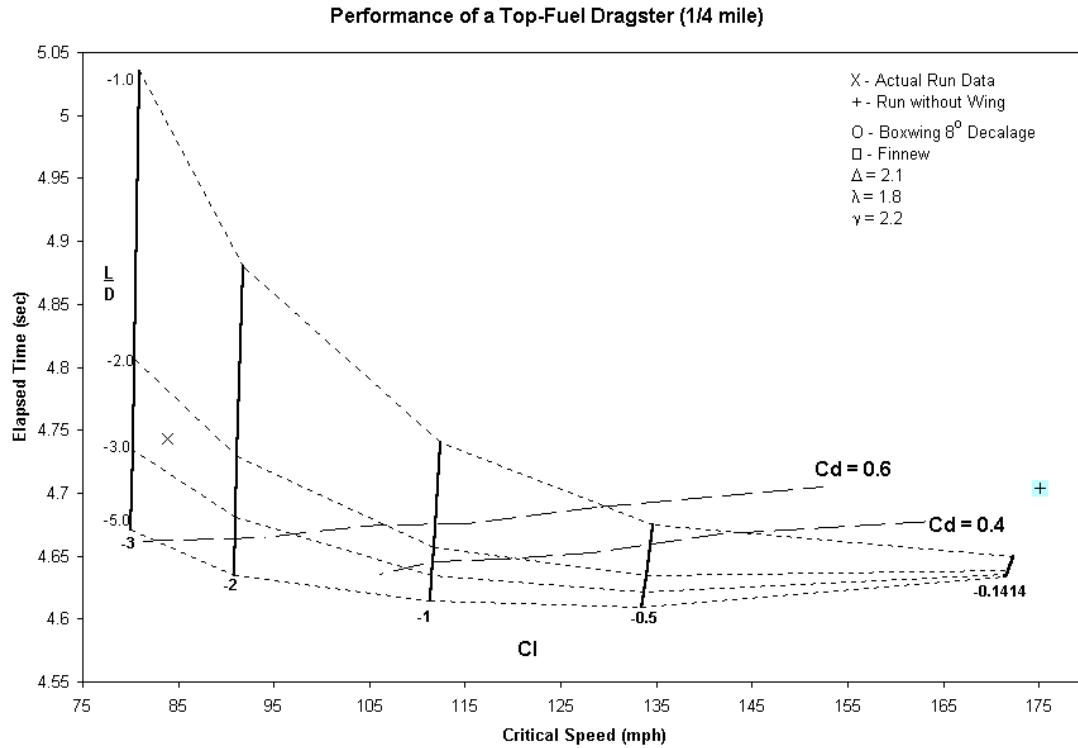


Figure 4-28: Elapsed Time and Critical Speed Data for Varying Lift Coefficient

These figures are somewhat misleading because if we are looking at changing the wing on the car then it is not simply looking at just changing the lift coefficient. Lets say for instance that you were looking at changing the angle of attack of a wing and you were able to increase the lift coefficient from -1 to -2. It is clear at to where the lift coefficient lines are and how they affect elapsed time but what now happens is that when the angle of attack changed not only did the lift coefficient change but the lift to drag ratio changed as well. So it is not as easy to see how it is affected because the lift to drag ratio is not constant and the user of the figures must determine the new lift to drag ratio.

Wing configurations will be plotted later in this paper but what I want to do is to talk about designing a new wing. From looking at the previous plots a wing that has a

lower lift coefficient with the highest lift to drag ratio will get us into a lower elapsed time. As was mentioned earlier the design of a boxwing was considered for many reasons and the results from STARS will be discussed in the next section.

4.6 Steady Results of Boxwing Design

The new boxwing design was analyzed computationally using STARS. The performance characteristics of this wing compared to the old style three-element wings will be looked at in this section. Various plots and figures are provided to show a variety of different comparisons between the wings including pressure plots, mach plots, coefficient of lift versus angle of attack, coefficient of drag versus angle of attack, coefficient of lift versus coefficient of drag, and several others.

4.6.1 Decalage Angle Comparisons

STARS simulations were performed for various boxwing configurations. The decalage angle was varied for three different angles. For every decalage angle the angle of attack was then varied over a wide range to find the characteristics of this particular type of wing. This data was used to analyze the performance of this wing and then use it also to compare this boxwing to existing wings.

4.6.1.1 Pressure Plots

The pressure plots are for three different decalage angles for a wide range of overall wing angle of attacks. The side view of the wing at zero angle of attack is also plotted on the graphs in order to clarify the two distinct sections of pressure distribution on the plots.

The two regions of pressure distribution clearly show the difference in loading of the two wings. The front wing is loaded too much while the back wing is not loaded enough. The reason that this happens is because the influence of the wings on each other. The front lower wing reduces the effective angle of attack of the back upper wing and the back upper wing increases the effective angle of attack that the lower front wing sees. This is why we change the decalage angle as to try to evenly load these wings to account for the influences of the wings on each other.

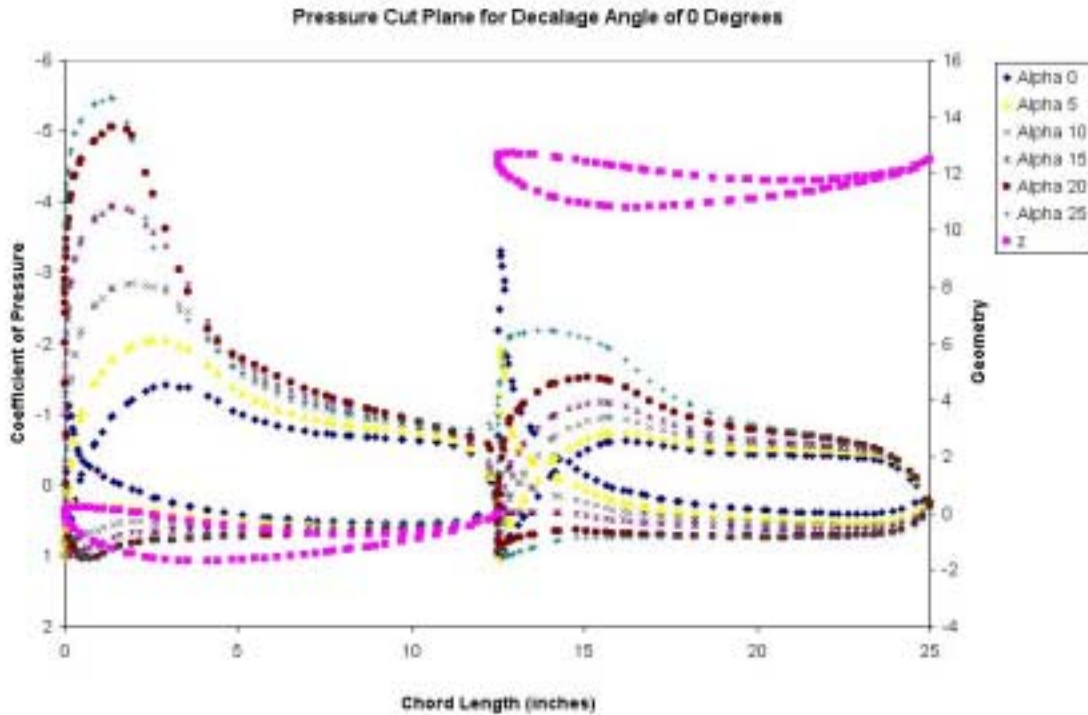


Figure 4-29: Pressure Plot for Boxwing at 0 Degree Decalage Angle

As can be seen in Figure 4-30 the pressure distribution is starting to level out and provide a more efficient wing. In this figure the decalage angle is 8° . As mentioned earlier the difference in angles between the two wings is the decalage angle. When the lower front wing is parallel to the ground, at a zero angle of attack, the upper back wing is turned at an 8° angle, where the tail of the wing is up.

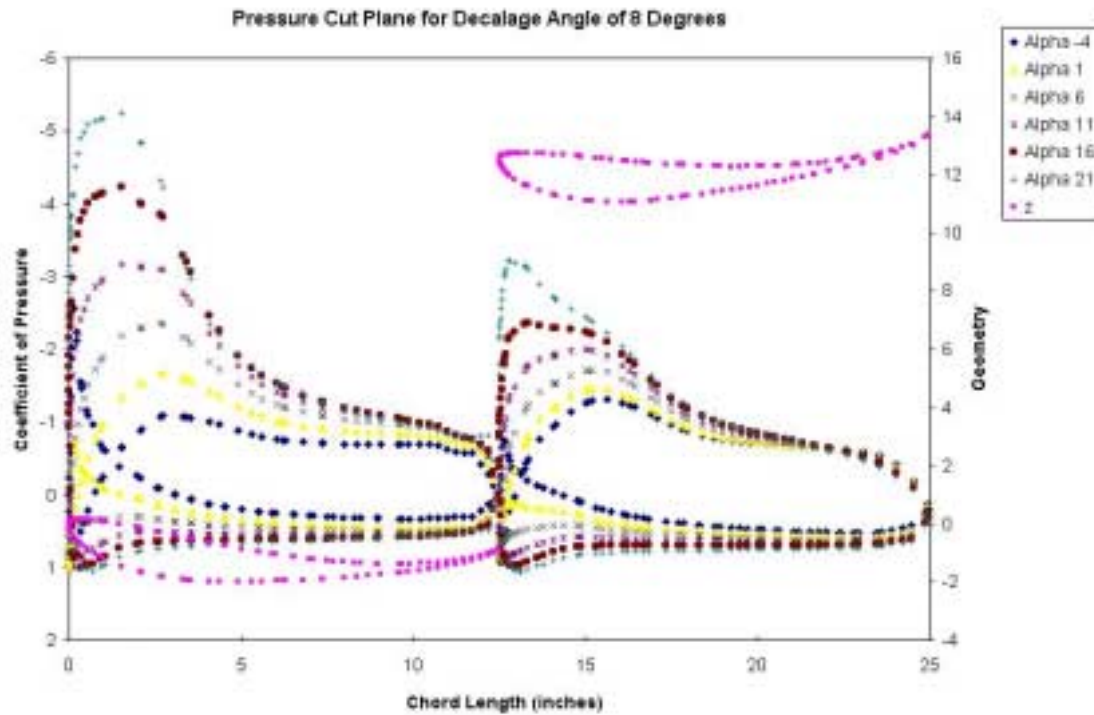


Figure 4-30: Pressure Plot for Boxwing at 8 Degree Decalage Angle

Since the distribution is still quite a bit off another decalage angle is studied. The pressure distribution of a 12° decalage angle boxwing is shown in Figure 4-31. There are only two overall angles of attacks that were run using STARS but the patterns for the more evenly distributed pressure contours can be seen. In these plots the side view of the boxwing is also plotted and in this figure the decalage angle is more noticeable.

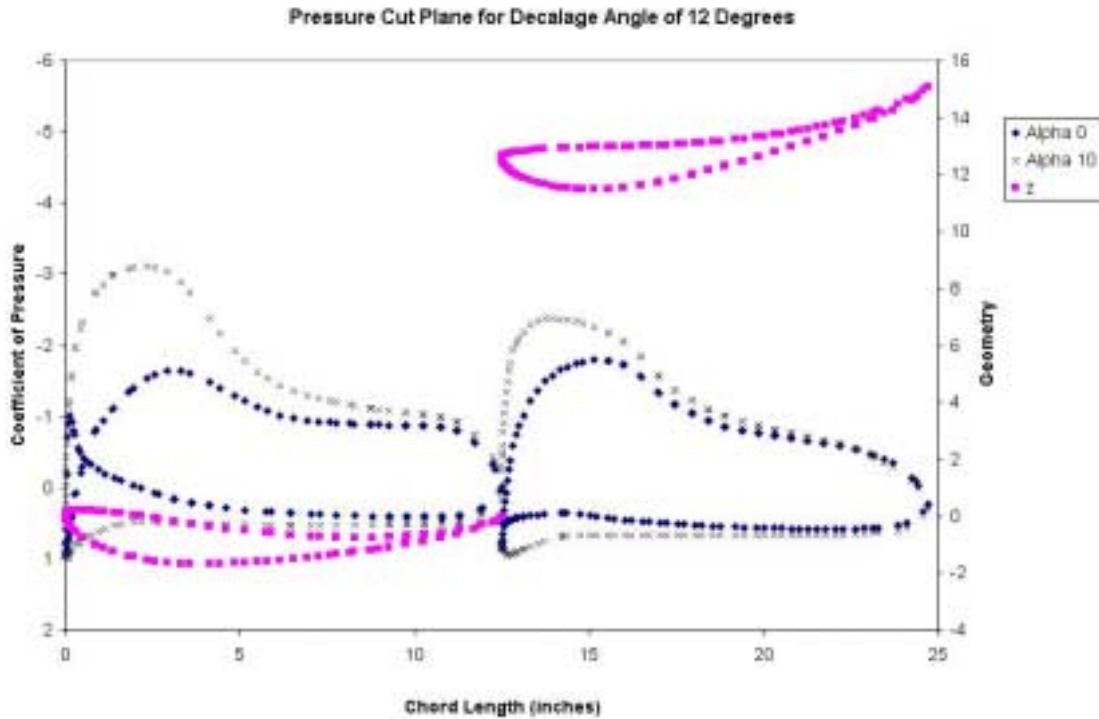


Figure 4-31: Pressure Plot for Boxwing at 12 Degree Decalage Angle

4.6.1.2 Mach Plots

Similarly to the pressure plots, the Mach plots are shown for three different decalage angles for a wide range of overall wing angle of attacks. The side view of the wing at zero angle of attack is also plotted on the graphs in order to clarify the two distinct sections of Mach distribution on the plots

The first plot, Figure 4-32, the decalage angle is 0° and once again the distribution of Mach number is distributed unevenly between the two wings. The Mach number on the lower front wing for high overall angles of attack has points where it is above Mach 1 but the upper back wing only sees subsonic flow no matter how high the overall angle of attack.

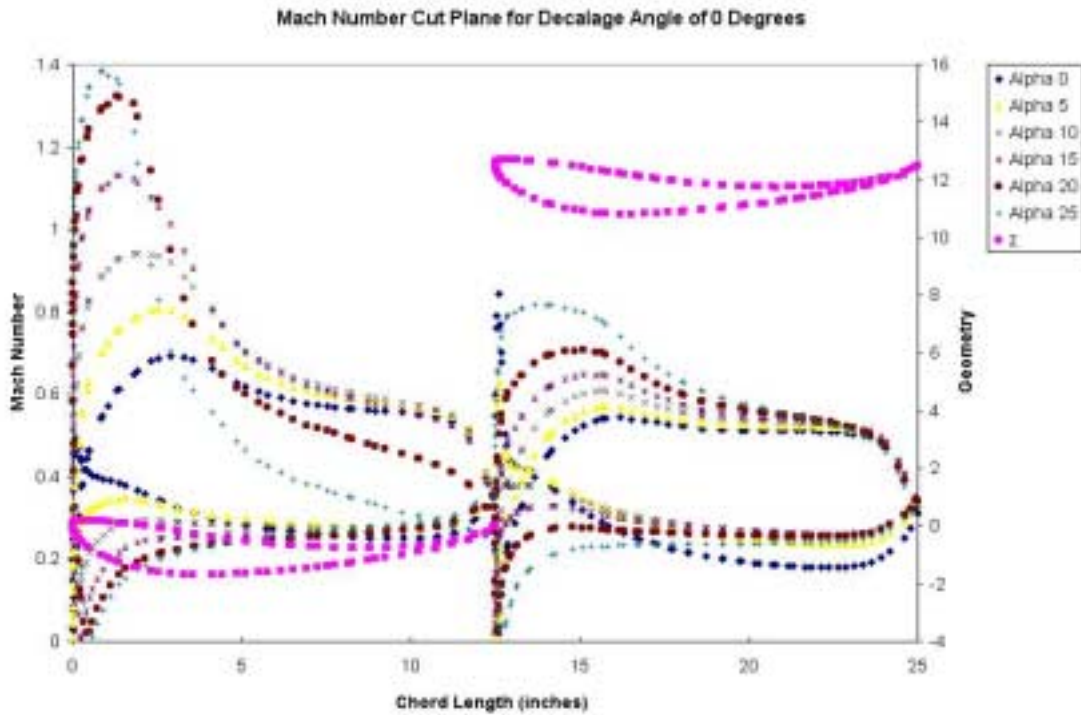


Figure 4-32: Mach Number Plot for Boxwing with 0 Degree Decalage Angle

The same patterns for the pressure plot for the 8° decalage angle occur for the Mach plot as well. In Figure 4-33 the distribution of Mach starts to even out. For the 21° angle of attack the upper back wing almost sees Mach 1 while the lower front wing sees Mach numbers to almost Mach 1.4.

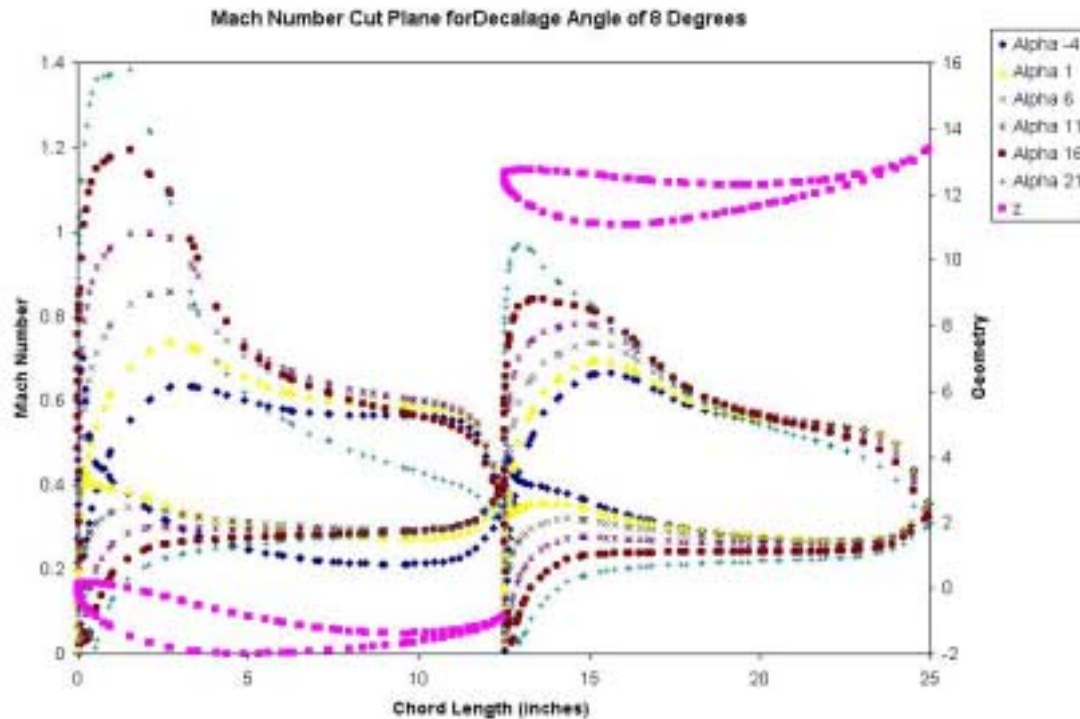


Figure 4-33: Mach Number Plot for Boxwing at 8 Degree Decalage Angle

The 12° decalage angle shown in Figure 4-34 once again looks like that of the pressure plot for the 12° decalage angle as expected. The angles of attack larger than 10° were not run but the patterns can be seen as the Mach distribution evens out even more. More decalage angles could have been run but the idea is not to get this wing to its optimal design but to look at a whole new approach to dragster wings to see if a better performance can be achieved which will be talked about in the next section.

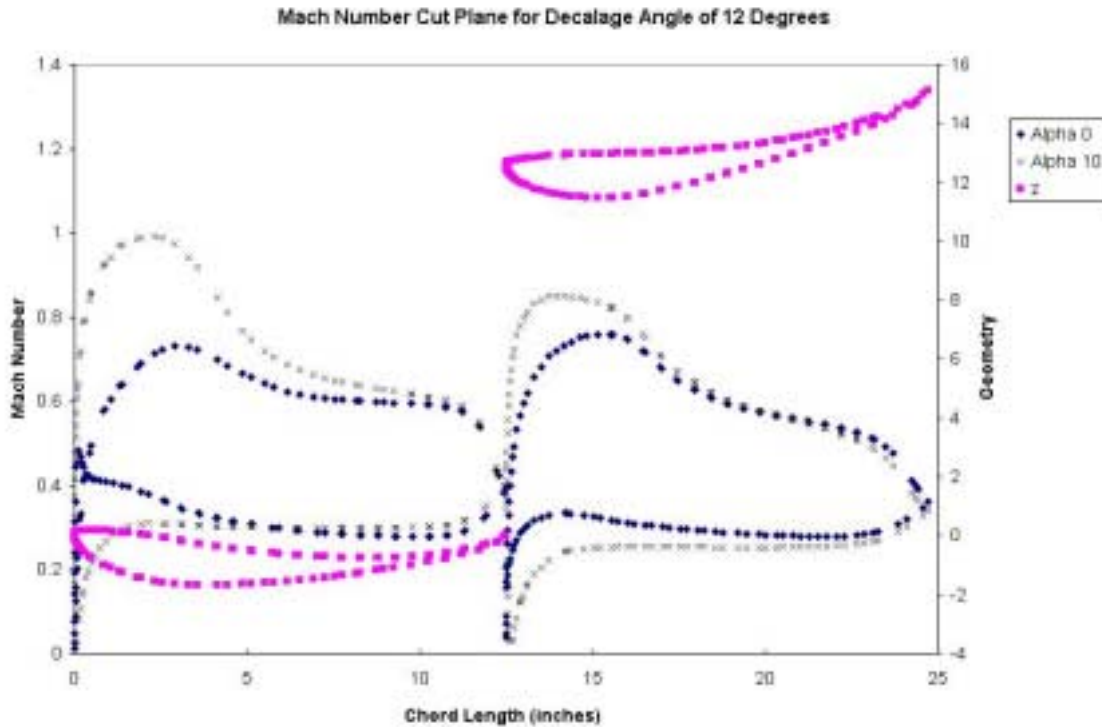


Figure 4-34: Mach Number Plot for Boxwing at 12 Degree Decalage Angle

4.6.2 Boxwing and Three-Element Wing Comparisons

In an attempt to compare these different wing types certain wing performance characteristics were studied and plotted. Some of these include coefficient of lift versus angle of attack, coefficient of drag versus angle of attack, coefficient of lift to coefficient of drag, and coefficient of lift to drag versus angle of attack.

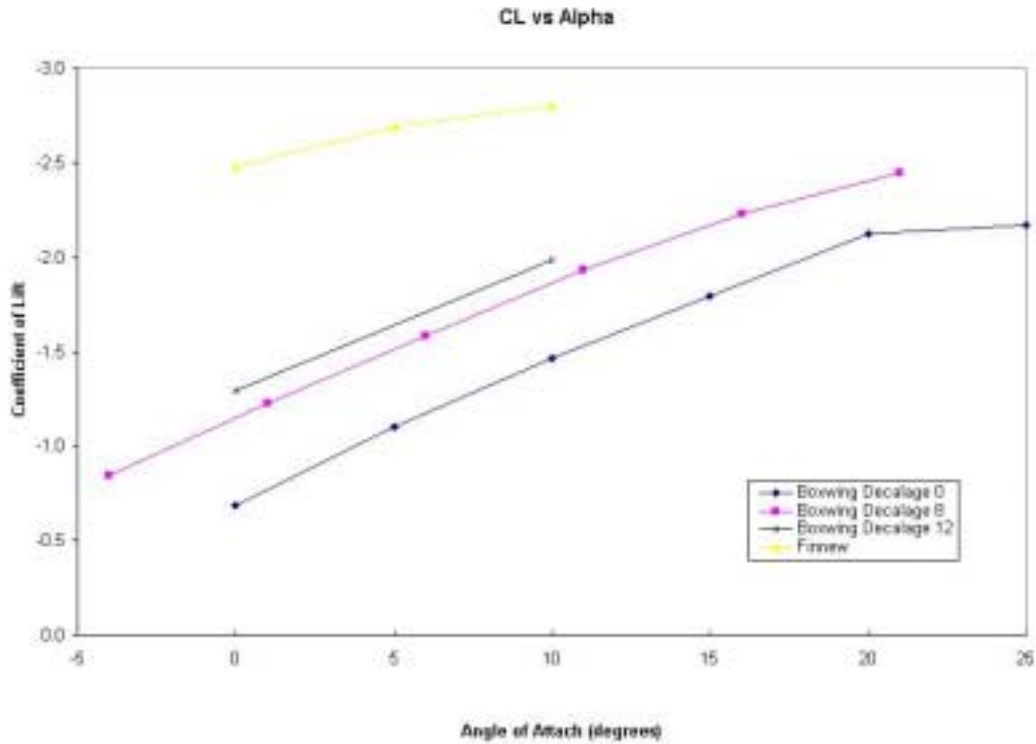


Figure 4-35: Coefficient of Lift vs Angle of Attack

The coefficient of lift versus angle of attack plot in Figure 4-35 shows how the lift coefficient a particular wing has when it is adjusted to a certain angle of attack. It can be seen that the wing labeled finnew, which is the three-element wing at a 0°-28°-65° configuration with the new endplate, has quite a bit higher $C_{L\alpha}$ than the other boxwing designs. The boxwing design with a decalage angle of 12 degrees has the potential of reaching the same coefficient of lift as the finnew wing if the boxwing is set to an overall angle of attack of 20°.

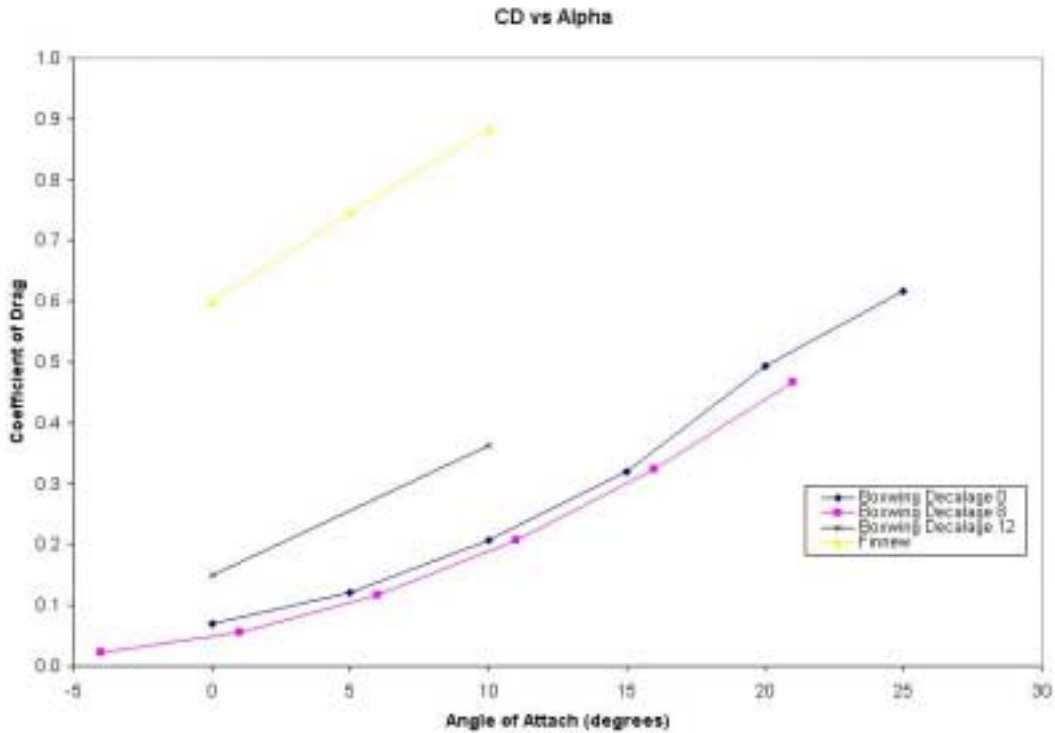


Figure 4-36: Coefficient of Drag vs Angle of Attack

The next plot above, Figure 4-36, is a plot of the coefficient of drag versus angle of attack.

This figure is deceiving at first because it looks like the boxwing design has a lot lower drag coefficient than the three-element design. This is not necessary true because the boxwing at these lower angles of attack does not produce the same lift as the three-element wing at the same angles of attack. It might be better to look at the coefficient of drag to the coefficient of lift to see a better comparison.

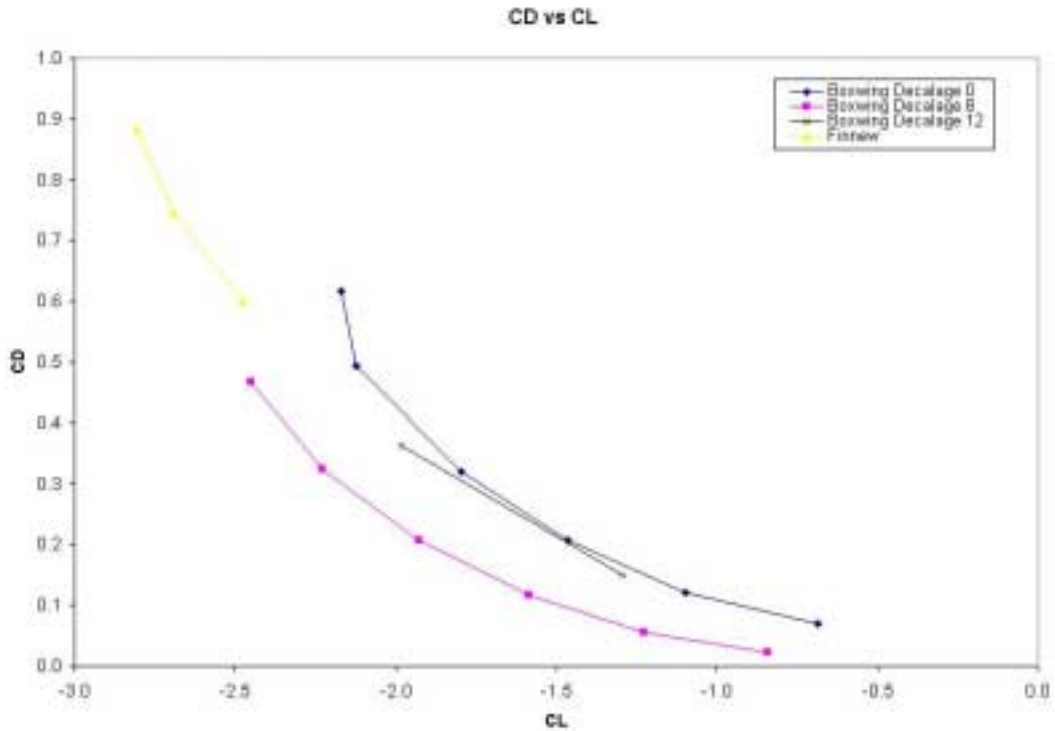


Figure 4-37: Coefficient of Drag vs Coefficient of Lift

Figure 4-37 above represents the coefficient of drag versus the coefficient of lift plot. This allows for the comparison of how efficient the wings can be if you will. This tells us how much lift we can get out of a wing with the punishment of the amount of drag that the wing had by nature.

It is hard to compare the boxwing to the three-element wing in this plot because they do not have the same lift coefficient. Therefore it is better to look at a plot that compares the ratio of the coefficients of lift to drag versus the coefficient of lift. This gives a better comparison of the wings.

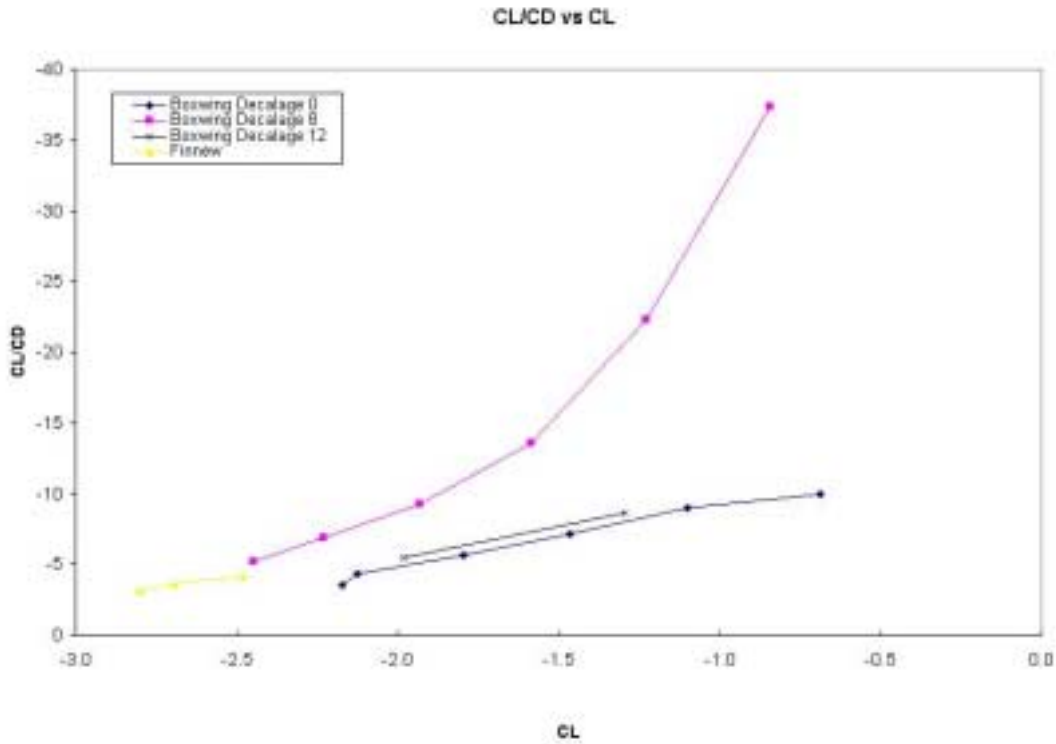


Figure 4-38: Coefficient of Lift to Drag vs Coefficient of Lift

This plot of the coefficients of lift to drag versus the coefficient of lift, shown in Figure 4-38, allows us to see the efficiency of the wings in a way. For a given coefficient of lift that is desired, a wing can be picked based upon its lift to drag ratio. A wing that has a better lift to drag ratio is punished less, in terms of drag, when there is an increase in the amount of lift produced. It is ideal to have a higher lift to drag ratio.

4.7 Dragster Performance Comparisons using the Dynamic Model

This portion of the results is what is the most important. Even though all the previous comparisons on wing performance was done the individual wing characteristics was not what this research was about fully. The true results is how these different wings and how the changes to these wings truly effected the overall performance of the

dragster. The improvements to the performance of the individual components is needed but the improvements should not be recognized without knowing how they will improve the performance of the dragster. Large improvements to a component might not necessarily provide large improvements to the performance of the dragster and vice versa.

A true test is to input these component changes into a dynamic model for the dragster and see how they affect the quarter mile time and speed. Since the dragster teams are concerned with the finishing times and top speeds of the dragsters then it is important to be able to give the teams a figure on how certain changes will affect the time and speed of their vehicles.

4.7.1 Performance Data for Various Rear Wings

Wing data from an actual dragster as well as the new boxwing design was used when running the model to determine how the aerodynamic changes would affect the performance. The wings were varied at different angles of attack since most dragster teams tamper with this feature. The data was plotted on the charts that were generated earlier and the results are shown in Figure 4-39.

The figure shows two wings with the first being the finnew design. This is a current wing that is being used on dragsters. It is varied for three different angles of attack from 0° to 10° . As the angle of attack increases so does the elapsed time while the top speed of the vehicle decreases.

The second wing that is analyzed is the boxwing configuration with an 8° decalage angle. This to was varied for several angles of attack. The angles range from -4° to 21° and are in increments of 5° . When the chord of the lower wing is parallel to ground then

the angle of attack is set to be at 0° . As the angle of attack is lowered from 21° the elapses time decreases and the top speed increases up until the wing is set to 1° . When the wing is set to a lower angle of attack the performance of elapsed time decreases but the top speed increases.

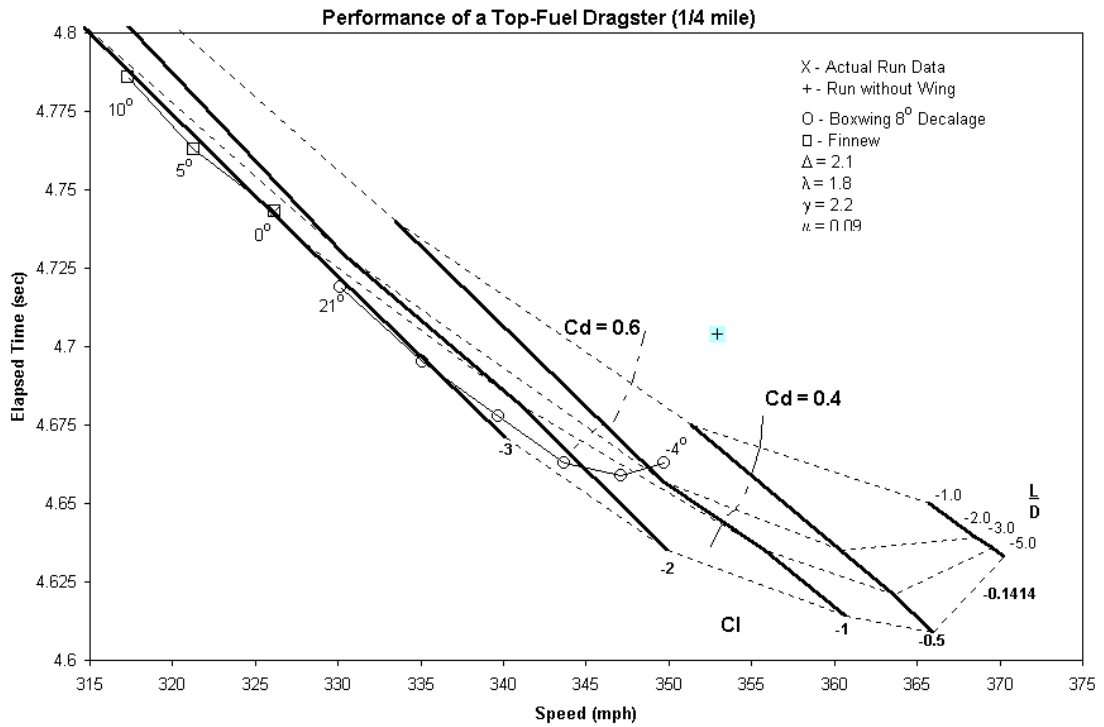


Figure 4-39: Elapsed Time and Speed Data with Different Wing Configurations

The next figure shows how this data affects the elapsed time and the critical speed of the dragster.

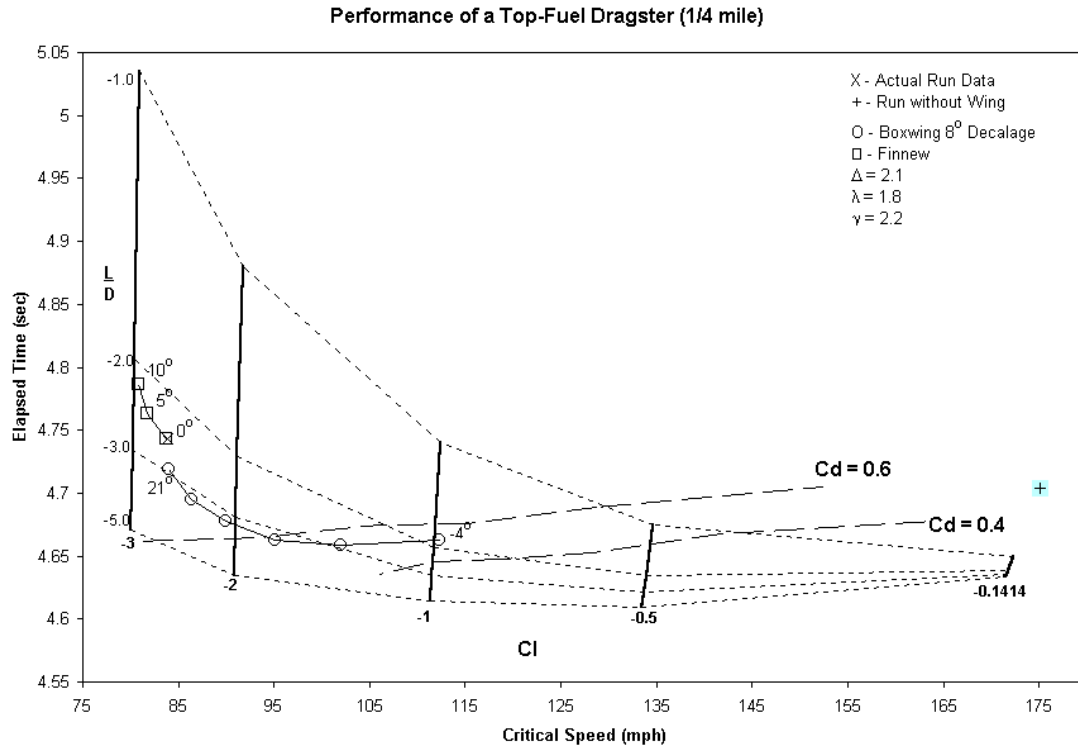


Figure 4-40: Elapsed Time and Speed Data with Different Wing Configurations

4.7.2 Performance Data for Various Input Power Curves

More data was studied looking at how the power input curve distribution effects the performance of the dragster. The wing and car properties were held constant and the input horsepower curve was varied. There are three power curves that were studied as can be seen in Figure 4-41.

The actual power curve depicted on the figure is a curve fit from an actual run of a top-fuel dragster. This is the power curve used as an input to the model to generate all the other model data. Two other power curves were generated to look at how and in what way would the horsepower curve effect the performance of the dragster.

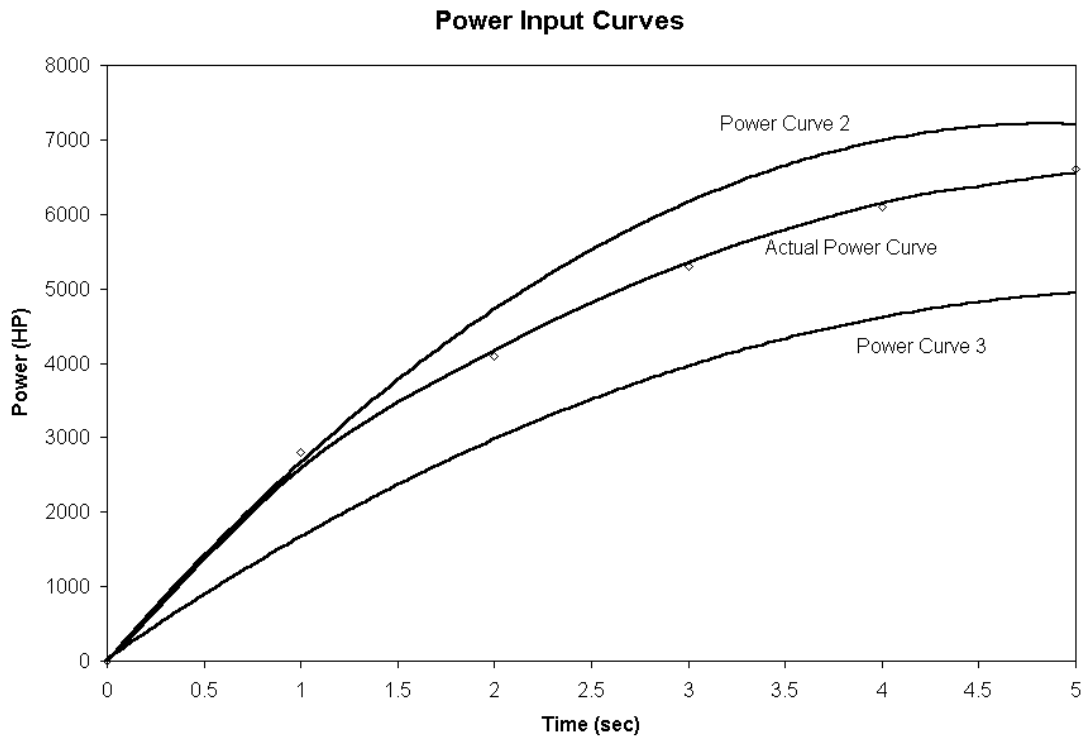


Figure 4-41: Model Power Input Curves to look at Horsepower Effects

This data was used for certain coefficients of lift and a constant drag coefficient of 1.0 to generate Figure 4-42, below. As can be seen the actual power curve is in the middle of the figure. When a lower power curve is used, simulating a dragster that has a reduced amount of power or maybe a slower start than usual, depicted by power curve three in Figure 4-41, the elapsed times increase and the top speed decrease considerably. For this power curve data the coefficients of lift can be looked at in more detail. For a higher lift coefficient like -3 the elapsed time is higher than that with a lower coefficient of lift such as -0.5. This is a different trend for larger power curves where the elapsed

time improves as the coefficient of lift is increased as can be seen for the actual power curve as well as power curve two.

Power curve two as seen in Figure 4-41 increases the top speed and decreases the elapsed time of the dragster. The power curve has a higher horsepower curve than that of the actual power curve. There is an improvement in the performance of the dragster. Even having this higher power curve with a coefficient of lift of -0.5 compared to the actual power curve with a higher coefficient of lift, such as -3, produces a lower elapsed time.

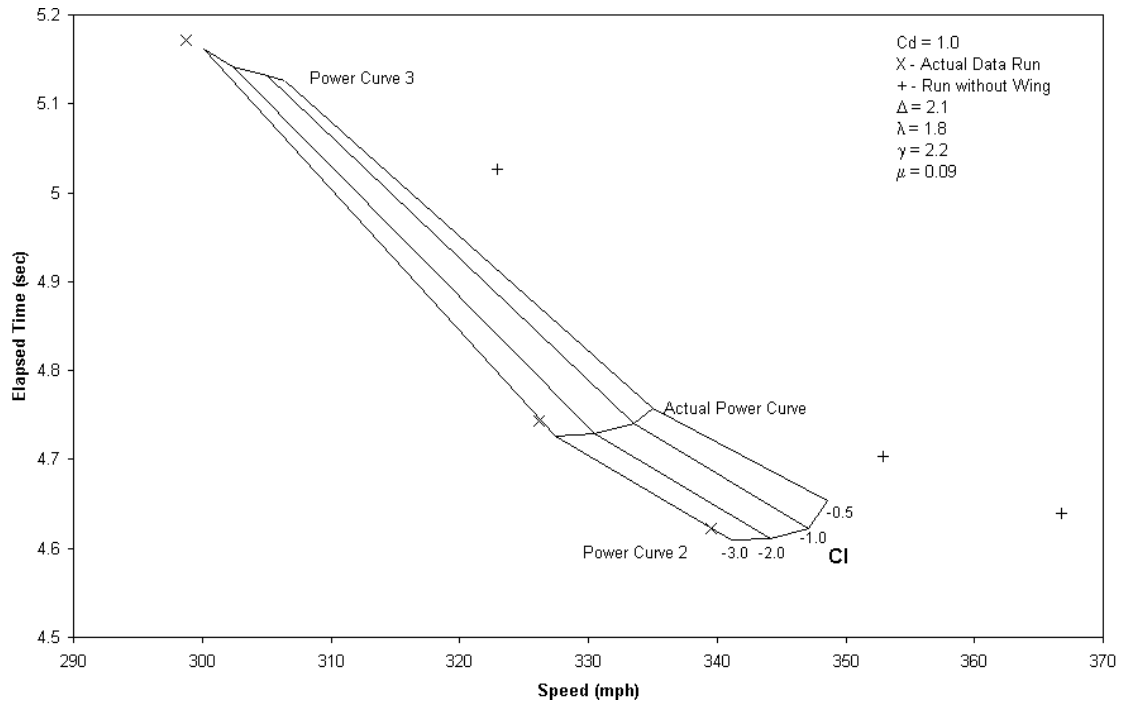


Figure 4-42: Power Curve Input Effects on Elapsed Time and Top Speed

This tells us that more power is important when it can be generated but whether more that power curve two is better has not been studied. Lower power curves, such as

power curve three, start to show that if the dragster has a reduction in power that it is better to have a lower lift coefficient. These three power curves were the only ones studied but a lot can be learned from them as far as performance effects are concerned.

What also should be noted in Figure 4-42 is the performance effects of the dragsters with and without the rear wing. The dragsters with the wings are represented by the "X" marks in the figure and the dragster without the wing is represented by the "+" marks. For the lower power curves the dragster without the wing out performs the dragster with the rear wing. For a dragster with greater power as in the actual power curve data, the dragster without the rear wing still has an advantage, elapsed time wise, over the dragster with the wing. When the highest power curve is looked at, power curve 2, the dragster with the wing has a lower elapsed time than the dragster without a rear wing.

This tells us that for lower powered dragsters, keeping all other parameters the same, it is better to take the rear wing off. If a dragster were to increase the power used today then the team would be more advantageous to put the wing on if having a rear wing or not were their only choices. I do want to reinstate the fact that these are not the only choices. As was shown previously, for the current dragsters today, using a lower drag wing with higher lift to drag ratios is better than no wing but using no rear wing right now is better than using the wings that the dragsters are currently using.

CHAPTER 5

5. CONCLUSIONS AND RECOMMENDATIONS

5.1 Conclusions

By modeling the performance of a dragster and looking at the effects that aerodynamics has of the performance of a dragster has proven very beneficial. It gives us an insight into the questions of how much down force is needed and how changing these aerodynamic characteristics will truly effect the performance of the dragster. It was always said that these dragsters want as much down force as possible but from this model it is not necessarily true. What was shown to be the most beneficial is the reduction of the drag and the reduction of the coefficient of lift up to a certain point. The improvement to the lift to drag ratio is important as well and was the case for the new endplate design.

5.1.1 Dynamic Dragster Model

The dragster model matched actual top-fuel dragster data very well. It functioned in a manner that allowed me to show how each of the aerodynamic parameters, lift and drag, affect the performance of the dragster. It led to the study of improving wind design

by improving the current wing and also led to the knowledge of how a different style of wing might improve the performance even better.

5.1.2 Endplate Effects on a Top-Fuel Dragster Rear Wing

The study of endplate effects on top-fuel dragster wings proved to be beneficial in understanding how and to what extent an endplate has on the flow over a wing. The results presented led to vast improvements in rear wing design and helped two different top-fuel dragsters prevail on top of two different world records.

The addition of the new endplate improved the effectiveness of the wing. It allowed for a more uniform load distribution over the entire span of the wing. This in turn produced a greater down force and since it reduced the amount of spillover, or disruptive flow to the suction side, it reduced the amount of induced drag. With the new endplate design there was an increase of almost 7.2%, over the wing with the style 3 endplate, in terms of the ratio of down force to drag.

It should be noted that this solution does not take into consideration compressibility effects and since there is not any experimental data to compare it to the percent error cannot be provided.

5.1.3 Boxwing Design

The boxwing design compared to the currently used dragster wings showed much improvement to the overall performance of the dragster. The model was able to show how the lift and drag effected the performance of the dragster and this provided the

insight as to what characteristics were needed for the new dragster rear wing. With this wing we were able to get to a lower elapsed time and a higher top speed.

This was done to reduce the drag since it takes so much horsepower to drag the currently used dragster rear wings through the air. By reducing the induced drag of the wing we were able to shift the horsepower that was saved into accelerating the car. This amounted to quicker elapsed times and faster speeds which was one of the motives behind this research.

5.2 Recommendations

Improvement to this research can be made in a number of ways. Recommendations will be made starting with modeling of the dragster and going thru to each of the parts of this project all the way to the boxwing design.

5.2.1 Dynamic Dragster Model

Although the dragster model worked well in showing the trends of the aerodynamic affects on performance it did not have some features that might be very beneficial to dragster teams. Many of the parameters for this program were not actual parameters but estimated parameters because this information was hard to get. Future work might include collecting data from actual runs that will show how close the estimations were to the actual parameters. The parameters did give accurate enough results to enable me to match actual run data that was shown in the validation section.

Other recommendations might be to add other features to the program that might enable a dragster team to get the dragster ready for a particular track and weather conditions. Such features could include track conditions as far as where the track is slippery or any conditions that a dragster team might look for when setting up the dragster. A feature that might be nice is adding a clutch that you can set up to shift for given parameters.

5.2.2 Endplate Design Improvements

Although improvements to the wing characteristics were made by changing the endplate geometry there can still be some changes made to further optimize the design. The shape of the wing was not truly optimized but merely a change in design of the endplate was chosen that would see the extent of the improvement that such a change could make. Further design could be done to improve upon this endplate so as to truly optimize it for design.

Another consideration would be to consider the cost of the wing and try to make changes that could not only improve the design but also reduce the cost of the wing itself. Since the wings are made of carbon fiber the cost can be expensive to produce. Improvements in design could reduce the amount of material used and therefore reduce the cost.

Further, structural analysis could be done using a finite element code, such as STARS, to look at the strength of the various parts of the wing. The inner workings of the wing as well as the attaching mechanism should be studied to see if modification could be done to reduce weight.

5.2.3 Boxwing Design

The boxwing design showed to reduce the elapsed time of the dragster as well as increase the top speed when compared to a wing that is currently being used on several top-fuel dragsters. This wing was in no way optimized to its full potential. There are many parameters that can be looked at such as the decalage angle as well as the endplate design used and looking into the structural and support of the wing could also be studied.

The decalage angles of 0° , 8° and 12° were studied and analyzed. Refining these angles would more than likely show better performance characteristics could be achieved. Having this range allowed me to see how this parameter affected this wing performance but not a lot of time was spent on getting the best decalage angle.

5.2.4 Stability of the Dragster

It is good to note that before the implementation of this new dragster wing that careful analysis be done on the stability of the dragsters. Since these wings have less drag and they allow the dragsters to function at higher speeds they should be once again analyzed to make sure that they are still safe.

BIBLIOGRAPHY

- Arena, A.S. Jr. (1998-2000). Associate Professor, Oklahoma State University. Personal Communications.
- Cogotti, A., "Aerodynamic Characteristics of Car Wheels," *International Journal of Vehicle Design*, Technological Advances in Vehicle Design Series, SP3, Impact of Aerodynamics on Vehicle Design, pp. 173-196, 1983.
- Gupta, K.K., "STARS-An Integrated, Multidisciplinary, Finite-Element, Structural, Fluids, Aeroelastic, and Aeroservoelastic Analysis Computer Program", NASA Technical Memorandum 4795, 1997.
- Hallum, C., "The Magic of the Drag Tire", Society of Automotive Engineers Inc. Paper No. 942484, 1994.
- Hawks, R.J. and C.L. Sayre, "Aerodynamics and Automobile Performance," *Advances in Road Vehicle Aerodynamics 1973*, pp. 1-13, BHRA Fluid Engineering (1973).
- Katz, J., *Race Car Aerodynamics: Designing for Speed*, Robert Bentley Publishers, 1995.
- Milliken, W.F. and D.L. Milliken, *Race Car Vehicle Dynamics*, Society of Automotive Engineers International, 1995.
- Munson, B.R., Young, D.F., and T.H. Okiishi, *Fundamentals of Fluid Mechanics*, 2nd Edition, John Wiley and Sons Inc., 1994.
- Raymer, D.P., *Aircraft Design: A Conceptual Approach*, 2nd Edition, American Institute of Aeronautics and Astronautics, 1992.
- Selig, M., Airfoil data for Selig 1223, University of Illinois, Urbana, Illinois, July 14, 1995.
- Smith, A.M.O., "High Lift Aerodynamics," *Journal of Aircraft*, Volume 12, Number 6, 1975, pp. 501-530.
- Stapleford, W.R. and G.W. Carr, "Aerodynamic Characteristics of Exposed Rotating Wheels", MIRA Report No. 1970/2, 1969.

Stephens, C.H., "CFD-Based Aeroservoelastic Predictions on a Benchmark Configuration using the Transpiration Method", *Masters Thesis*, Oklahoma State University, July 1998.

Winn, R.C., Kohlman, D.L., and Kenner, M.T., "Optimal Wing Design for Top-Fuel Dragsters", American Institute of Aeronautics and Astronautics, Paper No. 99-0464, 1999.

2000 NHRA Rulebook, National Hot Rod Association, 1999.

APPENDICES

APPENDIX A-1

STARS-CFD Geometry Data File (*fin.sur*)

1 Geometry definition...fin	335.7900 0.000 -123.43542	36
26 12	353.0100 0.000 -87.24390	0.000 0.000 0.000
Curves	362.8500 0.000 -54.66120	0.0355 0.000 -0.1650
1 1	367.7700 0.000 -24.56802	0.0500 0.000 -0.2000
21	369.0000 0.000 0.000	0.1250 0.000 -0.3438
-123.0000 0.000 0.000	3 1	0.1875 0.000 -0.4375
-121.7700 0.000 24.5680	36	0.3438 0.000 -0.6560
-116.8500 0.000 54.6612	0.000 0.000 0.000	0.5000 0.000 -0.8073
-107.0100 0.000 87.2439	0.0355 0.000 0.1008	0.7500 0.000 -1.0500
-89.7900 0.000 123.4354	0.0500 0.000 0.1280	1.0000 0.000 -1.2280
-68.8800 0.000 153.9419	0.1250 0.000 0.2295	1.5000 0.000 -1.5251
-39.3600 0.000 184.8124	0.1875 0.000 0.2700	2.0000 0.000 -1.7441
-7.3800 0.000 208.6080	0.3438 0.000 0.3338	2.5000 0.000 -1.9078
29.5200 0.000 227.5475	0.5000 0.000 0.3677	3.0000 0.000 -2.0330
71.3400 0.000 240.5142	0.7500 0.000 0.3750	3.5000 0.000 -2.1265
123.0000 0.000 246.0000	1.0000 0.000 0.3969	4.0000 0.000 -2.1939
174.6600 0.000 240.5142	1.5000 0.000 0.4207	4.5000 0.000 -2.2383
216.4800 0.000 227.5475	2.0000 0.000 0.4431	5.0000 0.000 -2.2599
253.3800 0.000 208.6080	2.5000 0.000 0.4654	5.5000 0.000 -2.2648
285.3600 0.000 184.8124	3.0000 0.000 0.4892	6.0000 0.000 -2.2554
314.8800 0.000 153.9419	3.5000 0.000 0.5135	6.5000 0.000 -2.2329
335.7900 0.000 123.4354	4.0000 0.000 0.5392	
353.0100 0.000 87.2439	4.5000 0.000 0.5639	7.0000 0.000 -2.1972
362.8500 0.000 54.6612	5.0000 0.000 0.5880	7.5000 0.000 -2.1456
367.7700 0.000 24.5680	5.5000 0.000 0.6091	8.0000 0.000 -2.0793
369.0000 0.000 0.000	6.0000 0.000 0.6275	8.5000 0.000 -1.9994
2 1	6.5000 0.000 0.6417	9.0000 0.000 -1.9026
21	7.0000 0.000 0.6471	9.5000 0.000 -1.7891
-123.00000 0.000 0.000	7.5000 0.000 0.6386	10.000 0.000 -1.6611
-121.77000 0.000 -24.56802	8.0000 0.000 0.6120	10.5000 0.000 -1.5153
-116.85000 0.000 -54.66120	8.5000 0.000 0.5693	11.0000 0.000 -1.3543
-107.01000 0.000 -87.24390	9.0000 0.000 0.5103	11.5000 0.000 -1.1782
-89.79000 0.000 -123.43542	9.5000 0.000 0.4324	12.0000 0.000 -0.9868
-68.88000 0.000 -153.94188	10.000 0.000 0.3359	12.5000 0.000 -0.7811
-39.36000 0.000 -184.81242	10.5000 0.000 0.2299	13.0000 0.000 -0.5588
-7.38000 0.000 -208.60800	11.0000 0.000 0.1166	13.5000 0.000 -0.3248
29.52000 0.000 -227.54754	11.5000 0.000 0.000	14.0000 0.000 -0.0699
71.34000 0.000 -240.51420	12.0000 0.000 -0.0946	14.1000 0.000 0.000
123.00000 0.000 -246.00000	12.5000 0.000 -0.1530	5 1
174.66000 0.000 -240.5142	13.0000 0.000 -0.1589	54
216.4800 0.000 -227.54754	13.5000 0.000 -0.1024	13.5405 0.000 0.7448
253.3800 0.000 -208.6080	14.0000 0.000 0.0251	13.5428 0.000 0.7860
285.3600 0.000 -184.81242	14.1000 0.000 0.000	13.5549 0.000 0.8269
314.8800 0.000 -153.94188	4 1	13.5766 0.000 0.8673

13.6076	0.000	0.9073	13.8110	0.000	0.5064	17.8346	0.000	4.0035
13.6475	0.000	0.9468	13.8898	0.000	0.4841	17.8647	0.000	4.0882
13.6960	0.000	0.9859	13.9779	0.000	0.4660	17.8992	0.000	4.1770
13.7525	0.000	1.0247	14.0748	0.000	0.4527	17.9376	0.000	4.2700
13.8167	0.000	1.0631	14.1800	0.000	0.4447	17.9797	0.000	4.3670
13.8880	0.000	1.1013	14.2930	0.000	0.4425	18.0250	0.000	4.4677
13.9660	0.000	1.1393	14.4130	0.000	0.4465	18.0732	0.000	4.5722
14.0503	0.000	1.1774	14.5394	0.000	0.4574	18.1239	0.000	4.6802
14.1403	0.000	1.2155	14.6714	0.000	0.4754	18.1766	0.000	4.7918
14.2355	0.000	1.2540	14.8081	0.000	0.5010	18.2314	0.000	4.9077
14.3354	0.000	1.2930	14.9486	0.000	0.5345	18.2905	0.000	5.0334
14.4398	0.000	1.3326	15.0921	0.000	0.5760	18.3530	0.000	5.1628
14.5480	0.000	1.3732	15.2376	0.000	0.6258	18.4185	0.000	5.2941
14.6598	0.000	1.4149	15.3843	0.000	0.6838	18.4864	0.000	5.4270
14.7746	0.000	1.4581	15.5312	0.000	0.7499	18.5565	0.000	5.5611
14.8923	0.000	1.5031	15.6774	0.000	0.8241	18.6283	0.000	5.6960
15.0123	0.000	1.5501	15.8192	0.000	0.9045	18.7015	0.000	5.8314
15.1343	0.000	1.5994	15.9552	0.000	0.9887	18.7757	0.000	5.9669
15.2581	0.000	1.6513	16.0900	0.000	1.0773	18.8505	0.000	6.1020
15.3861	0.000	1.7078	16.2233	0.000	1.1698	18.9255	0.000	6.2363
15.5197	0.000	1.7688	16.3544	0.000	1.2657	19.0004	0.000	6.3694
15.6547	0.000	1.8309	16.4830	0.000	1.3645	19.0748	0.000	6.5010
15.7906	0.000	1.8938	16.6087	0.000	1.4658	19.1485	0.000	6.6305
15.9269	0.000	1.9577	16.7310	0.000	1.5689	19.2209	0.000	6.7576
16.0631	0.000	2.0225	16.8496	0.000	1.6733	19.2920	0.000	6.8818
16.1987	0.000	2.0880	16.9643	0.000	1.7785	19.3613	0.000	7.0027
16.3332	0.000	2.1541	17.0747	0.000	1.8838	19.4286	0.000	7.1198
16.4662	0.000	2.2207	17.1805	0.000	1.9888	19.4936	0.000	7.2328
16.5971	0.000	2.2876	17.2816	0.000	2.0927	19.5561	0.000	7.3412
16.7255	0.000	2.3545	17.3777	0.000	2.1952	19.6159	0.000	7.4447
16.8509	0.000	2.4211	17.4687	0.000	2.2955	19.6726	0.000	7.5428
16.9729	0.000	2.4872	17.5544	0.000	2.3931	19.7262	0.000	7.6353
17.0911	0.000	2.5524	17.6348	0.000	2.4874	19.7763	0.000	7.7217
17.2050	0.000	2.6165	17.7097	0.000	2.5780	19.8228	0.000	7.8017
17.3142	0.000	2.6790	17.7790	0.000	2.6643	19.8655	0.000	7.8750
17.4184	0.000	2.7397	17.8428	0.000	2.7458	19.9042	0.000	7.9414
17.5171	0.000	2.7980	17.9009	0.000	2.8220	19.9388	0.000	8.0005
17.6101	0.000	2.8538	17.9535	0.000	2.8924	19.9691	0.000	8.0523
17.6970	0.000	2.9066	18.0004	0.000	2.9567	19.9950	0.000	8.0964
17.7774	0.000	2.9561	18.0417	0.000	3.0144	20.0163	0.000	8.1328
17.8512	0.000	3.0020	18.0775	0.000	3.0651	20.0330	0.000	8.1612
17.9179	0.000	3.0439	18.1076	0.000	3.1086	20.0450	0.000	8.1815
17.9774	0.000	3.0816	18.1323	0.000	3.1446	20.0522	0.000	8.1938
18.0295	0.000	3.1148	18.1514	0.000	3.1729	20.0546	0.000	8.1979
18.0739	0.000	3.1433	18.1651	0.000	3.1932	8	1	
18.1104	0.000	3.1669	18.1733	0.000	3.2054	54		
18.1390	0.000	3.1854	18.1760	0.000	3.2095	17.8359	0.000	3.4397
18.1595	0.000	3.1988	7	1		17.8704	0.000	3.4171
18.1719	0.000	3.2068	54			17.9104	0.000	3.4027
18.1760	0.000	3.2095	17.8359	0.000	3.4397	17.9558	0.000	3.3966
6	1		17.8074	0.000	3.4697	18.0063	0.000	3.3991
54			17.7857	0.000	3.5061	18.0619	0.000	3.4102
13.5405	0.000	0.7448	17.7707	0.000	3.5487	18.1221	0.000	3.4302
13.5483	0.000	0.7041	17.7621	0.000	3.5973	18.1867	0.000	3.4592
13.5664	0.000	0.6653	17.7599	0.000	3.6518	18.2551	0.000	3.4973
13.5948	0.000	0.6285	17.7637	0.000	3.7119	18.3268	0.000	3.5445
13.6336	0.000	0.5938	17.7734	0.000	3.7774	18.4013	0.000	3.6010
13.6826	0.000	0.5617	17.7886	0.000	3.8479	18.4780	0.000	3.6668
13.7418	0.000	0.5324	17.8091	0.000	3.9234	18.5561	0.000	3.7417

18.6349	0.000	3.8258	5.0000	29.7500	0.5880	54		
18.7138	0.000	3.9188	5.5000	29.7500	0.6091	13.5405	29.7500	0.7448
18.7921	0.000	4.0205	6.0000	29.7500	0.6275	13.5428	29.7500	0.7860
18.8690	0.000	4.1306	6.5000	29.7500	0.6417	13.5549	29.7500	0.8269
18.9439	0.000	4.2487	7.0000	29.7500	0.6471	13.5766	29.7500	0.8673
19.0161	0.000	4.3744	7.5000	29.7500	0.6386	13.6076	29.7500	0.9073
19.0846	0.000	4.5065	8.0000	29.7500	0.6120	13.6475	29.7500	0.9468
19.1466	0.000	4.6385	8.5000	29.7500	0.5693	13.6960	29.7500	0.9859
19.2062	0.000	4.7740	9.0000	29.7500	0.5103	13.7525	29.7500	1.0247
19.2642	0.000	4.9135	9.5000	29.7500	0.4324	13.8167	29.7500	1.0631
19.3204	0.000	5.0564	10.000	29.7500	0.3359	13.8880	29.7500	1.1013
19.3747	0.000	5.2022	10.5000	29.7500	0.2299	13.9660	29.7500	1.1393
19.4270	0.000	5.3503	11.0000	29.7500	0.1166	14.0503	29.7500	1.1774
19.4772	0.000	5.5001	11.5000	29.7500	0.000	14.1403	29.7500	1.2155
19.5253	0.000	5.6509	12.0000	29.7500	-0.0946	14.2355	29.7500	1.2540
19.5712	0.000	5.8023	12.5000	29.7500	-0.1530	14.3354	29.7500	1.2930
19.6149	0.000	5.9535	13.0000	29.7500	-0.1589	14.4398	29.7500	1.3326
19.6564	0.000	6.1040	13.5000	29.7500	-0.1024	14.5480	29.7500	1.3732
19.6956	0.000	6.2531	14.0000	29.7500	0.0251	14.6598	29.7500	1.4149
19.7325	0.000	6.4004	14.1000	29.7500	0.000	14.7746	29.7500	1.4581
19.7671	0.000	6.5452	10	1		14.8923	29.7500	1.5031
19.7995	0.000	6.6870	36			15.0123	29.7500	1.5501
19.8296	0.000	6.8252	0.000	29.7500	0.000	15.1343	29.7500	1.5994
19.8576	0.000	6.9592	0.0355	29.7500	-0.1650	15.2581	29.7500	1.6513
19.8833	0.000	7.0887	0.0500	29.7500	-0.2000	15.3861	29.7500	1.7078
19.9069	0.000	7.2130	0.1250	29.7500	-0.3438	15.5197	29.7500	1.7688
19.9284	0.000	7.3317	0.1875	29.7500	-0.4375	15.6547	29.7500	1.8309
19.9479	0.000	7.4443	0.3438	29.7500	-0.6560	15.7906	29.7500	1.8938
19.9654	0.000	7.5505	0.5000	29.7500	-0.8073	15.9269	29.7500	1.9577
19.9811	0.000	7.6497	0.7500	29.7500	-1.0500	16.0631	29.7500	2.0225
19.9950	0.000	7.7417	1.0000	29.7500	-1.2280	16.1987	29.7500	2.0880
20.0072	0.000	7.8261	1.5000	29.7500	-1.5251	16.3332	29.7500	2.1541
20.0178	0.000	7.9024	2.0000	29.7500	-1.7441	16.4662	29.7500	2.2207
20.0269	0.000	7.9705	2.5000	29.7500	-1.9078	16.5971	29.7500	2.2876
20.0345	0.000	8.0301	3.0000	29.7500	-2.0330	16.7255	29.7500	2.3545
20.0408	0.000	8.0809	3.5000	29.7500	-2.1265	16.8509	29.7500	2.4211
20.0459	0.000	8.1228	4.0000	29.7500	-2.1939	16.9729	29.7500	2.4872
20.0497	0.000	8.1555	4.5000	29.7500	-2.2383	17.0911	29.7500	2.5524
20.0524	0.000	8.1790	5.0000	29.7500	-2.2599	17.2050	29.7500	2.6165
20.0541	0.000	8.1931	5.5000	29.7500	-2.2648	17.3142	29.7500	2.6790
20.0546	0.000	8.1979	6.0000	29.7500	-2.2554	17.4184	29.7500	2.7397
9	1		6.5000	29.7500	-2.2329	17.5171	29.7500	2.7980
36			7.0000	29.7500	-2.1972	17.6101	29.7500	2.8538
0.000	29.7500	0.000	7.5000	29.7500	-2.1456	17.6970	29.7500	2.9066
0.0355	29.7500	0.1008	8.0000	29.7500	-2.0793	17.7774	29.7500	2.9561
0.0500	29.7500	0.1280	8.5000	29.7500	-1.9994	17.8512	29.7500	3.0020
0.1250	29.7500	0.2295	9.0000	29.7500	-1.9026	17.9179	29.7500	3.0439
0.1875	29.7500	0.2700	9.5000	29.7500	-1.7891	17.9774	29.7500	3.0816
0.3438	29.7500	0.3338	10.000	29.7500	-1.6611	18.0295	29.7500	3.1148
0.5000	29.7500	0.3677	10.5000	29.7500	-1.5153	18.0739	29.7500	3.1433
0.7500	29.7500	0.3750	11.0000	29.7500	-1.3543	18.1104	29.7500	3.1669
1.0000	29.7500	0.3969	11.5000	29.7500	-1.1782	18.1390	29.7500	3.1854
1.5000	29.7500	0.4207	12.0000	29.7500	-0.9868	18.1595	29.7500	3.1988
2.0000	29.7500	0.4431	12.5000	29.7500	-0.7811	18.1719	29.7500	3.2068
2.5000	29.7500	0.4654	13.0000	29.7500	-0.5588	18.1760	29.7500	3.2095
3.0000	29.7500	0.4892	13.5000	29.7500	-0.3248	12	1	
3.5000	29.7500	0.5135	14.0000	29.7500	-0.0699	54		
4.0000	29.7500	0.5392	14.1000	29.7500	0.000	13.5405	29.7500	0.7448
4.5000	29.7500	0.5639	11	1		13.5483	29.7500	0.7041

13.5664	29.7500	0.6653	17.7599	29.7500	3.6518	18.2551	29.7500	3.4973
13.5948	29.7500	0.6285	17.7637	29.7500	3.7119	18.3268	29.7500	3.5445
13.6336	29.7500	0.5938	17.7734	29.7500	3.7774	18.4013	29.7500	3.6010
13.6826	29.7500	0.5617	17.7886	29.7500	3.8479	18.4780	29.7500	3.6668
13.7418	29.7500	0.5324	17.8091	29.7500	3.9234	18.5561	29.7500	3.7417
13.8110	29.7500	0.5064	17.8346	29.7500	4.0035	18.6349	29.7500	3.8258
13.8898	29.7500	0.4841	17.8647	29.7500	4.0882	18.7138	29.7500	3.9188
13.9779	29.7500	0.4660	17.8992	29.7500	4.1770	18.7921	29.7500	4.0205
14.0748	29.7500	0.4527	17.9376	29.7500	4.2700	18.8690	29.7500	4.1306
14.1800	29.7500	0.4447	17.9797	29.7500	4.3670	18.9439	29.7500	4.2487
14.2930	29.7500	0.4425	18.0250	29.7500	4.4677	19.0161	29.7500	4.3744
14.4130	29.7500	0.4465	18.0732	29.7500	4.5722	19.0846	29.7500	4.5065
14.5394	29.7500	0.4574	18.1239	29.7500	4.6802	19.1466	29.7500	4.6385
14.6714	29.7500	0.4754	18.1766	29.7500	4.7918	19.2062	29.7500	4.7740
14.8081	29.7500	0.5010	18.2314	29.7500	4.9077	19.2642	29.7500	4.9135
14.9486	29.7500	0.5345	18.2905	29.7500	5.0334	19.3204	29.7500	5.0564
15.0921	29.7500	0.5760	18.3530	29.7500	5.1628	19.3747	29.7500	5.2022
15.2376	29.7500	0.6258	18.4185	29.7500	5.2941	19.4270	29.7500	5.3503
15.3843	29.7500	0.6838	18.4864	29.7500	5.4270	19.4772	29.7500	5.5001
15.5312	29.7500	0.7499	18.5565	29.7500	5.5611	19.5253	29.7500	5.6509
15.6774	29.7500	0.8241	18.6283	29.7500	5.6960	19.5712	29.7500	5.8023
15.8192	29.7500	0.9045	18.7015	29.7500	5.8314	19.6149	29.7500	5.9535
15.9552	29.7500	0.9887	18.7757	29.7500	5.9669	19.6564	29.7500	6.1040
16.0900	29.7500	1.0773	18.8505	29.7500	6.1020	19.6956	29.7500	6.2531
16.2233	29.7500	1.1698	18.9255	29.7500	6.2363	19.7325	29.7500	6.4004
16.3544	29.7500	1.2657	19.0004	29.7500	6.3694	19.7671	29.7500	6.5452
16.4830	29.7500	1.3645	19.0748	29.7500	6.5010	19.7995	29.7500	6.6870
16.6087	29.7500	1.4658	19.1485	29.7500	6.6305	19.8296	29.7500	6.8252
16.7310	29.7500	1.5689	19.2209	29.7500	6.7576	19.8576	29.7500	6.9592
16.8496	29.7500	1.6733	19.2920	29.7500	6.8818	19.8833	29.7500	7.0887
16.9643	29.7500	1.7785	19.3613	29.7500	7.0027	19.9069	29.7500	7.2130
17.0747	29.7500	1.8838	19.4286	29.7500	7.1198	19.9284	29.7500	7.3317
17.1805	29.7500	1.9888	19.4936	29.7500	7.2328	19.9479	29.7500	7.4443
17.2816	29.7500	2.0927	19.5561	29.7500	7.3412	19.9654	29.7500	7.5505
17.3777	29.7500	2.1952	19.6159	29.7500	7.4447	19.9811	29.7500	7.6497
17.4687	29.7500	2.2955	19.6726	29.7500	7.5428	19.9950	29.7500	7.7417
17.5544	29.7500	2.3931	19.7262	29.7500	7.6353	20.0072	29.7500	7.8261
17.6348	29.7500	2.4874	19.7763	29.7500	7.7217	20.0178	29.7500	7.9024
17.7097	29.7500	2.5780	19.8228	29.7500	7.8017	20.0269	29.7500	7.9705
17.7790	29.7500	2.6643	19.8655	29.7500	7.8750	20.0345	29.7500	8.0301
17.8428	29.7500	2.7458	19.9042	29.7500	7.9414	20.0408	29.7500	8.0809
17.9009	29.7500	2.8220	19.9388	29.7500	8.0005	20.0459	29.7500	8.1228
17.9535	29.7500	2.8924	19.9691	29.7500	8.0523	20.0497	29.7500	8.1555
18.0004	29.7500	2.9567	19.9950	29.7500	8.0964	20.0524	29.7500	8.1790
18.0417	29.7500	3.0144	20.0163	29.7500	8.1328	20.0541	29.7500	8.1931
18.0775	29.7500	3.0651	20.0330	29.7500	8.1612	20.0546	29.7500	8.1979
18.1076	29.7500	3.1086	20.0450	29.7500	8.1815	15	1	
18.1323	29.7500	3.1446	20.0522	29.7500	8.1938	2		
18.1514	29.7500	3.1729	20.0546	29.7500	8.1979	0.000	0.000	0.000
18.1651	29.7500	3.1932	14	1		0.000	29.7500	0.000
18.1733	29.7500	3.2054	54			16	1	
18.1760	29.7500	3.2095	17.8359	29.7500	3.4397	2		
13	1		17.8704	29.7500	3.4171	14.1000	0.000	0.000
54			17.9104	29.7500	3.4027	14.1000	29.7500	0.000
17.8359	29.7500	3.4397	17.9558	29.7500	3.3966	17	1	
17.8074	29.7500	3.4697	18.0063	29.7500	3.3991	2		
17.7857	29.7500	3.5061	18.0619	29.7500	3.4102	13.5405	0.000	0.7448
17.7707	29.7500	3.5487	18.1221	29.7500	3.4302	13.5405	29.7500	0.7448
17.7621	29.7500	3.5973	18.1867	29.7500	3.4592	18	1	

2			9.0000	30.000	-13.7000	-140.000	0.000	260.000
18.1760	0.000	3.2095	7.9500	30.000	-13.7000	380.000	0.000	260.000
18.1760	29.7500	3.2095	6.9500	30.000	-13.2500	2	1	
19	1		6.4500	30.000	-12.9000	21	21	
2			5.9000	30.000	-12.3500	-123.0000	0.000	0.000
17.8359	0.000	3.4397	4.8000	30.000	-11.0800	-121.7700	0.000	24.5680
17.8359	29.7500	3.4397	1.2000	30.000	-6.6100	-116.8500	0.000	54.6612
20	1		0.2000	30.000	-5.1800	-107.0100	0.000	87.2439
2			-0.3500	30.000	-4.3000	-89.7900	0.000	123.4354
20.0546	0.000	8.1979	-0.6800	30.000	-3.7500	-68.8800	0.000	153.9419
20.0546	29.7500	8.1979	-0.9200	30.000	-3.3500	-39.3600	0.000	184.8124
21	1		-1.1800	30.000	-2.7300	-7.3800	0.000	208.6080
41			-1.3500	30.000	-2.3500	29.5200	0.000	227.5475
21.3500	29.7500	-13.7000	-1.5000	30.000	-1.9500	71.3400	0.000	240.5142
15.0000	29.7500	-13.7000	-1.6500	30.000	-1.5500	123.0000	0.000	246.0000
10.000	29.7500	-13.7000	-1.8600	30.000	-1.0500	174.6600	0.000	240.5142
9.0000	29.7500	-13.7000	-2.0000	30.000	-0.6200	216.4800	0.000	227.5475
7.9500	29.7500	-13.7000	-2.0600	30.000	0.000	253.3800	0.000	208.6080
6.9500	29.7500	-13.2500	-2.0000	30.000	0.6200	285.3600	0.000	184.8124
6.4500	29.7500	-12.9000	-1.8600	30.000	1.0500	314.8800	0.000	153.9419
5.9000	29.7500	-12.3500	-1.6500	30.000	1.5500	335.7900	0.000	123.4354
4.8000	29.7500	-11.0800	-1.5000	30.000	1.9500	353.0100	0.000	87.2439
1.2000	29.7500	-6.6100	-1.3500	30.000	2.3500	362.8500	0.000	54.6612
0.2000	29.7500	-5.1800	-1.1800	30.000	2.7300	367.7700	0.000	24.5680
-0.3500	29.7500	-4.3000	-0.9200	30.000	3.3500	369.0000	0.000	0.000
-0.6800	29.7500	-3.7500	-0.6800	30.000	3.7500	-123.0000	0.000	0.000
-0.9200	29.7500	-3.3500	-0.3500	30.000	4.3000	-121.7700	3.8435	24.2679
-1.1800	29.7500	-2.7300	0.2000	30.000	5.1800	-116.8500	8.5511	53.9896
-1.3500	29.7500	-2.3500	1.2000	30.000	6.6100	-107.010	13.6479	86.1689
-1.5000	29.7500	-1.9500	4.8000	30.000	11.0800	-89.790	19.3096	121.9151
-1.6500	29.7500	-1.5500	5.9000	30.000	12.3500	-68.880	24.0818	152.0477
-1.8600	29.7500	-1.0500	6.4500	30.000	12.9000	-39.360	28.9108	182.5369
-2.0000	29.7500	-0.6200	6.9500	30.000	13.2500	-7.3800	32.6334	206.0398
-2.0600	29.7500	0.000	7.9500	30.000	13.7000	29.5200	35.5961	224.7456
-2.0000	29.7500	0.6200	9.0000	30.000	13.7000	71.3400	37.6247	237.5524
-1.8600	29.7500	1.0500	10.000	30.000	13.7000	123.000	38.4828	242.9717
-1.6500	29.7500	1.5500	15.0000	30.000	13.7000	174.660	37.6247	237.5524
-1.5000	29.7500	1.9500	21.3500	30.000	13.7000	216.480	35.5961	224.7456
-1.3500	29.7500	2.3500	23	1		253.380	32.6334	206.0398
-1.1800	29.7500	2.7300	2			285.360	28.9108	182.5369
-0.9200	29.7500	3.3500	21.3500	29.7500	13.7	314.880	24.0818	152.0477
-0.6800	29.7500	3.7500	21.3500	29.7500	-13.7	335.790	19.3096	121.9151
-0.3500	29.7500	4.3000	24	1		353.0100	13.6479	86.1689
0.2000	29.7500	5.1800	2			362.8500	8.5511	53.9896
1.2000	29.7500	6.6100	21.3500	30.000	13.7	367.7700	3.8435	24.2679
4.8000	29.7500	11.0800	21.3500	30.000	-13.7	369.0000	0.000	0.000
5.9000	29.7500	12.3500	25	1		-123.0000	0.000	0.000
6.4500	29.7500	12.9000	2			-121.7700	7.5923	23.3675
6.9500	29.7500	13.2500	21.3500	29.7500	13.7	-116.850	16.8916	51.9872
7.9500	29.7500	13.7000	21.3500	30.000	13.7	-107.010	26.9597	82.9733
9.0000	29.7500	13.7000	26	1		-89.7900	38.1438	117.3937
10.000	29.7500	13.7000	2			-68.880	47.5706	146.4069
15.0000	29.7500	13.7000	21.3500	29.7500	-13.7	-39.360	57.1098	175.7670
21.3500	29.7500	13.7000	21.3500	30.000	-13.7	-7.3800	64.4632	198.3965
22	1		Surfaces			29.5200	70.3157	216.4087
41			1	1		71.3400	74.3230	228.7431
21.3500	30.000	-13.7000	2	2		123.000	76.0181	233.9608
15.0000	30.000	-13.7000	-140.000	0.000	-260.000	174.660	74.3230	228.7431
10.000	30.000	-13.7000	380.000	0.000	-260.000	216.480	70.3157	216.4087

253.380	64.4632	198.3965	71.3400	170.0694	170.0696	-68.880	146.4073	47.5715
285.360	57.1098	175.7670	123.000	173.9482	173.9491	-39.360	175.7660	57.1089
314.880	47.5706	146.4069	174.660	170.0694	170.0696	-7.3800	198.3974	64.4643
335.790	38.1438	117.3937	216.480	160.8997	160.8988	29.5200	216.4097	70.3166
353.0100	26.9597	82.9733	253.380	147.5076	147.5090	71.3400	228.7428	74.3240
362.8500	16.8916	51.9872	285.360	130.6813	130.6826	123.000	233.9598	76.0189
367.7700	7.5923	23.3675	314.880	108.8532	108.8525	174.660	228.7428	74.3240
369.0000	0.000	0.000	335.7900	87.2823	87.2833	216.480	216.4097	70.3166
-123.0000	0.000	0.000	353.0100	61.6903	61.6894	253.380	198.3974	64.4643
-121.770	11.1542	21.8915	362.8500	38.6521	38.6515	285.360	175.7660	57.1089
-116.850	24.8162	48.7055	367.7700	17.3731	17.3725	314.880	146.4073	47.5715
-107.010	39.6076	77.7335	369.0000	0.000	0.000	335.790	117.3945	38.1448
-89.790	56.0387	109.9817	-123.0000	0.000	0.000	353.0100	82.9733	26.9591
-68.880	69.8880	137.1622	-121.770	19.8769	14.4427	362.8500	51.9870	16.8928
-39.360	83.9025	164.6675	-116.850	44.2228	32.1301	367.7700	23.3667	7.5916
-7.3800	94.7057	185.8702	-107.010	70.5813	51.2812	369.0000	0.000	0.000
29.520	103.3039	202.7458	-89.7900	99.8617	72.5528	-123.0000	0.000	0.000
71.340	109.1912	214.3004	-68.880	124.5414	90.4837	-121.7700	24.2667	3.8425
123.00	111.6816	219.1885	-39.360	149.5154	108.6287	-116.8500	53.9894	8.5510
174.660	109.1912	214.3004	-7.3800	168.7669	122.6162	-107.010	86.1692	13.6481
216.480	103.3039	202.7458	29.520	184.0890	133.7477	-89.7900	121.9162	19.3110
253.380	94.7057	185.8702	71.340	194.5802	141.3713	-68.880	152.0465	24.0809
285.360	83.9025	164.6675	123.000	199.0181	144.5963	-39.360	182.5360	28.9099
314.880	69.8880	137.1622	174.660	194.5802	141.3713	-7.3800	206.0391	32.6344
335.790	56.0387	109.9817	216.480	184.0890	133.7477	29.5200	224.7452	35.5962
353.0100	39.6076	77.7335	253.380	168.7669	122.6162	71.3400	237.5534	37.6257
362.8500	24.8162	48.7055	285.360	149.5154	108.6287	123.000	242.9713	38.4842
367.7700	11.1542	21.8915	314.880	124.5414	90.4837	174.660	237.5534	37.6257
369.0000	0.000	0.000	335.7900	99.8617	72.5528	216.480	224.7452	35.5962
-123.0000	0.000	0.000	353.0100	70.5813	51.2812	253.380	206.0391	32.6344
-121.770	14.4414	19.8768	362.8500	44.2228	32.1301	285.360	182.5360	28.9099
-116.850	32.1297	44.2234	367.7700	19.8769	14.4427	314.880	152.0465	24.0809
-107.010	51.2803	70.5823	369.0000	0.000	0.000	335.790	121.9162	19.3110
-89.7900	72.5537	99.8612	-123.0000	0.000	0.000	353.0100	86.1692	13.6481
-68.880	90.4846	124.5424	-121.770	21.8913	11.1536	362.8500	53.9894	8.5510
-39.360	108.6293	149.5163	-116.850	48.7045	24.8165	367.7700	24.2667	3.8425
-7.380	122.6163	168.7658	-107.010	77.7343	39.6085	369.0000	0.000	0.000
29.520	133.7485	184.0892	-89.7900	109.9821	56.0388	-123.0000	0.000	0.000
71.340	141.3708	194.5811	-68.8800	137.1630	69.8886	-121.7700	24.5692	0.000
123.000	144.5951	199.0189	-39.3600	164.6680	83.9032	-116.8500	54.6624	0.000
174.660	141.3708	194.5811	-7.3800	185.8705	94.7051	-107.0100	87.2433	0.000
216.480	133.7485	184.0892	29.5200	202.7455	103.3052	-89.7900	123.4359	0.000
253.380	122.6163	168.7658	71.3400	214.2999	109.1920	-68.8800	153.9418	0.000
285.360	108.6293	149.5163	123.000	219.1875	111.6815	-39.3600	184.8113	0.000
314.880	90.4846	124.5424	174.660	214.2999	109.1920	-7.3800	208.6074	0.000
335.7900	72.5537	99.8612	216.480	202.7455	103.3052	29.5200	227.5467	0.000
353.0100	51.2803	70.5823	253.380	185.8705	94.7051	71.3400	240.5145	0.000
362.8500	32.1297	44.2234	285.360	164.6680	83.9032	123.0000	246.0000	0.000
367.7700	14.4414	19.8768	314.880	137.1630	69.8886	174.6600	240.5145	0.000
369.0000	0.000	0.000	335.790	109.9821	56.0388	216.4800	227.5467	0.000
-123.0000	0.000	0.000	353.0100	77.7343	39.6085	253.3800	208.6074	0.000
-121.770	17.3731	17.3725	362.8500	48.7045	24.8165	285.3600	184.8113	0.000
-116.850	38.6521	38.6515	367.7700	21.8913	11.1536	314.8800	153.9418	0.000
-107.010	61.6903	61.6894	369.0000	0.000	0.000	335.7900	123.4359	0.000
-89.7900	87.2823	87.2833	-123.0000	0.000	0.000	353.0100	87.2433	0.000
-68.880	108.8532	108.8525	-121.7700	23.3667	7.5916	362.8500	54.6624	0.000
-39.360	130.6813	130.6826	-116.850	51.9870	16.8928	367.7700	24.5692	0.000
-7.3800	147.5076	147.5090	-107.010	82.9733	26.9591	369.0000	0.000	0.000
29.5200	160.8997	160.8988	-89.7900	117.3945	38.1448	-123.0000	0.000	0.000

-121.7700	24.2667	-3.8425	362.850	48.7046	-24.8165	285.36	108.6297	-149.5163
-116.8500	53.9894	-8.5510	367.770	21.8914	-11.1536	314.88	90.4850	-124.5424
-107.010	86.1692	-13.6481	369.0000	0.000	0.000	335.790	72.5540	-99.8612
-89.790	121.9162	-19.3085	-123.0000	0.000	0.000	353.010	51.2805	-70.5823
-68.880	152.0465	-24.0809	-121.770	19.8770	-14.4402	362.850	32.1298	-44.2234
-39.360	182.5360	-28.9099	-116.850	44.2229	-32.1301	367.7700	14.4415	-19.8768
-7.3800	206.0392	-32.6319	-107.010	70.5814	-51.2812	369.0000	0.000	0.000
29.520	224.7453	-35.5962	-89.7900	99.8619	-72.5528	-123.0000	0.000	0.000
71.340	237.5535	-37.6232	-68.880	124.5417	-90.4837	-121.770	11.1542	-21.8915
123.00	242.9714	-38.4818	-39.36	149.5157	-108.6287	-116.850	24.8163	-48.7055
174.660	237.5535	-37.6232	-7.380	168.7672	-122.6162	-107.010	39.6078	-77.7335
216.480	224.7453	-35.5962	29.520	184.0894	-133.7477	-89.790	56.0390	-109.9817
253.380	206.0392	-32.6319	71.340	194.5806	-141.3713	-68.880	69.8884	-137.1622
285.360	182.5360	-28.9099	123.00	199.0184	-144.5939	-39.360	83.9030	-164.6675
314.880	152.0465	-24.0809	174.66	194.5806	-141.3713	-7.3800	94.7062	-185.8702
335.790	121.9162	-19.3085	216.48	184.0894	-133.7477	29.52	103.3045	-202.7458
353.010	86.1692	-13.6481	253.38	168.7672	-122.6162	71.34	109.1918	-214.3004
362.8500	53.9894	-8.5510	285.36	149.5157	-108.6287	123.0	111.6822	-219.1885
367.7700	24.2667	-3.8425	314.88	124.5417	-90.4837	174.66	109.1918	-214.3004
369.0000	0.000	0.000	335.79	99.8619	-72.5528	216.48	103.3045	-202.7458
-123.0000	0.000	0.000	353.010	70.5814	-51.2812	253.38	94.7062	-185.8702
-121.7700	23.3667	-7.5916	362.850	44.2229	-32.1301	285.36	83.9030	-164.6675
-116.850	51.9871	-16.8904	367.770	19.8770	-14.4402	314.88	69.8884	-137.1622
-107.010	82.9734	-26.9591	369.0000	0.000	0.000	335.79	56.0390	-109.9817
-89.790	117.3946	-38.1448	-123.0000	0.000	0.000	353.01	39.6078	-77.7335
-68.880	146.4074	-47.5715	-121.770	17.3731	-17.3725	362.850	24.8163	-48.7055
-39.360	175.7661	-57.1089	-116.850	38.6522	-38.6515	367.770	11.1542	-21.8915
-7.3800	198.3975	-64.4618	-107.010	61.6905	-61.6894	369.0000	0.000	0.000
29.520	216.4099	-70.3166	-89.7900	87.2825	-87.2833	-123.0000	0.000	0.000
71.340	228.7430	-74.3215	-68.88	108.8535	-108.8525	-121.7700	7.5924	-23.3675
123.00	233.9600	-76.0189	-39.36	130.6816	-130.6801	-116.850	16.8917	-51.9872
174.66	228.7430	-74.3215	-7.380	147.5080	-147.5065	-107.010	26.9599	-82.9733
216.48	216.4099	-70.3166	29.520	160.9001	-160.8988	-89.790	38.1441	-117.3937
253.38	198.3975	-64.4618	71.340	170.0698	-170.0696	-68.880	47.5710	-146.4069
285.36	175.7661	-57.1089	123.00	173.9486	-173.9491	-39.360	57.1103	-175.7670
314.88	146.4074	-47.5715	174.66	170.0698	-170.0696	-7.3800	64.4637	-198.3965
335.79	117.3946	-38.1448	216.48	160.9001	-160.8988	29.520	70.3163	-216.4087
353.01	82.9734	-26.9591	253.38	147.5080	-147.5065	71.340	74.3236	-228.7431
362.85	51.9871	-16.8904	285.36	130.6816	-130.6801	123.00	76.0187	-233.9608
367.77	23.3667	-7.5916	314.88	108.8535	-108.8525	174.66	74.3236	-228.7431
369.00	0.000	0.000	335.79	87.2825	-87.2833	216.48	70.3163	-216.4087
-123.0000	0.000	0.000	353.010	61.6905	-61.6894	253.38	64.4637	-198.3965
-121.77	21.8914	-11.1536	362.850	38.6522	-38.6515	285.36	57.1103	-175.7670
-116.85	48.7046	-24.8165	367.770	17.3731	-17.3725	314.88	47.5710	-146.4069
-107.01	77.7345	-39.6085	369.0000	0.000	0.000	335.79	38.1441	-117.3937
-89.790	109.9823	-56.0388	-123.0000	0.000	0.000	353.010	26.9599	-82.9733
-68.880	137.1632	-69.8886	-121.770	14.4415	-19.8768	362.850	16.8917	-51.9872
-39.360	164.6683	-83.9032	-116.850	32.1298	-44.2234	367.7700	7.5924	-23.3675
-7.3800	185.8707	-94.7051	-107.010	51.2805	-70.5823	369.0000	0.000	0.000
29.520	202.7458	-103.3028	-89.7900	72.5540	-99.8612	-123.0000	0.000	0.000
71.340	214.3002	-109.1920	-68.880	90.4850	-124.5424	-121.7700	3.8435	-24.2679
123.0	219.1878	-111.6815	-39.36	108.6297	-149.5163	-116.8500	8.5512	-53.9896
174.66	214.3002	-109.1920	-7.380	122.6167	-168.7658	-107.010	13.6481	-86.1689
216.48	202.7458	-103.3028	29.520	133.7490	-184.0892	-89.790	19.3099	-121.9151
253.38	185.8707	-94.7051	71.340	141.3713	-194.5811	-68.880	24.0822	-152.0452
285.36	164.6683	-83.9032	123.00	144.5956	-199.0189	-39.360	28.9113	-182.5369
314.88	137.1632	-69.8886	174.66	141.3713	-194.5811	-7.3800	32.6339	-206.0398
335.79	109.9823	-56.0388	216.48	133.7490	-184.0892	29.520	35.5967	-224.7456
353.010	77.7345	-39.6085	253.38	122.6167	-168.7658	71.340	37.6254	-237.5524

123.00	38.4835	-242.9717	9.5000	0.000	0.4324	2.0000	0.000	-1.7441
174.66	37.6254	-237.5524	10.000	0.000	0.3359	2.5000	0.000	-1.9078
216.48	35.5967	-224.7456	10.5000	0.000	0.2299	3.0000	0.000	-2.0330
253.38	32.6339	-206.0398	11.0000	0.000	0.1166	3.5000	0.000	-2.1265
285.36	28.9113	-182.5369	11.5000	0.000	0.000	4.0000	0.000	-2.1939
314.88	24.0822	-152.0452	12.0000	0.000	-0.0946	4.5000	0.000	-2.2383
335.79	19.3099	-121.9151	12.5000	0.000	-0.1530	5.0000	0.000	-2.2599
353.010	13.6481	-86.1689	13.0000	0.000	-0.1589	5.5000	0.000	-2.2648
362.8500	8.5512	-53.9896	13.5000	0.000	-0.1024	6.0000	0.000	-2.2554
367.7700	3.8435	-24.2679	14.0000	0.000	0.0251	6.5000	0.000	-2.2329
369.0000	0.000	0.000	14.1000	0.000	0.000	7.0000	0.000	-2.1972
-123.0000	0.000	0.000	0.000	29.7500	0.000	7.5000	0.000	-2.1456
-121.7700	0.000	-24.5680	0.0355	29.7500	0.1008	8.0000	0.000	-2.0793
-116.8500	0.000	-54.6612	0.0500	29.7500	0.1280	8.5000	0.000	-1.9994
-107.0100	0.000	-87.2439	0.1250	29.7500	0.2295	9.0000	0.000	-1.9026
-89.7900	0.000	-123.4354	0.1875	29.7500	0.2700	9.5000	0.000	-1.7891
-68.8800	0.000	-153.9419	0.3438	29.7500	0.3338	10.000	0.000	-1.6611
-39.3600	0.000	-184.8124	0.5000	29.7500	0.3677	10.5000	0.000	-1.5153
-7.3800	0.000	-208.6080	0.7500	29.7500	0.3750	11.0000	0.000	-1.3543
29.5200	0.000	-227.5475	1.0000	29.7500	0.3969	11.5000	0.000	-1.1782
71.3400	0.000	-240.5142	1.5000	29.7500	0.4207	12.0000	0.000	-0.9868
123.0000	0.000	-246.0000	2.0000	29.7500	0.4431	12.5000	0.000	-0.7811
174.6600	0.000	-240.5142	2.5000	29.7500	0.4654	13.0000	0.000	-0.5588
216.4800	0.000	-227.5475	3.0000	29.7500	0.4892	13.5000	0.000	-0.3248
253.3800	0.000	-208.6080	3.5000	29.7500	0.5135	14.0000	0.000	-0.0699
285.3600	0.000	-184.8124	4.0000	29.7500	0.5392	14.1000	0.000	0.000
314.8800	0.000	-153.9419	4.5000	29.7500	0.5639	0.000	29.7500	0.000
335.7900	0.000	-123.4354	5.0000	29.7500	0.5880	0.0355	29.7500	-0.1650
353.0100	0.000	-87.2439	5.5000	29.7500	0.6091	0.0500	29.7500	-0.2000
362.8500	0.000	-54.6612	6.0000	29.7500	0.6275	0.1250	29.7500	-0.3438
367.7700	0.000	-24.5680	6.5000	29.7500	0.6417	0.1875	29.7500	-0.4375
369.0000	0.000	0.000	7.0000	29.7500	0.6471	0.3438	29.7500	-0.6560
3 1			7.5000	29.7500	0.6386	0.5000	29.7500	-0.8073
36 2			8.0000	29.7500	0.6120	0.7500	29.7500	-1.0500
0.000	0.000	0.000	8.5000	29.7500	0.5693	1.0000	29.7500	-1.2280
0.0355	0.000	0.1008	9.0000	29.7500	0.5103	1.5000	29.7500	-1.5251
0.0500	0.000	0.1280	9.5000	29.7500	0.4324	2.0000	29.7500	-1.7441
0.1250	0.000	0.2295	10.000	29.7500	0.3359	2.5000	29.7500	-1.9078
0.1875	0.000	0.2700	10.5000	29.7500	0.2299	3.0000	29.7500	-2.0330
0.3438	0.000	0.3338	11.0000	29.7500	0.1166	3.5000	29.7500	-2.1265
0.5000	0.000	0.3677	11.5000	29.7500	0.000	4.0000	29.7500	-2.1939
0.7500	0.000	0.3750	12.0000	29.7500	-0.0946	4.5000	29.7500	-2.2383
1.0000	0.000	0.3969	12.5000	29.7500	-0.1530	5.0000	29.7500	-2.2599
1.5000	0.000	0.4207	13.0000	29.7500	-0.1589	5.5000	29.7500	-2.2648
2.0000	0.000	0.4431	13.5000	29.7500	-0.1024	6.0000	29.7500	-2.2554
2.5000	0.000	0.4654	14.0000	29.7500	0.0251	6.5000	29.7500	-2.2329
3.0000	0.000	0.4892	14.1000	29.7500	0.000	7.0000	29.7500	-2.1972
3.5000	0.000	0.5135	4 1			7.5000	29.7500	-2.1456
4.0000	0.000	0.5392	36 2			8.0000	29.7500	-2.0793
4.5000	0.000	0.5639	0.000	0.000	0.000	8.5000	29.7500	-1.9994
5.0000	0.000	0.5880	0.0355	0.000	-0.1650	9.0000	29.7500	-1.9026
5.5000	0.000	0.6091	0.0500	0.000	-0.2000	9.5000	29.7500	-1.7891
6.0000	0.000	0.6275	0.1250	0.000	-0.3438	10.000	29.7500	-1.6611
6.5000	0.000	0.6417	0.1875	0.000	-0.4375	10.5000	29.7500	-1.5153
7.0000	0.000	0.6471	0.3438	0.000	-0.6560	11.0000	29.7500	-1.3543
7.5000	0.000	0.6386	0.5000	0.000	-0.8073	11.5000	29.7500	-1.1782
8.0000	0.000	0.6120	0.7500	0.000	-1.0500	12.0000	29.7500	-0.9868
8.5000	0.000	0.5693	1.0000	0.000	-1.2280	12.5000	29.7500	-0.7811
9.0000	0.000	0.5103	1.5000	0.000	-1.5251	13.0000	29.7500	-0.5588

13.5000	29.7500	-0.3248	13.5405	29.7500	0.7448	13.5948	0.000	0.6285
14.0000	29.7500	-0.0699	13.5428	29.7500	0.7860	13.6336	0.000	0.5938
14.1000	29.7500	0.000	13.5549	29.7500	0.8269	13.6826	0.000	0.5617
5 1			13.5766	29.7500	0.8673	13.7418	0.000	0.5324
54 2			13.6076	29.7500	0.9073	13.8110	0.000	0.5064
13.5405	0.000	0.7448	13.6475	29.7500	0.9468	13.8898	0.000	0.4841
13.5428	0.000	0.7860	13.6960	29.7500	0.9859	13.9779	0.000	0.4660
13.5549	0.000	0.8269	13.7525	29.7500	1.0247	14.0748	0.000	0.4527
13.5766	0.000	0.8673	13.8167	29.7500	1.0631	14.1800	0.000	0.4447
13.6076	0.000	0.9073	13.8880	29.7500	1.1013	14.2930	0.000	0.4425
13.6475	0.000	0.9468	13.9660	29.7500	1.1393	14.4130	0.000	0.4465
13.6960	0.000	0.9859	14.0503	29.7500	1.1774	14.5394	0.000	0.4574
13.7525	0.000	1.0247	14.1403	29.7500	1.2155	14.6714	0.000	0.4754
13.8167	0.000	1.0631	14.2355	29.7500	1.2540	14.8081	0.000	0.5010
13.8880	0.000	1.1013	14.3354	29.7500	1.2930	14.9486	0.000	0.5345
13.9660	0.000	1.1393	14.4398	29.7500	1.3326	15.0921	0.000	0.5760
14.0503	0.000	1.1774	14.5480	29.7500	1.3732	15.2376	0.000	0.6258
14.1403	0.000	1.2155	14.6598	29.7500	1.4149	15.3843	0.000	0.6838
14.2355	0.000	1.2540	14.7746	29.7500	1.4581	15.5312	0.000	0.7499
14.3354	0.000	1.2930	14.8923	29.7500	1.5031	15.6774	0.000	0.8241
14.4398	0.000	1.3326	15.0123	29.7500	1.5501	15.8192	0.000	0.9045
14.5480	0.000	1.3732	15.1343	29.7500	1.5994	15.9552	0.000	0.9887
14.6598	0.000	1.4149	15.2581	29.7500	1.6513	16.0900	0.000	1.0773
14.7746	0.000	1.4581	15.3861	29.7500	1.7078	16.2233	0.000	1.1698
14.8923	0.000	1.5031	15.5197	29.7500	1.7688	16.3544	0.000	1.2657
15.0123	0.000	1.5501	15.6547	29.7500	1.8309	16.4830	0.000	1.3645
15.1343	0.000	1.5994	15.7906	29.7500	1.8938	16.6087	0.000	1.4658
15.2581	0.000	1.6513	15.9269	29.7500	1.9577	16.7310	0.000	1.5689
15.3861	0.000	1.7078	16.0631	29.7500	2.0225	16.8496	0.000	1.6733
15.5197	0.000	1.7688	16.1987	29.7500	2.0880	16.9643	0.000	1.7785
15.6547	0.000	1.8309	16.3332	29.7500	2.1541	17.0747	0.000	1.8838
15.7906	0.000	1.8938	16.4662	29.7500	2.2207	17.1805	0.000	1.9888
15.9269	0.000	1.9577	16.5971	29.7500	2.2876	17.2816	0.000	2.0927
16.0631	0.000	2.0225	16.7255	29.7500	2.3545	17.3777	0.000	2.1952
16.1987	0.000	2.0880	16.8509	29.7500	2.4211	17.4687	0.000	2.2955
16.3332	0.000	2.1541	16.9729	29.7500	2.4872	17.5544	0.000	2.3931
16.4662	0.000	2.2207	17.0911	29.7500	2.5524	17.6348	0.000	2.4874
16.5971	0.000	2.2876	17.2050	29.7500	2.6165	17.7097	0.000	2.5780
16.7255	0.000	2.3545	17.3142	29.7500	2.6790	17.7790	0.000	2.6643
16.8509	0.000	2.4211	17.4184	29.7500	2.7397	17.8428	0.000	2.7458
16.9729	0.000	2.4872	17.5171	29.7500	2.7980	17.9009	0.000	2.8220
17.0911	0.000	2.5524	17.6101	29.7500	2.8538	17.9535	0.000	2.8924
17.2050	0.000	2.6165	17.6970	29.7500	2.9066	18.0004	0.000	2.9567
17.3142	0.000	2.6790	17.7774	29.7500	2.9561	18.0417	0.000	3.0144
17.4184	0.000	2.7397	17.8512	29.7500	3.0020	18.0775	0.000	3.0651
17.5171	0.000	2.7980	17.9179	29.7500	3.0439	18.1076	0.000	3.1086
17.6101	0.000	2.8538	17.9774	29.7500	3.0816	18.1323	0.000	3.1446
17.6970	0.000	2.9066	18.0295	29.7500	3.1148	18.1514	0.000	3.1729
17.7774	0.000	2.9561	18.0739	29.7500	3.1433	18.1651	0.000	3.1932
17.8512	0.000	3.0020	18.1104	29.7500	3.1669	18.1733	0.000	3.2054
17.9179	0.000	3.0439	18.1390	29.7500	3.1854	18.1760	0.000	3.2095
17.9774	0.000	3.0816	18.1595	29.7500	3.1988	13.5405	29.7500	0.7448
18.0295	0.000	3.1148	18.1719	29.7500	3.2068	13.5483	29.7500	0.7041
18.0739	0.000	3.1433	18.1760	29.7500	3.2095	13.5664	29.7500	0.6653
18.1104	0.000	3.1669	6 1			13.5948	29.7500	0.6285
18.1390	0.000	3.1854	54 2			13.6336	29.7500	0.5938
18.1595	0.000	3.1988	13.5405	0.000	0.7448	13.6826	29.7500	0.5617
18.1719	0.000	3.2068	13.5483	0.000	0.7041	13.7418	29.7500	0.5324
18.1760	0.000	3.2095	13.5664	0.000	0.6653	13.8110	29.7500	0.5064

13.8898	29.7500	0.4841	17.8647	0.000	4.0882	18.0732	29.7500	4.5722
13.9779	29.7500	0.4660	17.8992	0.000	4.1770	18.1239	29.7500	4.6802
14.0748	29.7500	0.4527	17.9376	0.000	4.2700	18.1766	29.7500	4.7918
14.1800	29.7500	0.4447	17.9797	0.000	4.3670	18.2314	29.7500	4.9077
14.2930	29.7500	0.4425	18.0250	0.000	4.4677	18.2905	29.7500	5.0334
14.4130	29.7500	0.4465	18.0732	0.000	4.5722	18.3530	29.7500	5.1628
14.5394	29.7500	0.4574	18.1239	0.000	4.6802	18.4185	29.7500	5.2941
14.6714	29.7500	0.4754	18.1766	0.000	4.7918	18.4864	29.7500	5.4270
14.8081	29.7500	0.5010	18.2314	0.000	4.9077	18.5565	29.7500	5.5611
14.9486	29.7500	0.5345	18.2905	0.000	5.0334	18.6283	29.7500	5.6960
15.0921	29.7500	0.5760	18.3530	0.000	5.1628	18.7015	29.7500	5.8314
15.2376	29.7500	0.6258	18.4185	0.000	5.2941	18.7757	29.7500	5.9669
15.3843	29.7500	0.6838	18.4864	0.000	5.4270	18.8505	29.7500	6.1020
15.5312	29.7500	0.7499	18.5565	0.000	5.5611	18.9255	29.7500	6.2363
15.6774	29.7500	0.8241	18.6283	0.000	5.6960	19.0004	29.7500	6.3694
15.8192	29.7500	0.9045	18.7015	0.000	5.8314	19.0748	29.7500	6.5010
15.9552	29.7500	0.9887	18.7757	0.000	5.9669	19.1485	29.7500	6.6305
16.0900	29.7500	1.0773	18.8505	0.000	6.1020	19.2209	29.7500	6.7576
16.2233	29.7500	1.1698	18.9255	0.000	6.2363	19.2920	29.7500	6.8818
16.3544	29.7500	1.2657	19.0004	0.000	6.3694	19.3613	29.7500	7.0027
16.4830	29.7500	1.3645	19.0748	0.000	6.5010	19.4286	29.7500	7.1198
16.6087	29.7500	1.4658	19.1485	0.000	6.6305	19.4936	29.7500	7.2328
16.7310	29.7500	1.5689	19.2209	0.000	6.7576	19.5561	29.7500	7.3412
16.8496	29.7500	1.6733	19.2920	0.000	6.8818	19.6159	29.7500	7.4447
16.9643	29.7500	1.7785	19.3613	0.000	7.0027	19.6726	29.7500	7.5428
17.0747	29.7500	1.8838	19.4286	0.000	7.1198	19.7262	29.7500	7.6353
17.1805	29.7500	1.9888	19.4936	0.000	7.2328	19.7763	29.7500	7.7217
17.2816	29.7500	2.0927	19.5561	0.000	7.3412	19.8228	29.7500	7.8017
17.3777	29.7500	2.1952	19.6159	0.000	7.4447	19.8655	29.7500	7.8750
17.4687	29.7500	2.2955	19.6726	0.000	7.5428	19.9042	29.7500	7.9414
17.5544	29.7500	2.3931	19.7262	0.000	7.6353	19.9388	29.7500	8.0005
17.6348	29.7500	2.4874	19.7763	0.000	7.7217	19.9691	29.7500	8.0523
17.7097	29.7500	2.5780	19.8228	0.000	7.8017	19.9950	29.7500	8.0964
17.7790	29.7500	2.6643	19.8655	0.000	7.8750	20.0163	29.7500	8.1328
17.8428	29.7500	2.7458	19.9042	0.000	7.9414	20.0330	29.7500	8.1612
17.9009	29.7500	2.8220	19.9388	0.000	8.0005	20.0450	29.7500	8.1815
17.9535	29.7500	2.8924	19.9691	0.000	8.0523	20.0522	29.7500	8.1938
18.0004	29.7500	2.9567	19.9950	0.000	8.0964	20.0546	29.7500	8.1979
18.0417	29.7500	3.0144	20.0163	0.000	8.1328	8	1	
18.0775	29.7500	3.0651	20.0330	0.000	8.1612	54	2	
18.1076	29.7500	3.1086	20.0450	0.000	8.1815	17.8359	0.000	3.4397
18.1323	29.7500	3.1446	20.0522	0.000	8.1938	17.8704	0.000	3.4171
18.1514	29.7500	3.1729	20.0546	0.000	8.1979	17.9104	0.000	3.4027
18.1651	29.7500	3.1932	17.8359	29.7500	3.4397	17.9558	0.000	3.3966
18.1733	29.7500	3.2054	17.8074	29.7500	3.4697	18.0063	0.000	3.3991
18.1760	29.7500	3.2095	17.7857	29.7500	3.5061	18.0619	0.000	3.4102
7	1		17.7707	29.7500	3.5487	18.1221	0.000	3.4302
54	2		17.7621	29.7500	3.5973	18.1867	0.000	3.4592
17.8359	0.000	3.4397	17.7599	29.7500	3.6518	18.2551	0.000	3.4973
17.8074	0.000	3.4697	17.7637	29.7500	3.7119	18.3268	0.000	3.5445
17.7857	0.000	3.5061	17.7734	29.7500	3.7774	18.4013	0.000	3.6010
17.7707	0.000	3.5487	17.7886	29.7500	3.8479	18.4780	0.000	3.6668
17.7621	0.000	3.5973	17.8091	29.7500	3.9234	18.5561	0.000	3.7417
17.7599	0.000	3.6518	17.8346	29.7500	4.0035	18.6349	0.000	3.8258
17.7637	0.000	3.7119	17.8647	29.7500	4.0882	18.7138	0.000	3.9188
17.7734	0.000	3.7774	17.8992	29.7500	4.1770	18.7921	0.000	4.0205
17.7886	0.000	3.8479	17.9376	29.7500	4.2700	18.8690	0.000	4.1306
17.8091	0.000	3.9234	17.9797	29.7500	4.3670	18.9439	0.000	4.2487
17.8346	0.000	4.0035	18.0250	29.7500	4.4677	19.0161	0.000	4.3744

19.0846	0.000	4.5065	19.3747	29.7500	5.2022	1.2000	29.7500	-6.6100
19.1466	0.000	4.6385	19.4270	29.7500	5.3503	0.2000	29.7500	-5.1800
19.2062	0.000	4.7740	19.4772	29.7500	5.5001	-0.3500	29.7500	-4.3000
19.2642	0.000	4.9135	19.5253	29.7500	5.6509	-0.6800	29.7500	-3.7500
19.3204	0.000	5.0564	19.5712	29.7500	5.8023	-0.9200	29.7500	-3.3500
19.3747	0.000	5.2022	19.6149	29.7500	5.9535	-1.1800	29.7500	-2.7300
19.4270	0.000	5.3503	19.6564	29.7500	6.1040	-1.3500	29.7500	-2.3500
19.4772	0.000	5.5001	19.6956	29.7500	6.2531	-1.5000	29.7500	-1.9500
19.5253	0.000	5.6509	19.7325	29.7500	6.4004	-1.6500	29.7500	-1.5500
19.5712	0.000	5.8023	19.7671	29.7500	6.5452	-1.8600	29.7500	-1.0500
19.6149	0.000	5.9535	19.7995	29.7500	6.6870	-2.0000	29.7500	-0.6200
19.6564	0.000	6.1040	19.8296	29.7500	6.8252	-2.0600	29.7500	0.000
19.6956	0.000	6.2531	19.8576	29.7500	6.9592	-2.0000	29.7500	0.6200
19.7325	0.000	6.4004	19.8833	29.7500	7.0887	-1.8600	29.7500	1.0500
19.7671	0.000	6.5452	19.9069	29.7500	7.2130	-1.6500	29.7500	1.5500
19.7995	0.000	6.6870	19.9284	29.7500	7.3317	-1.5000	29.7500	1.9500
19.8296	0.000	6.8252	19.9479	29.7500	7.4443	-1.3500	29.7500	2.3500
19.8576	0.000	6.9592	19.9654	29.7500	7.5505	-1.1800	29.7500	2.7300
19.8833	0.000	7.0887	19.9811	29.7500	7.6497	-0.9200	29.7500	3.3500
19.9069	0.000	7.2130	19.9950	29.7500	7.7417	-0.6800	29.7500	3.7500
19.9284	0.000	7.3317	20.0072	29.7500	7.8261	-0.3500	29.7500	4.3000
19.9479	0.000	7.4443	20.0178	29.7500	7.9024	0.2000	29.7500	5.1800
19.9654	0.000	7.5505	20.0269	29.7500	7.9705	1.2000	29.7500	6.6100
19.9811	0.000	7.6497	20.0345	29.7500	8.0301	4.8000	29.7500	11.0800
19.9950	0.000	7.7417	20.0408	29.7500	8.0809	5.9000	29.7500	12.3500
20.0072	0.000	7.8261	20.0459	29.7500	8.1228	6.4500	29.7500	12.9000
20.0178	0.000	7.9024	20.0497	29.7500	8.1555	6.9500	29.7500	13.2500
20.0269	0.000	7.9705	20.0524	29.7500	8.1790	7.9500	29.7500	13.7000
20.0345	0.000	8.0301	20.0541	29.7500	8.1931	9.0000	29.7500	13.7000
20.0408	0.000	8.0809	20.0546	29.7500	8.1979	10.000	29.7500	13.7000
20.0459	0.000	8.1228	9 1			15.0000	29.7500	13.7000
20.0497	0.000	8.1555	2 2			21.3500	29.7500	13.7000
20.0524	0.000	8.1790	-30.000	29.7500	-30.000	21.3500	30.000	-13.7000
20.0541	0.000	8.1931	30.000	29.7500	-30.000	15.0000	30.000	-13.7000
20.0546	0.000	8.1979	-30.000	29.7500	30.000	10.000	30.000	-13.7000
17.8359	29.7500	3.4397	30.000	29.7500	30.000	9.0000	30.000	-13.7000
17.8704	29.7500	3.4171	10 1			7.9500	30.000	-13.7000
17.9104	29.7500	3.4027	2 2			6.9500	30.000	-13.2500
17.9558	29.7500	3.3966	-30.000	30.000	-30.000	6.4500	30.000	-12.9000
18.0063	29.7500	3.3991	30.000	30.000	-30.000	5.9000	30.000	-12.3500
18.0619	29.7500	3.4102	-30.000	30.000	30.000	4.8000	30.000	-11.0800
18.1221	29.7500	3.4302	30.000	30.000	30.000	1.2000	30.000	-6.6100
18.1867	29.7500	3.4592	11 1			0.2000	30.000	-5.1800
18.2551	29.7500	3.4973	2 2			-0.3500	30.000	-4.3000
18.3268	29.7500	3.5445	21.3500	29.7500	-13.7000	-0.6800	30.000	-3.7500
18.4013	29.7500	3.6010	21.3500	30.000	-13.7000	-0.9200	30.000	-3.3500
18.4780	29.7500	3.6668	21.3500	29.7500	13.7000	-1.1800	30.000	-2.7300
18.5561	29.7500	3.7417	21.3500	30.000	13.7000	-1.3500	30.000	-2.3500
18.6349	29.7500	3.8258	12 1			-1.5000	30.000	-1.9500
18.7138	29.7500	3.9188	41 2			-1.6500	30.000	-1.5500
18.7921	29.7500	4.0205	21.3500	29.7500	-13.7000	-1.8600	30.000	-1.0500
18.8690	29.7500	4.1306	15.0000	29.7500	-13.7000	-2.0000	30.000	-0.6200
18.9439	29.7500	4.2487	10.000	29.7500	-13.7000	-2.0600	30.000	0.000
19.0161	29.7500	4.3744	9.0000	29.7500	-13.7000	-2.0000	30.000	0.6200
19.0846	29.7500	4.5065	7.9500	29.7500	-13.7000	-1.8600	30.000	1.0500
19.1466	29.7500	4.6385	6.9500	29.7500	-13.2500	-1.6500	30.000	1.5500
19.2062	29.7500	4.7740	6.4500	29.7500	-12.9000	-1.5000	30.000	1.9500
19.2642	29.7500	4.9135	5.9000	29.7500	-12.3500	-1.3500	30.000	2.3500
19.3204	29.7500	5.0564	4.8000	29.7500	-11.0800	-1.1800	30.000	2.7300

-0.9200	30.000	3.3500	15	10	16	4
-0.6800	30.000	3.7500	5	5	1	
-0.3500	30.000	4.3000	4			
0.2000	30.000	5.1800	17	5	18	11
1.2000	30.000	6.6100	6	6	1	
4.8000	30.000	11.0800	4			
5.9000	30.000	12.3500	17	12	18	6
6.4500	30.000	12.9000	7	7	1	
6.9500	30.000	13.2500	4			
7.9500	30.000	13.7000	19	7	20	13
9.0000	30.000	13.7000	8	8	1	
10.000	30.000	13.7000	4			
15.0000	30.000	13.7000	19	14	20	8
21.3500	30.000	13.7000	9	9	1	
Mesh generation			8			
26	12		21	23	9	-10 11 -12 13 -14
Curves segments			10	10	1	
1	1	1	2			
2	2	1	22	24		
3	3	1	11	11	1	
4	4	1	4			
5	5	1	23	26	24	25
6	6	1	12	12	1	
7	7	1	4			
8	8	1	21	25	-22	-26
9	9	1				
10	10	1				
11	11	1				
12	12	1				
13	13	1				
14	14	1				
15	15	1				
16	16	1				
17	17	1				
18	18	1				
19	19	1				
20	20	1				
21	21	1				
22	22	1				
23	23	1				
24	24	1				
25	25	1				
26	26	1				
Surface Regions						
1	1	1				
8						
1	-2	-3	4	-5	6	-7 8
2	2	1				
2						
1	2					
3	3	1				
4						
15	3	16	9			
4	4	1				
4						

APPENDIX A-2

STARS-CFD Background Mesh Data File (*fin.bac*)

Background Mesh....fin

4 1 0 0 7

1 -1800 -100 -2400

1 0 0 20

0 1 0 20

0 0 1 20

2 1800 -100 -2400

1 0 0 20

0 1 0 20

0 0 1 20

3 0 -100 2400

1 0 0 20

0 1 0 20

0 0 1 20

4 0 2400 0

1 0 0 20

0 1 0 20

0 0 1 20

1 1 2 3 4

* Point Sources

* Line Sources

* Triangle Sources

1. Source for fin 1

0.000 0.000 0.000 0.4 0.8 3

0.000 30.000 0.000 0.4 0.8 3

14.10000 0.000 0.000 0.4 0.8 3

2. Source for fin 1

14.10000 0.000 0.000 0.4 0.8 3

0.000 30.000 0.000 0.4 0.8 3

14.10000 30.000 0.000 0.4 0.8 3

3. Source for fin 2

13.54051 0.000 0.74475 0.4 0.8 3

13.54051 30.000 0.74475 0.4 0.8 3

18.17598 0.000 3.20948 0.4 0.8 3

4. Source for fin 2
18.17598 0.000 3.20948 0.4 0.8 3
13.54051 30.000 0.74475 0.4 0.8 3
18.17598 30.000 3.20948 0.4 0.8 3

5. Source for fin 3
17.83585 0.000 3.43973 0.4 0.8 3
17.83585 30.000 3.43973 0.4 0.8 3
20.05219 0.000 8.19376 0.4 0.8 3

6. Source for fin 3
20.05219 0.000 8.19376 0.4 0.8 3
17.83585 30.000 3.43973 0.4 0.8 3
20.05219 30.000 8.19376 0.4 0.8 3

7. Source for endplate
21.00000 30.000 13.0000 0.6 0.8 5
21.00000 30.000 -13.000 0.6 0.8 5
-2.00000 30.000 0.000 0.6 0.8 5

APPENDIX A-3

STARS-CFD Boundary Conditions Data File (*fin.bco*)

Fin Boundary Condition File	17	0
12 26	18	1
Surface Regions	19	0
1 2	20	1
2 3	21	1
3 1	22	1
4 1	23	1
5 1	24	1
6 1	25	1
7 1	26	1
8 1		
9 1		
10 1		
11 1		
12 1		
Curve Segments		
1 0		
2 0		
3 4		
4 4		
5 4		
6 4		
7 4		
8 4		
9 4		
10 4		
11 4		
12 4		
13 4		
14 4		
15 0		
16 1		

APPENDIX A-4

STARS-CFD Parameter Control File (*fin.cons*)

```
&control
nout   = 50,
nstep  = 1,
ncycl  = 5000,
nstpe  = 20,
cfl    = 0.3,
nsmth  = 0,
smofc  = 0.2,
relax  = 1.0,
mach   = 0.434,
alpha  = 0.0,
beta   = 0.0,
restart = 0,
amplitude= 1.0,
/
```

APPENDIX B-1

STARS-CFD Geometry Data File (*boxwing.sur*)

1 Geometry definition...felisa	314.8800 0.000 -153.9419	4 1
boxwing	335.7900 0.000 -123.4354	46
26 12	353.0100 0.000 -87.2439	100.000625 0.000 -0.022250
Curves	362.8500 0.000 -54.6612	100.019375 0.000 -0.129125
1 1	367.7700 0.000 -24.5680	100.061875 0.000 -0.246125
21	369.0000 0.000 0.000	100.1285 0.000 -0.369250
-123.0000 0.000 0.000	3 1	100.219375 0.000 -0.495125
-121.7700 0.000 24.5680	36	100.33675 0.000 -0.620750
-116.8500 0.000 54.6612	100.000625 0.000 -0.02225	100.481875 0.000 -0.746000
-107.0100 0.000 87.2439	100.0055 0.000 0.070125	100.652875 0.000 -0.870625
-89.7900 0.000 123.4354	100.033 0.000 0.140000	100.848625 0.000 -0.992500
-68.8800 0.000 153.9419	100.098625 0.0000 0.178375	101.068125 0.000 -1.109875
-39.3600 0.000 184.8124	100.21475 0.000 0.193750	101.31025 0.000 -1.221250
-7.3800 0.000 208.6080	100.37575 0.000 0.198000	101.573875 0.000 -1.324750
29.5200 0.000 227.5475	100.578375 0.0000 0.191500	101.857875 0.000 -1.419375
71.3400 0.000 240.5142	100.820125 0.0000 0.175500	102.16075 0.000 -1.503250
123.0000 0.000 246.0000	101.098375 0.0000 0.150250	102.48075 0.000 -1.574250
174.6600 0.000 240.5142	101.41025 0.000 0.115625	102.817625 0.000 -1.629625
216.4800 0.000 227.5475	101.7525 0.000 0.070375	103.17125 0.000 -1.668250
253.3800 0.000 208.6080	102.12575 0.000 0.009375	103.543375 0.000 -1.688125
285.3600 0.000 184.8124	102.53475 0.0000 -0.066875	103.936 0.000 -1.690750
314.8800 0.000 153.9419	102.98 0.000 -0.151625	104.347125 0.000 -1.680875
335.7900 0.000 123.4354	103.459125 0.0000 -0.241000	104.774125 0.000 -1.658875
353.0100 0.000 87.2439	103.96875 0.0000 -0.331500	105.215125 0.000 -1.626375
362.8500 0.000 54.6612	104.5055 0.000 -0.419750	105.6675 0.000 -1.585375
367.7700 0.000 24.5680	105.064875 0.000 -0.502625	106.128125 0.000 -1.537875
369.0000 0.000 0.000	105.642375 0.000 -0.577250	106.593 0.000 -1.485125
2 1	106.2325 0.000 -0.641125	107.058125 0.000 -1.428125
21	106.829875 0.000 -0.691750	107.51975 0.000 -1.366875
-123.0000 0.000 0.000	107.4285 0.000 -0.727500	107.97475 0.000 -1.301500
-121.7700 0.000 -24.5680	108.022 0.000 -0.747000	108.42 0.000 -1.232375
-116.8500 0.000 -54.6612	108.604 0.000 -0.749250	108.852875 0.000 -1.159625
-107.0100 0.000 -87.2439	109.168 0.000 -0.734000	109.27075 0.000 -1.083875
-89.7900 0.000 -123.4354	109.7075 0.000 -0.701500	109.671125 0.000 -1.005500
-68.8800 0.000 -153.9419	110.216125 0.000 -0.652375	110.0515 0.000 -0.925250
-39.3600 0.000 -184.8124	110.6875 0.000 -0.588250	110.409625 0.000 -0.843625
-7.3800 0.000 -208.6080	111.116 0.000 -0.511000	110.743375 0.000 -0.761125
29.5200 0.000 -227.5475	111.49575 0.000 -0.423375	111.05075 0.000 -0.678375
71.3400 0.000 -240.5142	111.821625 0.000 -0.328000	111.330125 0.000 -0.596000
123.0000 0.000 -246.0000	112.086625 0.000 -0.227750	111.579875 0.000 -0.514500
174.6600 0.000 -240.5142	112.281875 0.000 -0.132500	111.798625 0.000 -0.434500
216.4800 0.000 -227.5475	112.4085 0.000 -0.058500	111.9855 0.000 -0.356625
253.3800 0.000 -208.6080	112.478125 0.000 -0.014375	112.138875 0.000 -0.281250
285.3600 0.000 -184.8124	112.5 0.000 0.000	112.259375 0.000 -0.205750

112.353125	0.000	-0.129625	115.317625	0.000	10.870375	110.216125	29.750	-0.652375
112.427125	0.000	-0.061750	115.67125	0.000	10.831750	110.6875	29.750	-0.588250
112.47975	0.000	-0.015750	116.043375	0.000	10.811875	111.116	29.750	-0.511000
112.5	0.000	0.000	116.436	0.000	10.809250	111.49575	29.750	-0.423375
5	1		116.847125	0.000	10.819125	111.821625	29.750	-0.32800
36			117.274125	0.000	10.841125	112.086625	29.750	-0.22775
112.500625	0.000	12.477750	117.715125	0.000	10.873625	112.281875	29.750	-0.13250
112.5055	0.000	12.570125	118.1675	0.000	10.914625	112.4085	29.750	-0.058500
112.533	0.000	12.640000	118.628125	0.000	10.962125	112.478125	29.750	-0.014375
112.598625	0.000	12.678375	119.093	0.000	11.014875	112.5	29.750	0.000
112.71475	0.000	12.693750	119.558125	0.000	11.071875	8	1	
112.87575	0.000	12.698000	120.01975	0.000	11.133125	46		
113.078375	0.000	12.691500	120.47475	0.000	11.198500	100.000625	29.750	-0.02225
113.320125	0.000	12.675500	120.92	0.000	11.267625	100.019375	29.750	-0.129125
113.598375	0.000	12.650250	121.352875	0.000	11.340375	100.061875	29.75	-0.246125
113.91025	0.000	12.615625	121.77075	0.000	11.416125	100.12850	29.750	-0.369250
114.2525	0.000	12.570375	122.171125	0.000	11.494500	100.219375	29.750	-0.495125
114.62575	0.000	12.509375	122.5515	0.000	11.574750	100.336750	29.750	-0.62075
115.03475	0.000	12.433125	122.909625	0.000	11.656375	100.481875	29.750	-0.74600
115.48	0.000	12.348375	123.243375	0.000	11.738875	100.652875	29.750	-0.870625
115.959125	0.000	12.259000	123.55075	0.000	11.821625	100.848625	29.750	-0.99250
116.46875	0.000	12.168500	123.830125	0.000	11.904000	101.068125	29.750	-1.109875
117.0055	0.000	12.080250	124.079875	0.000	11.985500	101.310250	29.750	-1.22125
117.564875	0.000	11.997375	124.298625	0.000	12.065500	101.573875	29.750	-1.32475
118.142375	0.000	11.922750	124.4855	0.000	12.143375	101.857875	29.750	-1.419375
118.7325	0.000	11.858875	124.638875	0.000	12.218750	102.160750	29.750	-1.50325
119.329875	0.000	11.808250	124.759375	0.000	12.294250	102.480750	29.750	-1.57425
119.9285	0.000	11.772500	124.853125	0.000	12.370375	102.817625	29.750	-1.629625
120.522	0.000	11.753000	124.927125	0.000	12.438250	103.171250	29.750	-1.66825
121.104	0.000	11.750750	124.97975	0.000	12.484250	103.543375	29.750	-1.688125
121.668	0.000	11.766000	125	0.000	12.500000	103.93600	29.750	-1.69075
122.2075	0.000	11.798500	7	1		104.347125	29.750	-1.680875
122.716125	0.000	11.847625	36			104.774125	29.750	-1.658875
123.1875	0.000	11.911750	100.000625	29.7500	-0.02225	105.215125	29.750	-1.626375
123.616	0.000	11.989000	100.0055	29.7500	0.070125	105.66750	29.750	-1.585375
123.99575	0.000	12.076625	100.033	29.75000	0.140000	106.128125	29.750	-1.537875
124.321625	0.000	12.172000	100.098625	29.750	0.178375	106.593000	29.750	-1.485125
124.586625	0.000	12.272250	100.21475	29.750	0.193750	107.058125	29.750	-1.428125
124.781875	0.000	12.367500	100.37575	29.750	0.198000	107.519750	29.750	-1.366875
124.9085	0.000	12.441500	100.578375	29.750	0.191500	107.974750	29.750	-1.30150
124.978125	0.000	12.485625	100.820125	29.750	0.175500	108.420000	29.750	-1.232375
125	0.000	12.500000	101.098375	29.750	0.150250	108.852875	29.750	-1.159625
6	1		101.41025	29.750	0.115625	109.270750	29.750	-1.083875
46			101.7525	29.750	0.070375	109.671125	29.750	-1.00550
112.500625	0.000	12.477750	102.12575	29.750	0.009375	110.051500	29.750	-0.92525
112.519375	0.000	12.370875	102.53475	29.750	-0.066875	110.409625	29.750	-0.843625
112.561875	0.000	12.253875	102.98	29.750	-0.151625	110.743375	29.750	-0.761125
112.6285	0.000	12.130750	103.459125	29.750	-0.24100	111.050750	29.750	-0.678375
112.719375	0.000	12.004875	103.96875	29.750	-0.331500	111.330125	29.750	-0.596000
112.83675	0.000	11.879250	104.5055	29.750	-0.419750	111.579875	29.750	-0.514500
112.981875	0.000	11.754000	105.064875	29.750	-0.502625	111.798625	29.750	-0.434500
113.152875	0.000	11.629375	105.642375	29.750	-0.577250	111.985500	29.750	-0.356625
113.348625	0.000	11.507500	106.2325	29.750	-0.641125	112.138875	29.750	-0.281250
113.568125	0.000	11.390125	106.829875	29.750	-0.691750	112.259375	29.750	-0.205750
113.81025	0.000	11.278750	107.4285	29.750	-0.727500	112.353125	29.750	-0.129625
114.073875	0.000	11.175250	108.022	29.750	-0.747000	112.427125	29.750	-0.061750
114.357875	0.000	11.080625	108.604	29.750	-0.749250	112.479750	29.750	-0.015750
114.66075	0.000	10.996750	109.168	29.750	-0.734000	112.500000	29.750	0.000
114.98075	0.000	10.925750	109.7075	29.750	-0.701500	9	1	

36									
112.500625	29.750	12.47775	117.274125	29.75	10.841125	19	1		
112.50550	29.750	12.570125	117.715125	29.75	10.873625	2			
112.53300	29.750	12.640000	118.16750	29.75	10.914625	125.8	29.750	-3.200000	
112.598625	29.750	12.67837	118.628125	29.75	10.962125	98.6	29.750	-3.200000	
112.71475	29.750	12.693750	119.093000	29.75	11.014875	20	1		
112.87575	29.750	12.698000	119.558125	29.75	11.071875	2			
113.078375	29.750	12.69150	120.019750	29.75	11.133125	125.80000	30.000	-3.200000	
113.320125	29.750	12.67550	120.474750	29.75	11.198500	98.600000	30.000	-3.200000	
113.598375	29.750	12.65025	120.920000	29.75	11.267625	21	1		
113.91025	29.750	12.615625	121.352875	29.75	11.340375	2			
114.25250	29.750	12.570375	121.770750	29.75	11.416125	125.8	29.750	-3.200000	
114.62575	29.750	12.509375	122.171125	29.75	11.494500	125.8	30.000	-3.200000	
115.03475	29.750	12.433125	122.551500	29.75	11.574750	22	1		
115.48000	29.750	12.348375	122.909625	29.75	11.656375	2			
115.959125	29.750	12.25900	123.243375	29.75	11.738875	125.8	29.750	14.400000	
116.468750	29.750	12.16850	123.550750	29.75	11.821625	125.8	29.750	-3.200000	
117.005500	29.750	12.08025	123.830125	29.75	11.904000	23	1		
117.564875	29.750	11.99737	124.079875	29.75	11.985500	2			
118.142375	29.750	11.92275	124.298625	29.75	12.065500	125.8000	30.000	14.400000	
118.73250	29.750	11.858875	124.485500	29.75	12.143375	125.8000	30.000	-3.200000	
119.329875	29.750	11.80825	124.638875	29.75	12.218750	24	1		
119.92850	29.750	11.772500	124.759375	29.75	12.294250	2			
120.52200	29.750	11.753000	124.853125	29.75	12.370375	125.8	29.750	14.400000	
121.10400	29.750	11.750750	124.927125	29.75	12.438250	125.8	30.000	14.400000	
121.66800	29.750	11.766000	124.979750	29.75	12.484250	25	1		
122.20750	29.750	11.798500	125.000000	29.75	12.500000	2			
122.716125	29.75	11.847625	11	1		125.8	29.750	14.400000	
123.18750	29.750	11.911750	2			98.6	29.750	14.400000	
123.61600	29.750	11.989000	100.000625	0.000	-0.022250	26	1		
123.99575	29.750	12.076625	100.000625	29.750	-0.022250	2			
124.321625	29.750	12.17200	12	1		125.8000	30.000	14.400000	
124.586625	29.750	12.27225	2			98.60000	30.000	14.400000	
124.781875	29.750	12.36750	112.500000	0.000	0.000	Surfaces			
124.908500	29.750	12.44150	112.500000	29.750	0.000	1	1		
124.978125	29.75	12.485625	13	1		2	2		
125.00000	29.750	12.500000	2			-140.000	0.000	-260.000	
10	1		112.500625	0.000	12.477750	380.000	0.000	-260.000	
46			112.500625	29.750		-140.000	0.000	260.000	
112.500625	29.750	12.47775	12.477750			380.000	0.000	260.000	
112.519375	29.75	12.370875	14	1		2	1		
112.561875	29.75	12.253875	2			21	21		
112.62850	29.750	12.130750	125.000000	0.000	12.500000	-123.0000	0.000	0.000	
112.719375	29.75	12.004875	125.000000	29.75	12.500000	-121.7700	0.000	24.5680	
112.83675	29.750	11.879250	15	1		-116.8500	0.000	71.3400	
112.981875	29.750	11.75400	2			-107.0100	0.000	87.2439	
113.152875	29.75	11.629375	98.6	29.750	14.400000	-89.7900	0.000	123.4354	
113.348625	29.750	11.50750	98.6	29.750	-3.200000	-68.8800	0.000	153.9419	
113.568125	29.75	11.390125	16	1		-39.3600	0.000	184.8124	
113.810250	29.750	11.27875	2			-7.3800	0.000	208.6080	
114.073875	29.750	11.17525	98.600000	30.000	14.400000	29.5200	0.000	227.5475	
114.357875	29.75	11.080625	98.600000	30.000	-3.200000	71.3400	0.000	240.5142	
114.660750	29.750	10.99675	17	1		123.0000	0.000	246.0000	
114.980750	29.750	10.92575	2			174.6600	0.000	240.5142	
115.317625	29.75	10.870375	98.6	29.750	14.400000	216.4800	0.000	227.5475	
115.671250	29.750	10.83175	98.6	30.000	14.400000	253.3800	0.000	208.6080	
116.043375	29.75	10.811875	18	1		285.3600	0.000	184.8124	
116.43600	29.750	10.809250	2			314.8800	0.000	153.9419	
116.847125	29.75	10.819125	98.6	29.750	-3.200000	335.7900	0.000	123.4354	
			98.6	30.000	-3.200000	353.0100	0.000	87.2439	

362.8500	0.000	54.6612	285.3600	83.9025	164.6675	123.000	199.0181	144.5963
367.7700	0.000	24.5680	314.8800	69.8880	137.1622	174.660	194.5802	141.3713
369.0000	0.000	0.000	335.7900	56.0387	109.9817	216.480	184.0890	133.7477
-123.0000	0.000	0.000	353.0100	39.6076	77.7335	253.380	168.7669	122.6162
-121.7700	3.8435	24.2679	362.8500	24.8162	48.7055	285.360	149.5154	108.6287
-116.8500	8.5511	53.9896	367.7700	11.1542	21.8915	314.8800	124.5414	90.4837
-107.0100	13.6479	86.1689	369.0000	0.000	0.000	335.7900	99.8617	72.5528
-89.7900	19.3096	121.9151	-123.0000	0.000	0.000	353.0100	70.5813	51.2812
-68.8800	24.0818	152.0477	-121.7700	14.4414	19.8768	362.8500	44.2228	32.1301
-39.3600	28.9108	182.5369	-116.8500	32.1297	44.2234	367.7700	19.8769	14.4427
-7.3800	32.6334	206.0398	-107.0100	51.2803	70.5823	369.0000	0.000	0.000
29.5200	35.5961	224.7456	-89.7900	72.5537	99.8612	-123.0000	0.000	0.000
71.3400	37.6247	237.5524	-68.8800	90.4846	124.5424	-121.7700	21.8913	11.1536
123.0000	38.4828	242.9717	-39.3600	108.6293	149.5163	-116.8500	48.7045	24.8165
174.6600	37.6247	237.5524	-7.3800	122.6163	168.7658	-107.0100	77.7343	39.6085
216.4800	35.5961	224.7456	29.5200	133.7485	184.0892	-89.7900	109.9821	56.0388
253.3800	32.6334	206.0398	71.3400	141.3708	194.5811	-68.8800	137.1630	69.8886
285.3600	28.9108	182.5369	123.000	144.5951	199.0189	-39.3600	164.6680	83.9032
314.8800	24.0818	152.0477	174.660	141.3708	194.5811	-7.3800	185.8705	94.7051
335.7900	19.3096	121.9151	216.480	133.7485	184.0892	29.5200	202.7455	103.3052
353.0100	13.6479	86.1689	253.380	122.6163	168.7658	71.3400	214.2999	109.1920
362.8500	8.5511	53.9896	285.360	108.6293	149.5163	123.000	219.1875	111.6815
367.7700	3.8435	24.2679	314.8800	90.4846	124.5424	174.660	214.2999	109.1920
369.0000	0.000	0.000	335.7900	72.5537	99.8612	216.480	202.7455	103.3052
-123.0000	0.000	0.000	353.0100	51.2803	70.5823	253.3800	185.8705	94.7051
-121.7700	7.5923	23.3675	362.8500	32.1297	44.2234	285.3600	164.6680	83.9032
-116.8500	16.8916	51.9872	367.7700	14.4414	19.8768	314.8800	137.1630	69.8886
-107.0100	26.9597	82.9733	369.0000	0.000	0.000	335.7900	109.9821	56.0388
-89.7900	38.1438	117.3937	-123.0000	0.000	0.000	353.0100	77.7343	39.6085
-68.8800	51.6600	120.5400	-121.7700	17.3731	17.3725	362.8500	48.7045	24.8165
-39.3600	57.1098	175.7670	-116.8500	38.6521	38.6515	367.7700	21.8913	11.1536
-7.3800	64.4632	198.3965	-107.0100	61.6903	61.6894	369.0000	0.000	0.000
29.5200	66.4200	204.1800	-89.7900	87.2823	87.2833	-123.0000	0.000	0.000
71.3400	70.3157	216.4087	-68.8800	108.8532	108.8525	-121.7700	23.3667	7.5916
123.0000	76.0181	233.9608	-39.3600	130.6813	130.6826	-116.8500	51.9870	16.8928
174.6600	74.3230	228.7431	-7.3800	147.5076	147.5090	-107.0100	82.9733	26.9591
216.4800	70.3157	216.4087	29.5200	160.8997	160.8988	-89.7900	117.3945	38.1448
253.3800	64.4632	198.3965	71.3400	170.0694	170.0696	-68.8800	146.4073	47.5715
285.3600	57.1098	175.7670	123.000	173.9482	173.9491	-39.3600	175.7660	57.1089
314.8800	47.5706	146.4069	174.660	170.0694	170.0696	-7.3800	198.3974	64.4643
335.7900	38.1438	117.3937	216.480	160.8997	160.8988	29.5200	216.4097	70.3166
353.0100	26.9597	82.9733	253.380	147.5076	147.5090	71.3400	228.7428	74.3240
362.8500	16.8916	51.9872	285.360	130.6813	130.6826	123.0000	233.9598	76.0189
367.7700	7.5923	23.3675	314.880	108.8532	108.8525	174.6600	228.7428	74.3240
369.0000	0.000	0.000	335.7900	87.2823	87.2833	216.4800	216.4097	70.3166
-123.0000	0.000	0.000	353.0100	61.6903	61.6894	253.3800	198.3974	64.4643
-121.7700	11.1542	21.8915	362.8500	38.6521	38.6515	285.3600	175.7660	57.1089
-116.8500	24.8162	48.7055	367.7700	17.3731	17.3725	314.8800	146.4073	47.5715
-107.0100	39.6076	77.7335	369.0000	0.000	0.000	335.7900	117.3945	38.1448
-89.7900	56.0387	109.9817	-123.0000	0.000	0.000	353.0100	82.9733	26.9591
-68.8800	69.8880	137.1622	-121.7700	19.8769	14.4427	362.8500	51.9870	16.8928
-39.3600	83.9025	164.6675	-116.8500	44.2228	32.1301	367.7700	23.3667	7.5916
-7.3800	94.7057	185.8702	-107.0100	70.5813	51.2812	369.0000	0.000	0.000
29.5200	103.3039	202.7458	-89.7900	99.8617	72.5528	-123.0000	0.000	0.000
71.3400	109.1912	214.3004	-68.8800	124.5414	90.4837	-121.7700	24.2667	3.8425
123.000	111.6816	219.1885	-39.3600	149.5154	108.6287	-116.8500	53.9894	8.5510
174.660	109.1912	214.3004	-7.3800	168.7669	122.6162	-107.0100	86.1692	13.6481
216.480	103.3039	202.7458	29.5200	184.0890	133.7477	-89.7900	121.9162	19.3110
253.3800	94.7057	185.8702	71.3400	194.5802	141.3713	-68.8800	152.0465	24.0809

-39.3600	182.5360	28.9099	-116.8500	51.9871	-16.8904	367.7700	19.8770	-14.4402
-7.3800	206.0391	32.6344	-107.0100	82.9734	-26.9591	369.0000	0.000	0.000
29.5200	224.7452	35.5962	-89.7900	117.3946	-38.1448	-123.0000	0.000	0.000
71.3400	237.5534	37.6257	-68.8800	146.4074	-47.5715	-121.7700	17.3731	-17.3725
123.0000	242.9713	38.4842	-39.3600	175.7661	-57.1089	-116.8500	38.6522	-38.6515
174.6600	237.5534	37.6257	-7.3800	198.3975	-64.4618	-107.0100	61.6905	-61.6894
216.4800	224.7452	35.5962	29.5200	216.4099	-70.3166	-89.7900	87.2825	-87.2833
253.3800	206.0391	32.6344	71.3400	228.7430	-74.3215	-68.880	108.8535	-108.8525
285.3600	182.5360	28.9099	123.0000	233.9600	-76.0189	-39.360	130.6816	-130.6801
314.8800	152.0465	24.0809	174.6600	228.7430	-74.3215	-7.3800	147.5080	-147.5065
335.7900	121.9162	19.3110	216.4800	216.4099	-70.3166	29.5200	160.9001	-160.8988
353.0100	86.1692	13.6481	253.3800	198.3975	-64.4618	71.3400	170.0698	-170.0696
362.8500	53.9894	8.5510	285.3600	175.7661	-57.1089	123.000	173.9486	-173.9491
367.7700	24.2667	3.8425	314.8800	146.4074	-47.5715	174.660	170.0698	-170.0696
369.0000	0.000	0.000	335.7900	117.3946	-38.1448	216.480	160.9001	-160.8988
-123.0000	0.000	0.000	353.0100	82.9734	-26.9591	253.380	147.5080	-147.5065
-121.7700	24.5692	0.000	362.8500	51.9871	-16.8904	285.360	130.6816	-130.6801
-116.8500	54.6624	0.000	367.7700	23.3667	-7.5916	314.880	108.8535	-108.8525
-107.0100	87.2433	0.000	369.0000	0.000	0.000	335.7900	87.2825	-87.2833
-89.7900	123.4359	0.000	-123.0000	0.000	0.000	353.0100	61.6905	-61.6894
-68.8800	153.9418	0.000	-121.7700	21.8914	-11.1536	362.8500	38.6522	-38.6515
-39.3600	184.8113	0.000	-116.8500	48.7046	-24.8165	367.7700	17.3731	-17.3725
-7.3800	208.6074	0.000	-107.0100	77.7345	-39.6085	369.0000	0.000	0.000
29.5200	227.5467	0.000	-89.7900	109.9823	-56.0388	-123.0000	0.000	0.000
71.3400	240.5145	0.000	-68.8800	137.1632	-69.8886	-121.7700	14.4415	-19.8768
123.0000	246.0000	0.000	-39.3600	164.6683	-83.9032	-116.8500	32.1298	-44.2234
174.6600	240.5145	0.000	-7.3800	185.8707	-94.7051	-107.0100	51.2805	-70.5823
216.4800	227.5467	0.000	29.5200	202.7458	-103.3028	-89.7900	72.5540	-99.8612
253.3800	208.6074	0.000	71.3400	214.3002	-109.1920	-68.8800	90.4850	-124.5424
285.3600	184.8113	0.000	123.000	219.1878	-111.6815	-39.360	108.6297	-149.5163
314.8800	153.9418	0.000	174.660	214.3002	-109.1920	-7.3800	122.6167	-168.7658
335.7900	123.4359	0.000	216.480	202.7458	-103.3028	29.5200	133.7490	-184.0892
353.0100	87.2433	0.000	253.3800	185.8707	-94.7051	71.3400	141.3713	-194.5811
362.8500	54.6624	0.000	285.3600	164.6683	-83.9032	123.000	144.5956	-199.0189
367.7700	24.5692	0.000	314.8800	137.1632	-69.8886	174.660	141.3713	-194.5811
369.0000	0.000	0.000	335.7900	109.9823	-56.0388	216.480	133.7490	-184.0892
-123.0000	0.000	0.000	353.0100	77.7345	-39.6085	253.380	122.6167	-168.7658
-121.7700	24.2667	-3.8425	362.8500	48.7046	-24.8165	285.360	108.6297	-149.5163
-116.8500	53.9894	-8.5510	367.7700	21.8914	-11.1536	314.8800	90.4850	-124.5424
-107.0100	86.1692	-13.6481	369.0000	0.000	0.000	335.7900	72.5540	-99.8612
-89.7900	121.9162	-19.3085	-123.0000	0.000	0.000	353.0100	51.2805	-70.5823
-68.8800	152.0465	-24.0809	-121.7700	19.8770	-14.4402	362.8500	32.1298	-44.2234
-39.3600	182.5360	-28.9099	-116.8500	44.2229	-32.1301	367.7700	14.4415	-19.8768
-7.3800	206.0392	-32.6319	-107.0100	70.5814	-51.2812	369.0000	0.000	0.000
29.5200	224.7453	-35.5962	-89.7900	99.8619	-72.5528	-123.0000	0.000	0.000
71.3400	237.5535	-37.6232	-68.8800	124.5417	-90.4837	-121.7700	11.1542	-21.8915
123.0000	242.9714	-38.4818	-39.360	149.5157	-108.6287	-116.8500	24.8163	-48.7055
174.6600	237.5535	-37.6232	-7.3800	168.7672	-122.6162	-107.0100	39.6078	-77.7335
216.4800	224.7453	-35.5962	29.5200	184.0894	-133.7477	-89.7900	56.0390	-109.9817
253.3800	206.0392	-32.6319	71.3400	194.5806	-141.3713	-68.8800	69.8884	-137.1622
285.3600	182.5360	-28.9099	123.000	199.0184	-144.5939	-39.3600	83.9030	-164.6675
314.8800	152.0465	-24.0809	174.660	194.5806	-141.3713	-7.3800	94.7062	-185.8702
335.7900	121.9162	-19.3085	216.480	184.0894	-133.7477	29.5200	103.3045	-202.7458
353.0100	86.1692	-13.6481	253.380	168.7672	-122.6162	71.3400	109.1918	-214.3004
362.8500	53.9894	-8.5510	285.360	149.5157	-108.6287	123.000	111.6822	-219.1885
367.7700	24.2667	-3.8425	314.8800	124.5417	-90.4837	174.660	109.1918	-214.3004
369.0000	0.000	0.000	335.7900	99.8619	-72.5528	216.480	103.3045	-202.7458
-123.0000	0.000	0.000	353.0100	70.5814	-51.2812	253.3800	94.7062	-185.8702
-121.7700	23.3667	-7.5916	362.8500	44.2229	-32.1301	285.3600	83.9030	-164.6675

314.8800	69.8884	-137.1622	174.6600	0.000	-240.5142	102.12575	29.750	0.009375
335.7900	56.0390	-109.9817	216.4800	0.000	-227.5475	102.53475	29.750	-0.066875
353.0100	39.6078	-77.7335	253.3800	0.000	-208.6080	102.98	29.750	-0.151625
362.8500	24.8163	-48.7055	285.3600	0.000	-184.8124	103.459125	29.75	-0.241000
367.7700	11.1542	-21.8915	314.8800	0.000	-153.9419	103.96875	29.750	-0.331500
369.0000	0.000	0.000	335.7900	0.000	-123.4354	104.5055	29.750	-0.419750
-123.0000	0.000	0.000	353.0100	0.000	-87.2439	105.064875	29.75	-0.502625
-121.7700	7.5924	-23.3675	362.8500	0.000	-54.6612	105.642375	29.75	-0.577250
-116.8500	16.8917	-51.9872	367.7700	0.000	-24.5680	106.2325	29.750	-0.641125
-107.0100	26.9599	-82.9733	369.0000	0.000	0.000	106.829875	29.75	-0.691750
-89.7900	38.1441	-117.3937	3	1		107.4285	29.750	-0.727500
-68.8800	47.5710	-146.4069	36	2		108.022	29.750	-0.747000
-39.3600	57.1103	-175.7670	100.000625	0.000	-0.022250	108.604	29.750	-0.749250
-7.3800	64.4637	-198.3965	100.0055	0.000	0.070125	109.168	29.750	-0.734000
29.5200	70.3163	-216.4087	100.033	0.000	0.140000	109.7075	29.750	-0.701500
71.3400	74.3236	-228.7431	100.098625	0.000	0.178375	110.216125	29.75	-0.652375
123.0000	76.0187	-233.9608	100.21475	0.000	0.193750	110.6875	29.750	-0.588250
174.6600	74.3236	-228.7431	100.37575	0.000	0.198000	111.116	29.750	-0.511000
216.4800	70.3163	-216.4087	100.578375	0.000	0.191500	111.49575	29.750	-0.423375
253.3800	64.4637	-198.3965	100.820125	0.000	0.175500	111.821625	29.75	-0.328000
285.3600	57.1103	-175.7670	101.098375	0.000	0.150250	112.086625	29.75	-0.227750
314.8800	47.5710	-146.4069	101.41025	0.000	0.115625	112.281875	29.75	-0.132500
335.7900	38.1441	-117.3937	101.7525	0.000	0.070375	112.4085	29.750	-0.058500
353.0100	26.9599	-82.9733	102.12575	0.000	0.009375	112.478125	29.75	-0.014375
362.8500	16.8917	-51.9872	102.53475	0.000	-0.066875	112.5	29.750	0.000
367.7700	7.5924	-23.3675	102.98	0.000	-0.151625	4	1	
369.0000	0.000	0.000	103.459125	0.000	-0.241000	46	2	
-123.0000	0.000	0.000	103.96875	0.000	-0.331500	100.000625	0.000	-0.022250
-121.7700	3.8435	-24.2679	104.5055	0.000	-0.419750	100.019375	0.000	-0.129125
-116.8500	8.5512	-53.9896	105.064875	0.000	-0.502625	100.061875	0.000	-0.246125
-107.0100	13.6481	-86.1689	105.642375	0.000	-0.577250	100.1285	0.000	-0.369250
-89.7900	19.3099	-121.9151	106.2325	0.000	-0.641125	100.219375	0.000	-0.495125
-68.8800	24.0822	-152.0452	106.829875	0.000	-0.691750	100.33675	0.000	-0.620750
-39.3600	28.9113	-182.5369	107.4285	0.000	-0.727500	100.481875	0.000	-0.746000
-7.3800	32.6339	-206.0398	108.022	0.000	-0.747000	100.652875	0.000	-0.870625
29.5200	35.5967	-224.7456	108.604	0.000	-0.749250	100.848625	0.000	-0.992500
71.3400	37.6254	-237.5524	109.168	0.000	-0.734000	101.068125	0.000	-1.109875
123.0000	38.4835	-242.9717	109.7075	0.000	-0.701500	101.31025	0.000	-1.221250
174.6600	37.6254	-237.5524	110.216125	0.000	-0.652375	101.573875	0.000	-1.324750
216.4800	35.5967	-224.7456	110.6875	0.000	-0.588250	101.857875	0.000	-1.419375
253.3800	32.6339	-206.0398	111.116	0.000	-0.511000	102.16075	0.000	-1.503250
285.3600	28.9113	-182.5369	111.49575	0.000	-0.423375	102.48075	0.000	-1.574250
314.8800	24.0822	-152.0452	111.821625	0.000	-0.328000	102.817625	0.000	-1.629625
335.7900	19.3099	-121.9151	112.086625	0.000	-0.227750	103.17125	0.000	-1.668250
353.0100	13.6481	-86.1689	112.281875	0.000	-0.132500	103.543375	0.000	-1.688125
362.8500	8.5512	-53.9896	112.4085	0.000	-0.058500	103.936	0.000	-1.690750
367.7700	3.8435	-24.2679	112.478125	0.000	-0.014375	104.347125	0.000	-1.680875
369.0000	0.000	0.000	112.5	0.000	0.000	104.774125	0.000	-1.658875
-123.0000	0.000	0.000	100.000625	29.750	-0.02225	105.215125	0.000	-1.626375
-121.7700	0.000	-24.5680	100.0055	29.750	0.070125	105.6675	0.000	-1.585375
-116.8500	0.000	-54.6612	100.033	29.750	0.140000	106.128125	0.000	-1.537875
-107.0100	0.000	-87.2439	100.098625	29.75	0.178375	106.593	0.000	-1.485125
-89.7900	0.000	-123.4354	100.21475	29.750	0.193750	107.058125	0.000	-1.428125
-68.8800	0.000	-153.9419	100.37575	29.750	0.198000	107.51975	0.000	-1.366875
-39.3600	0.000	-184.8124	100.578375	29.75	0.191500	107.97475	0.000	-1.301500
-7.3800	0.000	-208.6080	100.820125	29.750	0.175500	108.42	0.000	-1.232375
29.5200	0.000	-227.5475	101.098375	29.75	0.150250	108.852875	0.000	-1.159625
71.3400	0.000	-240.5142	101.41025	29.750	0.115625	109.27075	0.000	-1.083875
123.0000	0.000	-246.0000	101.7525	29.750	0.070375	109.671125	0.000	-1.005500

110.0515	0.000	-0.925250	112.5	29.75	0.000	119.329875	29.75	11.80825
110.409625	0.000	-0.843625	5	1		119.9285	29.75	11.772500
110.743375	0.000	-0.761125	36	2		120.522	29.75	11.753000
111.05075	0.000	-0.678375	112.500625	0.000	12.47775	121.104	29.75	11.750750
111.330125	0.000	-0.596000	112.5055	0.000	12.570125	121.668	29.75	11.766000
111.579875	0.000	-0.514500	112.533	0.000	12.640000	122.2075	29.75	11.798500
111.798625	0.000	-0.434500	112.598625	0.00	12.678375	122.716125	29.75	11.847625
111.9855	0.000	-0.356625	112.71475	0.000	12.693750	123.1875	29.75	11.911750
112.138875	0.000	-0.281250	112.87575	0.000	12.698000	123.616	29.75	11.989000
112.259375	0.000	-0.205750	113.078375	0.000	12.69150	123.99575	29.75	12.076625
112.353125	0.000	-0.129625	113.320125	0.000	12.67550	124.321625	29.75	12.17200
112.427125	0.000	-0.061750	113.598375	0.000	12.65025	124.586625	29.75	12.27225
112.47975	0.000	-0.015750	113.91025	0.000	12.615625	124.781875	29.75	12.36750
112.5	0.000	0.000	114.2525	0.000	12.570375	124.9085	29.75	12.441500
100.000625	29.750	-0.02225	114.62575	0.000	12.509375	124.978125	29.75	12.485625
100.019375	29.75	-0.129125	115.03475	0.000	12.433125	125	29.75	12.500000
100.061875	29.75	-0.246125	115.48	0.000	12.348375	6	1	
100.1285	29.750	-0.369250	115.959125	0.000	12.25900	46	2	
100.219375	29.75	-0.495125	116.46875	0.000	12.168500	112.500625	0.000	12.47775
100.33675	29.750	-0.620750	117.0055	0.000	12.080250	112.519375	0.000	12.370875
100.481875	29.75	-0.746000	117.564875	0.00	11.997375	112.561875	0.000	12.253875
100.652875	29.75	-0.870625	118.142375	0.000	11.92275	112.6285	0.000	12.130750
100.848625	29.75	-0.992500	118.7325	0.000	11.858875	112.719375	0.000	12.004875
101.068125	29.75	-1.109875	119.329875	0.000	11.80825	112.83675	0.000	11.879250
101.31025	29.75	-1.221250	119.9285	0.000	11.772500	112.981875	0.000	11.75400
101.573875	29.75	-1.324750	120.522	0.000	11.753000	113.152875	0.000	11.629375
101.857875	29.75	-1.419375	121.104	0.000	11.750750	113.348625	0.000	11.50750
102.16075	29.75	-1.503250	121.668	0.000	11.766000	113.568125	0.000	11.390125
102.48075	29.75	-1.574250	122.2075	0.000	11.798500	113.81025	0.000	11.278500
102.817625	29.75	-1.629625	122.716125	0.00	11.847625	114.073875	0.000	11.17525
103.17125	29.75	-1.668250	123.1875	0.000	11.911750	114.357875	0.000	11.080625
103.543375	29.75	-1.688125	123.616	0.000	11.989000	114.66075	0.000	10.996750
103.936	29.75	-1.690750	123.99575	0.000	12.076625	114.98075	0.000	10.925750
104.347125	29.75	-1.680875	124.321625	0.000	12.17200	115.317625	0.000	10.870375
104.774125	29.75	-1.658875	124.586625	0.000	12.27225	115.67125	0.000	10.831750
105.215125	29.75	-1.626375	124.781875	0.000	12.36750	116.043375	0.000	10.811875
105.6675	29.75	-1.585375	124.9085	0.000	12.441500	116.436	0.000	10.809250
106.128125	29.75	-1.537875	124.978125	0.00	12.485625	116.847125	0.000	10.819125
106.593	29.75	-1.485125	125	0.000	12.500000	117.274125	0.000	10.841125
107.058125	29.75	-1.428125	112.500625	29.75	12.47775	117.715125	0.000	10.873625
107.51975	29.75	-1.366875	112.5055	29.75	12.570125	118.1675	0.000	10.914625
107.97475	29.75	-1.301500	112.533	29.75	12.640000	118.628125	0.000	11.0962125
108.42	29.75	-1.232375	112.598625	9.75	12.678375	119.093	0.000	11.014875
108.852875	29.75	-1.159625	112.71475	29.75	12.693750	119.558125	0.000	11.071875
109.27075	29.75	-1.083875	112.87575	29.75	12.698000	120.01975	0.000	11.133125
109.671125	29.75	-1.005500	113.078375	29.75	12.69150	120.47475	0.000	11.198500
110.0515	29.75	-0.925250	113.320125	29.75	12.67550	120.92	0.000	11.267625
110.409625	29.75	-0.843625	113.598375	29.75	12.65025	121.352875	0.000	11.340375
110.743375	29.75	-0.761125	113.91025	29.75	12.615625	121.77075	0.000	11.416125
111.05075	29.75	-0.678375	114.2525	29.75	12.570375	122.171125	0.000	11.49450
111.330125	29.75	-0.596000	114.62575	29.75	12.509375	122.5515	0.000	11.574750
111.579875	29.75	-0.514500	115.03475	29.75	12.433125	122.909625	0.000	11.656375
111.798625	29.75	-0.434500	115.48	29.75	12.348375	123.243375	0.000	11.738875
111.9855	29.75	-0.356625	115.959125	29.75	12.25900	123.55075	0.000	11.821625
112.138875	29.75	-0.281250	116.46875	29.75	12.168500	123.830125	0.000	11.90400
112.259375	29.75	-0.205750	117.0055	29.75	12.080250	124.079875	0.000	11.98550
112.353125	29.75	-0.129625	117.564875	29.75	11.997375	124.298625	0.000	12.06550
112.427125	29.75	-0.061750	118.142375	29.75	11.92275	124.4855	0.000	12.143375
112.47975	29.75	-0.015750	118.7325	29.75	11.858875	124.638875	0.000	12.21875

124.759375	0.000	12.29425	2	2	Surface Regions
124.853125	0.000	12.370375	70	30.000 -30.000	1 1 1
124.927125	0.000	12.43825	130	30.000 -30.000	6
124.97975	0.000	12.484250	70	30.000 30.000	1 -2 -3 4 -5 6
125	0.000	12.500000	130	30.000 30.000	2 2 1
112.500625	29.75	12.47775	9	1	2
112.519375	29.75	12.370875	2	2	1 2
112.561875	29.75	12.253875	98.6	29.75 -3.200000	3 3 1
112.6285	29.75	12.130750	98.6	30.000 -3.200000	4
112.719375	29.75	12.004875	98.6	29.75 14.400000	11 3 12 7
112.83675	29.75	11.879250	98.6	30.000 14.400000	4 4 1
112.981875	29.75	11.75400	10	1	4
113.152875	29.75	11.629375	2	2	11 8 12 4
113.348625	29.75	11.50750	98.6	29.75 -3.200000	5 5 1
113.568125	29.75	11.390125	98.6	30.000 -3.200000	4
113.81025	29.75	11.278750	125.8	29.75 -3.200000	13 5 14 9
114.073875	29.75	11.17525	125.8	30.000 -3.200000	6 6 1
114.357875	29.75	11.080625	11	1	4
114.66075	29.75	10.996750	2	2	13 10 14 6
114.98075	29.75	10.925750	125.8	29.75 -3.200000	7 7 1
115.317625	29.75	10.870375	125.8	30.000 -3.200000	8
115.67125	29.75	10.831750	125.8	29.75 14.400000	25 15 -19 -22 7 -8 9 -10
116.043375	29.75	10.811875	125.8	30.000 14.400000	8 8 1
116.436	29.75	10.809250	12	1	4
116.847125	29.75	10.819125	2	2	23 20 -16 -26
117.274125	29.75	10.841125	98.600000	29.75 14.400000	9 9 1
117.715125	29.75	10.873625	98.60000	30.000 14.400000	4
118.1675	29.75	10.914625	125.80000	29.75 14.400000	17 16 -18 -15
118.628125	29.75	10.962125	125.8000	30.000 14.400000	10 10 1
119.093	29.75	11.014875	Mesh generation		4
119.558125	29.75	11.071875	26	12	19 18 -20 -21
120.01975	29.75	11.133125	Curves segments		11 11 1
120.47475	29.75	11.198500	1	1 1	4
120.92	29.75	11.267625	2	2 1	22 21 -23 -24
121.352875	29.75	11.340375	3	3 1	12 12 1
121.77075	29.75	11.416125	4	4 1	4
122.171125	29.75	11.494500	5	5 1	24 26 -17 -25
122.5515	29.75	11.574750	6	6 1	
122.909625	29.75	11.656375	7	7 1	
123.243375	29.75	11.738875	8	8 1	
123.55075	29.75	11.821625	9	9 1	
123.830125	29.75	11.904000	10	10 1	
124.079875	29.75	11.985500	11	11 1	
124.298625	29.75	12.065500	12	12 1	
124.4855	29.75	12.143375	13	13 1	
124.638875	29.75	12.218750	14	14 1	
124.759375	29.75	12.294250	15	15 1	
124.853125	29.75	12.370375	16	16 1	
124.927125	29.75	12.438250	17	17 1	
124.97975	29.75	12.484250	18	18 1	
125	29.75	12.500000	19	19 1	
7	1		20	20 1	
2	2		21	21 1	
70	29.75	-30.000	22	22 1	
130	29.75	-30.000	23	23 1	
70	29.75	30.000	24	24 1	
130	29.75	30.000	25	25 1	
8	1		26	26 1	

APPENDIX B-2

STARS-CFD Background Mesh Data File (*boxwing.bac*)

Background Mesh....boxwing

```

4      1      0      3      6
1     -1800  -100  -2400
      1      0      0     40
      0      1      0     40
      0      0      1     40
2     1800  -100  -2400
      1      0      0     40
      0      1      0     40
      0      0      1     40
3      0     -100   2400
      1      0      0     40
      0      1      0     40
      0      0      1     40
4      0     2400   0
      1      0      0     40
      0      1      0     40
      0      0      1     40
1      1      2      3      4

```

* Point Sources

* Line Sources

1. Leading Edge of Lower Wing

```

100.00000  0.00000  -0.02224  0.07  0.07  0.35
100.00000  30.00000  -0.02224  0.07  0.07  0.35

```

2. Leading Edge of Upper Wing

```

112.50063  0.00000  12.57013  0.07  0.07  0.35
112.50063  30.00000  12.57013  0.07  0.07  0.35

```

3. In the middle

```

112.50063  0.00000  6.00000  0.8  6  15.00000
112.50063  30.00000  6.00000  0.8  6  15.00000

```

* Triangle Sources

1. Source for lower wing

```

100.00000  0.00000  0.00000  0.5  1  3
100.00000  30.00000  0.00000  0.5  1  3

```


112.50000	0.00000	0.00000	0.5	1	3
2. Source for lower wing					
112.50000	0.00000	0.00000	0.5	1	3
100.00000	30.00000	0.00000	0.5	1	3
112.50000	30.00000	0.00000	0.5	1	3
3. Source for upper wing					
112.50063	0.00000	12.57013	0.5	1	3
112.50063	30.00000	12.57013	0.5	1	3
125.00000	0.00000	12.57013	0.5	1	3
4. Source for upper wing					
125.00000	0.00000	12.57013	0.5	1	3
112.50063	30.00000	12.57013	0.5	1	3
125.00000	30.00000	12.57013	0.5	1	3
5. Source for endplate					
98.60000	30.00000	14.40000	0.5	1	3
125.80000	30.00000	-3.20000	0.5	1	3
125.80000	30.00000	14.40000	0.5	1	3
6. Source for endplate					
98.60000	30.00000	14.40000	0.5	1	3
125.80000	30.00000	-3.20000	0.5	1	3
98.60000	30.00000	-3.20000	0.5	1	3

APPENDIX B-3

STARS-CFD Boundary Conditions Data File (*boxwing.bco*)

Fin Boundary Condition File	19	3
12 26	20	3
Surface Regions	21	1
1 2	22	1
2 3	23	1
3 1	24	1
4 1	25	3
5 1	26	3
6 1		
7 1		
8 1		
9 1		
10 1		
11 1		
12 1		
Curve Segments		
1 0		
2 0		
3 0		
4 0		
5 0		
6 0		
7 3		
8 3		
9 3		
10 3		
11 0		
12 1		
13 0		
14 1		
15 1		
16 1		
17 1		
18 1		

APPENDIX B-4

STARS-CFD Parameter Control File (*boxwing.cons*)

```
&control  
nout = 50,  
nstep = 1,  
ncycl = 5000,  
nstpe = 20,  
nsmth = 0,  
smofc = 0.25,  
cfl = 0.20,  
mach = 0.434,  
alpha = 0.0,  
beta = 0.0,  
relax = 1.0,  
amplitude= 1.0,  
restart = 0,  
/
```

APPENDIX C-1

Selig 1223 Airfoil Coordinate Data

X	Y		
0.00005	-0.00178	0.83277	-0.06749
0.00155	-0.01033	0.85947	-0.06089
0.00495	-0.01969	0.88406	-0.05427
0.01028	-0.02954	0.90641	-0.04768
0.01755	-0.03961	0.92639	-0.04116
0.02694	-0.04966	0.94389	-0.03476
0.03855	-0.05968	0.95884	-0.02853
0.05223	-0.06965	0.97111	-0.02250
0.06789	-0.07940	0.98075	-0.01646
0.08545	-0.08879	0.98825	-0.01037
0.10482	-0.09770	0.99417	-0.00494
0.12591	-0.10598	0.99838	-0.00126
0.14863	-0.11355	1.00000	0.00000
0.17286	-0.12026	0.00044	0.00561
0.19846	-0.12594	0.00264	0.01120
0.22541	-0.13037	0.00789	0.01427
0.25370	-0.13346	0.01718	0.01550
0.28347	-0.13505	0.03006	0.01584
0.31488	-0.13526	0.04627	0.01532
0.34777	-0.13447	0.06561	0.01404
0.38193	-0.13271	0.08787	0.01202
0.41721	-0.13011	0.11282	0.00925
0.45340	-0.12683	0.14020	0.00563
0.49025	-0.12303	0.17006	0.00075
0.52744	-0.11881	0.20278	-0.00535
0.56465	-0.11425	0.23840	-0.01213
0.60158	-0.10935	0.27673	-0.01928
0.63798	-0.10412	0.31750	-0.02652
0.67360	-0.09859	0.36044	-0.03358
0.70823	-0.09277	0.40519	-0.04021
0.74166	-0.08671	0.45139	-0.04618
0.77369	-0.08044	0.49860	-0.05129
0.80412	-0.07402	0.54639	-0.05534
		0.59428	-0.05820

0.64176	-0.05976
0.68832	-0.05994
0.73344	-0.05872
0.77660	-0.05612
0.81729	-0.05219
0.85500	-0.04706
0.88928	-0.04088
0.91966	-0.03387
0.94573	-0.02624
0.96693	-0.01822
0.98255	-0.01060
0.99268	-0.00468
0.99825	-0.00115
1.00000	0.00000

VITA

Tony Michael Buratti

Candidate for the Degree of
Masters of Science

Thesis: TOP-FUEL DRAGSTER WING DESIGN USING CFD AND ITS INFLUENCE
ON VEHICLE DYNAMIC PERFORMANCE

Major Field: Mechanical Engineering

Biography:

Personal Data: Born in Oklahoma City, Oklahoma March 12, 1976. The son of Richard M. and Joyce K. Buratti.

Education: Graduated from John Marshall High School, Oklahoma City, Oklahoma in May 1994; received a Bachelor of Science degree in Mechanical Engineering in July 1998 from Oklahoma State University, Stillwater, Oklahoma. Completed requirements for the Masters of Science degree with a major in Mechanical at Oklahoma State University in December, 2000.

Experience: Field Engineer, Boeing Aerospace Operations, 1997-1998; Teaching Assistant, Oklahoma State University School of Mechanical and Aerospace Engineering, 1998-2000; Graduate Research Assistant, Oklahoma State University School of Mechanical Engineering, 1998-2000.

Professional Memberships: American Institute of Aeronautics and Astronautics, American Society of Mechanical Engineers, Society of Automotive Engineers, American Pool Players Association, Phi Kappa Phi, Tau Beta Pi, Pi Tau Sigma, and Golden Key National Honor Society.

Name: Tony Michael Buratti

Date of Degree: December, 2000

Institution: Oklahoma State University

Location: Stillwater, Oklahoma

Title of Study: TOP-FUEL DRAGSTER WING DESIGN USING CFD AND ITS
INFLUENCE ON VEHICLE DYNAMIC PERFORMANCE

Pages in Study: 144

Candidate for the Degree of Masters of Science

Major Field: Mechanical Engineering

Scope and Method of Study: The scope of the thesis is to develop a dynamic dragster model that will provide insight into the aerodynamics of the rear wing effects on a top-fuel dragster's overall performance. It was never know how much down force is needed for these vehicles but study of this dynamic model provides this information. This research focuses on top-fuel dragsters running on a quarter mile drag strip. By using a CFD code to analyze rear wing designs this data can be implemented into the dynamic model and can determine how the wing effects the dragster performance. Lift and drag will be varied in the dynamic model and plots will show how each parameter effects the elapsed time and top speed of the dragster.

Findings and Conclusions: Development of the dragster model proved beneficial in understanding how the aerodynamic characteristics affect the performance of the dragster. This model allows us to understand the questions of how much down force is needed and how changing these aerodynamic characteristics will truly effect the performance of the dragster. Development of these elapsed time versus speed curves for various lift and drag coefficients allows us to determine a trend as to how these aerodynamic characteristics can improve performance. It was always said that these dragsters want as much down force as possible but from this model it is not necessarily true. What was shown to be the most beneficial is the reduction of the drag and the reduction of the coefficient of lift up to a certain point. The current wings used on top-fuel dragsters produce an enormous amount of down force and along with this comes an enormous amount of induced drag. Designing a wing that will take advantage of the knowledge gained from this model proved to increase the top speed but more importantly reduce the elapsed time which is how you win races.

ADVISOR'S APPROVAL: _____